

**FOURIER TRANSFORM INFRARED SPECTROSCOPY STUDY
OF SMALL TRANSITION-METAL CARBIDE CLUSTERS**

by

RAYMOND EDWARD KINZER, JR.

Bachelor of Science, 2004
Texas Christian University
Fort Worth, TX

Submitted to the Graduate Faculty of the
College of Science and Engineering
Texas Christian University
in partial fulfillment of the requirements
for the degree of

Doctor of Philosophy

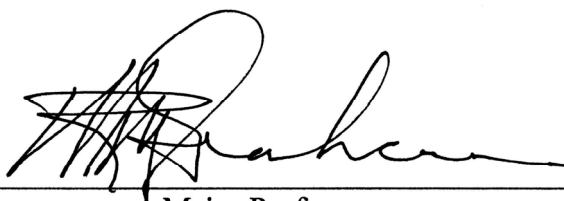
August 2009

FOURIER TRANSFORM INFRARED SPECTROSCOPY STUDY
OF SMALL TRANSITION-METAL CARBIDE CLUSTERS

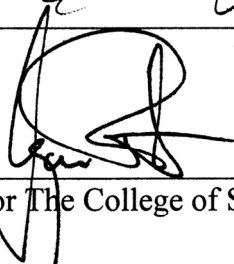
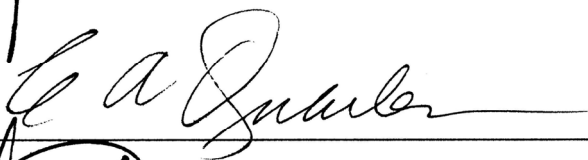
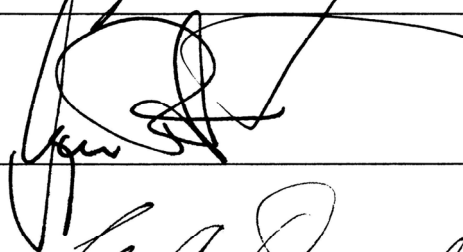
by

Raymond Edward Kinzer, Jr.

Dissertation approved:



Major Professor



For The College of Science and Engineering

Copyright by
Raymond Edward Kinzer, Jr.

2009

ACKNOWLEDGEMENTS

I wish to express my deepest appreciation to my advisor, Dr. W. R. M. Graham, for his guidance and support in my research and education.

Thanks to Dr. C. M. L. Rittby for his assistance with computer simulations and providing theoretical insight in this research.

Thanks to M. Murdock, D. Yale, and G. Katchinska for their assistance in maintaining the laboratory equipment.

Thanks to my family and friends who supported and encouraged me in my studies.

Funding for this research and equipment by the Welch Foundation, the W. M. Keck Foundation, and the TCU Research and Creative Activities Fund is gratefully acknowledged.

TABLE OF CONTENTS

ACKNOWLEDGEMENTS	ii
LIST OF FIGURES	vi
LIST OF TABLES	xi
CHAPTER I INTRODUCTION: MOTIVATION AND PREVIOUS RESEARCH	1
1.1 ASTROPHYSICAL MOTIVATION	1
1.2 METALLOCARBOHEDRENES AND THEIR BUILDING BLOCKS	7
1.3 PREVIOUS RESEARCH	9
1.3.1 <i>Previous Experimental Results</i>	9
1.3.2 <i>Previous Theoretical Results</i>	11
1.4 OVERVIEW OF THE DISSERTATION RESEARCH	12
CHAPTER II TECHNIQUES AND PROCEDURES	14
2.1 MATRIX TRAPPING	14
2.2 EXPERIMENTAL PROCEDURES	15
2.2.1 <i>General Experimental Procedures</i>	15
2.2.2 <i>Special Experimental Considerations</i>	16
2.3 ISOTOPIC SUBSTITUTION	20
2.4 SAMPLE ROD PREPARATION	25
2.4.1 <i>Carbon Sample Rods</i>	25
2.4.2 <i>Metal Sample Rods</i>	26
2.5 THE “LOW-POWER” EVAPORATION TECHNIQUE	26
2.6 THEORETICAL SIMULATIONS	28

CHAPTER III FTIR OBSERVATION OF THE $\nu_3(\sigma_u)$ VIBRATIONAL	
FUNDAMENTAL OF LINEAR NiC₃Ni IN SOLID Ar	30
3.1 INTRODUCTION AND PREVIOUS RESEARCH.....	30
3.2 EXPERIMENTAL PROCEDURES.....	33
3.3 EXPERIMENTAL RESULTS AND ANALYSIS.....	34
3.4 THEORETICAL MODELING AND ANALYSIS.....	38
3.5 CONCLUSIONS.....	44
CHAPTER IV FTIR OBSERVATION OF VIBRATIONAL FUNDAMENTALS OF TiC₃	
IN SOLID Ar.....	45
4.1 INTRODUCTION AND PREVIOUS RESEARCH.....	45
4.2 THEORETICAL CALCULATIONS	50
4.3 EXPERIMENTAL PROCEDURES.....	51
4.4 RESULTS AND ANALYSIS	55
4.4.1 <i>The $\nu_5(b_2)$ vibrational fundamental</i>	56
4.4.2 <i>The $\nu_3(a_1)$ vibrational fundamental</i>	60
4.4.3 <i>The $\nu_4(b_1)$ vibrational fundamental</i>	61
4.4.4 <i>Other vibrational fundamentals of TiC₃</i>	64
4.5 CONCLUSIONS.....	64
CHAPTER V FTIR OBSERVATION OF VIBRATIONAL FUNDAMENTALS OF ScC₃	
IN SOLID Ar.....	65
5.1 INTRODUCTION AND PREVIOUS RESEARCH.....	65
5.2 THEORETICAL MODELING.....	66
5.3 EXPERIMENTAL PROCEDURES.....	71

5.4	RESULTS AND ANALYSIS	71
5.4.1	<i>The $\nu_5(b_2)$ vibrational fundamental</i>	73
5.4.2	<i>The $\nu_3(a_1)$ vibrational fundamental</i>	77
5.4.3	<i>The $\nu_1(a_1)$ vibrational fundamental</i>	83
5.4.4	<i>Other vibrational fundamentals of ScC_3</i>	86
5.5	CONCLUSIONS.....	86
CHAPTER VI CONCLUSIONS AND FUTURE RESEARCH.....		87
6.1	CONCLUSIONS.....	87
6.1.1	<i>Linear NiC_3Ni</i>	87
6.1.2	<i>Cyclic TiC_3</i>	88
6.1.3	<i>Cyclic ScC_3</i>	89
6.2	FUTURE RESEARCH.....	89
6.2.1	<i>Transition-Metal Carbides</i>	89
6.2.2	<i>Other Metal Carbides</i>	91
6.2.3	<i>Transition Metal–Silicon–Carbon Clusters</i>	92
REFERENCES.....		94

VITA

ABSTRACT

LIST OF FIGURES

- Figure 1.1 The original Ti_8C_{12} metcar structures proposed (a) by Castleman *et al.* (Ref. 15) and (b) modeled by Dance (Ref. 20). Dance's structure in (c) is a better representative of the currently accepted structure and demonstrates the TiC_2 building block which is not observed in (a) or (b).....8
- Figure 2.1 General schematic of the experimental apparatus. Only one laser optics system is shown. The sample deposition chamber (shown in the blue, shaded box) is enlarged in Fig. 2.2. The Au mirror here is positioned for scanning by the Bomem (deposition and scanning are not done simultaneously). [Modeled after Bates (Ref. 39)]......17
- Figure 2.2 Top-view schematic (not to scale) of the sample deposition chamber during deposition. [Modeled after Bates (Ref. 39).]18
- Figure 2.3 Carbon sites in C_3 . C_α denotes equivalent C sites and C_β denotes the unique site. Shaded discs represent single ^{13}C substitutions in (b) the two equivalent isotopomers and (c) the unique isotopomer.22
- Figure 2.4 The isotopic shift spectrum of the $\nu_3(\sigma_u)$ fundamental of linear C_3 . The isotopomers corresponding to the isotopic shifts are labeled in the $\text{C}_\alpha\text{-C}_\beta\text{-C}_\alpha$ convention of Fig. 2.3.23
- Figure 2.5 Commonly predicted structures for MC_3 transition-metal carbide clusters. Equivalent and unique carbon sites are labeled in the fashion of Fig. 2.3. The arrows represent the principal axis of symmetry for each geometry.24

Figure 3.1	<p>The (a) kite-shaped, (b) linear, and (c) fanlike geometries modeled for NiC₃. The fanlike is predicted to be the ground state structure. Bond lengths are in angstroms (Å) (linear and fanlike only). [(a) adapted from Longo <i>et al.</i> (Ref. 57); (b)-(c) adapted from Froudakis <i>et al.</i> (Ref. 56).].....</p>	32
Figure 3.2	<p>A survey spectrum in the 1800-2100 cm⁻¹ range showing the spectra produced (a) from the ablation of nickel and graphite rods and (b) from graphite ablation only. Vibrational fundamentals of known carbon bands are labeled. The intense absorption at 1950.8 cm⁻¹ is unique to (a) which suggests it belongs to a nickel-carbon cluster.....</p>	35
Figure 3.3	<p>The ¹³C isotopic substituted spectra in the 1860-1960 cm⁻¹ range showing (a) the spectrum with ~12% ¹³C enrichment and (b) ~50% ¹³C enrichment. Isotopomers are assigned in (b) following the convention of Table 3.2 and Fig. 3.4. Spectrum (c) shows the 50% ¹³C-enriched DFT calculated isotopic spectrum for linear NiC₃Ni off 1950.8 cm⁻¹. All isotopic shifts, including the full Ni¹³C₃Ni isotopomer, are scaled off the fundamental.....</p>	37
Figure 3.4	<p>The structure of linear NiC₃Ni in the ¹Σ_g⁺ and relaxed ¹A₁ electronic states. Bond lengths are in angstroms (Å) and are the same for both linear and relaxed structures. The angles denote the bending calculated for the relaxed structure. The vectors above the molecule indicate the displacement of the carbon atoms in the ν₃(σ_u) vibrational mode of the linear structure which corresponds to the ν₇(b₂) vibrational mode of the relaxed structure.</p>	42

Figure 4.1	Geometries of TiC_3 investigated in the DFT study by Sumathi and Hendrickx (Ref. 65). Bond lengths are given in angstroms (\AA) for singlet, triplet (), and quintet [] electronic states.47
Figure 4.2	Energy level diagram plotting the relative energies of the TiC_3 isomers in Fig. 4.1 by Sumathi and Hendrickx (Ref. 65). The electronic states are singlet (s), triplet (t), and quintet (q). Solid lines represent stable minima and dashed lines represent higher order saddle points or stationary points.48
Figure 4.3	Ground state structures for (a)-(c) TiC_n ($n=2-4$) and (d)-(e) Ti_2C_n ($n=2,3$) clusters calculated in the DFT investigations of Sumathi and Hendrickx (Ref. 63,65-67). Bond lengths are in angstroms (\AA).49
Figure 4.4	The DFT-B3LYP/6-311G(3df, 3pd) calculated fanlike (C_{2v}) isomer of TiC_3 in the 1A_1 ground state. Bond lengths are in angstroms (\AA). Equivalent carbon sites are denoted C_α , and the unique carbon site by C_β52
Figure 4.5	The DFT-B3LYP/6-311G(3df, 3pd) calculated vibrational modes of fanlike (1A_1) TiC_3 . Vectors show the displacement of the atoms.54
Figure 4.6	The $\nu_5(b_2)=1484.2 \text{ cm}^{-1}$ fundamental of TiC_3 . (a) The spectrum produced in the 1430-1490 cm^{-1} region by the simultaneous evaporation of a carbon rod with 10% ^{13}C isotopic enrichment and a titanium rod and (b) the spectrum of the sample after annealing at 24 K. The labeling of isotopic shifts in (b) follows the convention of Table 4.2 and Fig. 4.4 (the metal atom is omitted for brevity). (c) The DFT-B3LYP/6-311G(3df, 3pd) simulated spectrum.58

- Figure 4.7 The $\nu_3(a_1)=624.3\text{ cm}^{-1}$ and tentatively assigned $\nu_4(b_1)=573.8\text{ cm}^{-1}$ fundamentals of TiC_3 . (a) The spectrum produced in the $540\text{-}640\text{ cm}^{-1}$ region by simultaneous evaporation of a carbon rod with 10% ^{13}C isotopic enrichment and a titanium rod after annealing at 16 K. The labeling of the isotopic shifts follows the convention in Table 4.3 and Fig 4.4 (the metal atom is omitted for brevity). (b) The DFT-B3LYP/6-311G(3df, 3pd) simulated spectrum.62
- Figure 5.1 Geometry of fanlike (C_{2v}) ScC_3 in the (a) 2A_2 electronic state and (b) 4B_1 state. Bond lengths in angstroms (\AA) are shown for the B3LYP/6-311G(3df, 3pd) simulation. Equivalent and unique carbon sites are labeled C_α and C_β , respectively.68
- Figure 5.2 [(a)-(f)] The B3LYP/6-311G(3df, 3pd) predicted vibrational modes for ScC_3 in the 2A_2 electronic state. Vectors show the displacement of the atoms. (g) In the $\nu_3(a_1)$ fundamental in the 4B_1 state, the C_β atom significantly participates in the vibration.70
- Figure 5.3 The $\nu_5(b_2)=1478.0\text{ cm}^{-1}$ fundamental of fanlike ScC_3 . (a) ^{13}C -enriched isotopic spectrum after annealing at 30 K; the DFT-B3LYP/6-311G(3df, 3pd) simulated isotopic spectra using 25% ^{13}C enrichment for the (b) 2A_2 and (c) 4B_1 electronic states over the $1410\text{-}1480\text{ cm}^{-1}$ region. The isotopic spectrum for C_5 is labeled. Isotopic shift frequencies and isotopomers in the spectrum in (a) are labeled according to the convention of Table 5.2 and Fig. 5.1.75
- Figure 5.4 The $\nu_3(a_1)=557.0\text{ cm}^{-1}$ fundamental of fanlike ScC_3 . (a) The ^{13}C -enriched isotopic spectrum after annealing at 30 K; the DFT-B3LYP/6-311G(3df, 3pd) simulated

isotopic spectra using 25% ^{13}C enrichment for the (b) 2A_2 and (c) 4B_1 electronic states over the 540-560 cm^{-1} region. Measured and predicted isotopic shift frequencies are labeled. The isotopomers are labeled in (a) following the convention of Table 5.3 and Fig. 5.1.79

Figure 5.5 (a) The ^{13}C -enriched isotopic spectra after annealing at 30 K in the 620-680 cm^{-1} range. The 4B_1 simulation of the $\nu_2(a_1)$ isotopic spectrum is scaled for comparison with the bands observed at (b) 658.9 and (c) 673.2 cm^{-1} . None of the bands is a suitable candidate for the $\nu_2(a_1)$ fundamental of the quartet state.82

Figure 5.6 The $\nu_1(a_1)=1190.7 \text{ cm}^{-1}$ fundamental of fanlike ScC_3 . (a) The ^{13}C -enriched isotopic spectrum after annealing at 30 K; the DFT-B3LYP/6-311G(3df, 3pd) simulated isotopic spectra using 25% ^{13}C enrichment for the (b) 2A_2 and (c) 4B_1 electronic states over the 1150-1200 cm^{-1} region. The isotopic spectrum for C_6 is labeled. Spectrum (a) shows the isotopic shift frequencies, and isotopomers are labeled following the convention of Table 5.4 and Fig. 5.1.84

LIST OF TABLES

Table 1.1	A listing of molecules observed in the interstellar medium and/or circumstellar shells as recorded by the Cologne Database for Molecular Spectroscopy (CDMS) in May 2009 (Ref. 2). Additional listings from Al Wooten’s database (Ref. 3) are denoted by (W). Tentative identifications are denoted by ?.....3
Table 1.2	Molecules observed in the circumstellar shells of carbon star IRC+10216 as of 2006 (Ref. 10).5
Table 3.1	DFT-B3LYP/6-311G* calculated vibrational frequencies for $^1\Sigma_g^+$ linear and 1A_1 “relaxed” NiC ₃ Ni (see Fig. 3.4).41
Table 3.2	Comparison of observed and DFT-B3LYP/6-311G* calculated isotopic shifts for linear $^1\Sigma_g^+$ NiC ₃ Ni (see Fig. 3.3).43
Table 4.1	DFT-B3LYP/6-311G(3 <i>df</i> , 3 <i>pd</i>) predicted vibrational frequencies (cm ⁻¹) and infrared intensities (km/mol) for the 1A_1 fanlike (<i>C</i> _{2<i>v</i>}) isomer of TiC ₃ (see Fig. 4.4 and 4.5).53
Table 4.2	Comparison between the observed ¹³ C shift frequencies (cm ⁻¹) and the DFT-B3LYP/6-311G(3 <i>df</i> , 3 <i>pd</i>) predicted isotopomer frequencies for the $\nu_5(b_2)$ mode of the 1A_1 fanlike (<i>C</i> _{2<i>v</i>}) isomer of TiC ₃ (see Fig. 4.6).59
Table 4.3	Comparison between the observed ¹³ C shift frequencies (cm ⁻¹) and the DFT-B3LYP/6-311G(3 <i>df</i> , 3 <i>pd</i>) predicted isotopomer frequencies for the $\nu_3(a_1)$ mode of the 1A_1 fanlike (<i>C</i> _{2<i>v</i>}) isomer of TiC ₃ (see Fig. 4.7).63

Table 5.1	DFT-B3LYP/6-311G(3 <i>df</i> , 3 <i>pd</i>) predicted vibrational modes, frequencies (cm ⁻¹), and infrared intensities (km/mol) for cyclic (fanlike, C _{2v}) ScC ₃ in ² A ₂ and ⁴ B ₁ electronic states (see Fig. 5.1 and 5.2).....69
Table 5.2	Comparison of observed ¹³ C isotopic shift frequencies (cm ⁻¹) to DFT-B3LYP/6-311G(3 <i>df</i> , 3 <i>pd</i>) predicted isotopic frequencies for the ν ₅ (b ₂) mode of fanlike (C _{2v}) ScC ₃ in the ² A ₂ and ⁴ B ₁ electronic states (see Fig. 5.3).....76
Table 5.3	Comparison of observed ¹³ C isotopic shift frequencies (cm ⁻¹) to DFT-B3LYP/6-311G(3 <i>df</i> , 3 <i>pd</i>) predicted isotopic frequencies for the ν ₃ (a ₁) mode of fanlike (C _{2v}) ScC ₃ in the ² A ₂ and ⁴ B ₁ electronic states (see Fig. 5.4).....80
Table 5.4	Comparison of observed ¹³ C isotopic shift frequencies (cm ⁻¹) to DFT-B3LYP/6-311G(3 <i>df</i> , 3 <i>pd</i>) predicted isotopic frequencies for the ν ₁ (a ₁) mode of fanlike (C _{2v}) ScC ₃ in the ² A ₂ and ⁴ B ₁ electronic states (see Fig.5.6).....85

CHAPTER I

INTRODUCTION: MOTIVATION AND PREVIOUS RESEARCH

Molecules composed of transition metal and carbon atoms have received special attention for their wide range of applications. Such molecules are of interest because of their potential for observation in astrophysical environments and the insight they may provide into the formation of larger transition metal and carbon complexes such as metallocarbohedrenes. Additional potential applications of these molecules exist in the study of superconductors, semiconductors, quantum dot devices, and possibly catalysts.¹

The following discussion will outline the motivation for studying small transition-metal carbide molecules, including their potential astrophysical significance and their relevance to the study of metallocarbohedrenes and other metal-carbon complexes. Previous experimental and theoretical research on small transition-metal carbide clusters will also be discussed.

1.1 ASTROPHYSICAL MOTIVATION

Small transition-metal carbides are potential astrophysically significance species. To date (May 2009) approximately 150 molecules have been observed in the interstellar medium or circumstellar shells as recorded by the Cologne Database for Molecular Spectroscopy (CDMS).² Table 1.1 lists these molecules according to the number of atoms they contain.^{2,3} Among the molecules listed are carbon chains (*e.g.*, C₃, C₄, C₅) and a number of molecules with carbon chain backbones (*e.g.*, CCCN, HC₄N, C₅N, HC₉). Numerous metal-bearing molecules observed in circumstellar shells are also listed in Table 1.1 (*e.g.*, MgCN, AINC, FeO).

Additionally, transition metals and molecules containing transition metals have been observed in stellar environments. For example, neutral metal absorption lines (*e.g.*, Fe I, Cr I, Mn I) are observed in the spectra of F-stars and become stronger in M-stars. Spectra of M-stars are dominated by absorption bands of molecules such as TiO and VO. Other transition metal-bearing molecules, such as TiH, CrH, FeH,⁴ have been observed in very cool stars (700-2200 K).

Furthermore, there has been recent debate concerning titanium carbide structures in meteorites and carbon-rich post-asymptotic giant branch (AGB) stars (also referred to as protoplanetary nebulae or PPN's).^{5,6} Graphite grains embedded with titanium are observed in meteorites, and Von Helden *et al.*⁵ have speculated that post-AGB stars may be the source of these grains. They observed an infrared emission at 20.1 μm in gas-phase titanium carbide nanocrystals which seemed to correspond to a feature observed at the same wavelength (commonly referred to as the "21 μm " line) in the spectra of post-AGB stars,⁷ suggesting these stars could possibly be the origin of the micrometer sized graphite grains with embedded titanium carbide grains in meteorites. In a later study, Kimura *et al.*⁶ suggest that the 20.1 μm feature may be from the vibrational interaction of titanium atoms bonded to carbon cage fullerenes. Kimura observed another feature, also found in post-AGB spectra, at 19.0 μm that might be attributed to a vibration of C₆₀ (the buckminsterfullerene). Among other suggested carriers of the 20.1 μm line are iron oxides, hydrogenated amorphous carbon, SiS₂, SiC, SiO₂, among many others, but none of the proposed carriers, including titanium carbide nanocrystals, provides a convincing identification.^{8,9} The point remains, however, that complex titanium-bearing species in astrophysical sources are already the subject of considerable interest and speculation.

Table 1.1 A listing of molecules observed in the interstellar medium and/or circumstellar shells as recorded by the Cologne Database for Molecular Spectroscopy (CDMS) in May 2009 (Ref. 2). Additional listings from Al Wooten's database (Ref. 3) are denoted by (W). Tentative identifications are denoted by ?.

<u>2 atoms</u>	<u>3 atoms</u>	<u>4 atoms</u>	<u>5 atoms</u>	<u>6 atoms</u>	<u>7 atoms</u>	<u>8 atoms</u>	<u>9 atoms</u>
H ₂	C ₃	<i>c</i> -C ₃ H	C ₅	C ₅ H	C ₆ H	CH ₃ C ₃ N	CH ₃ C ₄ H
AlF	C ₂ H	<i>l</i> -C ₃ H	C ₄ H	<i>l</i> -H ₂ C ₄	CH ₂ CHCN	HC(O)OCH ₃	CH ₃ CH ₂ CN
AlCl	C ₂ O	C ₃ N	C ₄ Si	C ₂ H ₄	CH ₃ C ₂ H	CH ₃ COOH	(CH ₃) ₂ O
C ₂	C ₂ S	C ₃ O	<i>l</i> -C ₃ H ₂	CH ₃ CN	HC ₃ N	C ₇ H	CH ₃ CH ₂ OH
CH, CH ⁺	CH ₂	C ₃ S	<i>c</i> -C ₃ H ₂	CH ₃ NC	CH ₃ CHO	H ₂ C ₆	HC ₇ N
CN	HCN	C ₂ H ₂	H ₂ CCN	CH ₃ OH	CH ₃ NH ₂	CH ₂ OHCHO	C ₈ H
CO, CO ⁺	HCO, HCO ⁺	NH ₃	CH ₄	CH ₃ SH	<i>c</i> -C ₂ H ₄ O	<i>l</i> -HC ₆ H ?	CH ₃ C(O)NH ₂
CP	HCS ⁺	HCCN	HC ₃ N	HC ₃ NH ⁺	H ₂ CCHOH	CH ₂ CHCHO ?	C ₈ H ⁻
SiC	HOC ⁺	HCNH ⁺	HC ₂ NC	HC ₂ CHO	C ₆ H ⁻	CH ₂ CCHCN	C ₃ H ₆
HCl	H ₂ O	HNCO	HCOOH	NH ₂ CHO		H ₂ NCH ₂ CN	
KCl	H ₂ S	HNCS	H ₂ CNH	C ₅ N			
NH	HNC	HOCO ⁺	H ₂ C ₂ O	<i>l</i> -HC ₄ H ?			
NO	HNO	H ₂ CO	H ₂ NCN	<i>l</i> -HC ₄ N			
NS	MgCN	H ₂ CN	HNC ₃	<i>c</i> -H ₂ C ₃ O			
NaCl	MgNC	H ₂ CS	SiH ₄	H ₂ CCNH ?			
OH	N ₂ H ⁺	H ₃ O ⁺	H ₂ COH ⁺	C ₅ N ⁻			
PN	N ₂ O	<i>c</i> -SiC ₃	C ₄ H ⁻				
SO, SO ⁺	NaCN	CH ₃	HC(O)CN				
SiN	OCS	C ₄ ^(W)					
SiO	SO ₂	CH ₂ D ⁺ ^(W)					
SiS	<i>c</i> -SiC ₂	C ₃ N ⁻					
CS	CO ₂	PH ₃ ?		<u>10 atoms</u>	<u>11 atoms</u>	<u>12 atoms</u>	<u>13 atoms</u>
HF	NH ₂	HCNO		CH ₃ C ₅ N	HC ₉ N	C ₆ H ₆ ?	HC ₁₁ N
SH	H ₃ ⁺			(CH ₃) ₂ CO	CH ₃ C ₆ H	C ₂ H ₅ OCH ₃ ?	
HD	H ₂ D ⁺ , HD ₂ ⁺			(CH ₂ OH) ₂	C ₂ H ₅ OCHO	<i>n</i> -C ₃ H ₇ CN	
FeO ?	SiCN			CH ₃ CH ₂ CHO			
O ₂	AlNC						
CF ⁺	SiNC						
SiH ?	HCP						
PO	CCP						
AlO							

Therefore, when one considers the abundance of small C_n chains in circumstellar shells and the interstellar medium, the observations of numerous molecules composed of C_n chains, the variety of metal-bearing molecules observed in space, the observations of diatomic transition metal-bearing species (*e.g.*, TiH, CrH) in astrophysical sources, and even the speculation on TiC nanocrystals and Ti-fullerenes existing in more evolved stars, it seems plausible that small transition-metal carbide clusters might be observed as well. However, before such molecules can be identified in stellar environments or the interstellar medium, their structures and spectra must be measured in the laboratory. To date there have been few spectroscopic investigations of small transition-metal carbide clusters.

Many of the carbon-bearing molecules of Table 1.1 have been observed in carbon stars known for their rich variety of carbon-bearing molecules (*e.g.*, C_2 , CH, and CN). Table 1.2 shows a listing of molecules¹⁰ observed in one carbon star in particular, the red giant IRC+10216, which is a popular target of radio and infrared observations mainly because of its proximity to Earth (~ 600 ly). Though dim in visible light ($\sim 18^{\text{th}}$ magnitude) because of surrounding clouds of gas and dust, it is a strong source of infrared and radio light. This is a fine illustration of the need for infrared astronomy in general. Higher energy light (visible, ultraviolet, *etc.*) is absorbed and scattered by dust and gas in the interstellar medium. However, lower energy light (infrared, *etc.*) can pass through the interstellar medium with considerably less loss, revealing details that would otherwise be obscured.

Most of the molecules in Table 1.1 were observed using microwave spectroscopy which observes a molecule's rotational transitions.² To be observed by rotational spectroscopy, the molecule must have a permanent dipole moment. This is not the case for homonuclear chains (*e.g.*, C_3 , C_4 , C_5), molecules with a center of inversion, and some non-linear molecules (*e.g.*, CCl_4).¹¹ Such molecules are hidden to radio astronomers because they do not have permanent

Table 1.2 Molecules observed in the circumstellar shells of carbon star IRC+10216 as of 2006 (Ref. 10).

CO	CCH	HC ₃ N	CCS	SiO	NaCl
CS	C ₃ H	HC ₅ N	C ₃ S	SiS	AlCl
CN	C ₃ O	HC ₇ N	C ₃ N	SiC	KCl
HCN	C ₄ H	HC ₉ N	C ₅ N	SiN	AlF
HCCH	C ₅ H	H ₂ C ₄	HC ₄ N	SiC ₂	MgNC
HNC	C ₆ H	H ₂ C ₆	<i>c</i> -C ₃ H ₂	SiC ₃	MgCN
H ₂ CCH ₂	C ₇ H	HC ₂ N	CH ₃ CN	SiCN	AlNC
CH ₄	C ₈ H	C ₃	CP	SiC ₄	KCN
NH ₃	C ₂	C ₅	PN	SiH ₄	NaCN
H ₂ S					

dipole moments and, hence, rotational transitions cannot be observed; however, this does not rule out their detection via infrared spectroscopy. Therefore, infrared spectroscopic observations are an important tool for identifying astrophysically significant molecules, and these identifications rely on laboratory measurements such as those obtained in this research.

An additional problem in observing astrophysical molecules in the infrared is equipment. Space-based telescopes are necessary for astronomers to study astronomical objects at infrared wavelengths. Infrared observations from Earth's surface are complicated by significant absorption of radiation by H₂O and CO₂ in the Earth's atmosphere, thus limiting ground-based infrared measurements to narrow windows through which infrared radiation can pass with minimal absorption. The observation of the $\nu_3(\sigma_u^+) \approx 2169.4 \text{ cm}^{-1}$ ($\sim 4.6 \text{ }\mu\text{m}$) fundamental of C₅ in IRC+10216 demonstrates this problem.¹² This fundamental is in a spectroscopic region that has low atmospheric transmission because of CO₂ absorption. However, it was observed at Kitt Peak National Observatory in the 2115 to 2195 cm⁻¹ range (using a filter) by taking the ratio of the lunar spectrum (which is intrinsically featureless over this range) to the IRC+10216 spectrum in the same air mass, thus removing the telluric (*i.e.*, atmospheric) spectrum. Space-based and upper atmosphere observatories mitigate the problem of atmospheric absorption. Among the most important of these is the Spitzer Space Telescope (formerly the Space Infrared Telescope or SIRTf) launched in August 2003. At 0.85 m, Spitzer is the largest infrared telescope yet launched into space and is able to take spectroscopic measurements at wavelengths 5-40 μm . Another infrared observatory that is beginning operations is the Stratospheric Observatory for Infrared Astronomy (SOFIA).¹³ This facility observes in the far-infrared (50-200 μm) with a 2.5 m reflecting telescope mounted in a Boeing 747SP. At an altitude of 41,000 ft., the telescope operates above 95% of atmospheric water.¹⁴ Such new telescopes and others that will follow

generate the need for laboratory synthesizing of molecules and the measurement of their infrared spectra.

In summary, there is the possibility that transition metal–carbon clusters may be observed in astrophysical environments such as stars and their outer shells. Space-based telescopes can facilitate the observation of new molecules, but positive identification depends critically on prior laboratory measurements of the spectra of potential species, which is the principal objective of the present research.

1.2 METALCARBOHEDRENES AND THEIR BUILDING BLOCKS

In addition to their potential astrophysical significance, small transition metal–carbon molecules serve as potential building blocks of metallocarbohedrenes and other large transition metal–carbon clusters.

Research on transition-metal carbides was prompted by the discovery of $\text{Ti}_8\text{C}_{12}^+$ metallocarbohedrene (henceforth called “metcar”) by Castleman *et al.*¹⁵ and additional $M_8\text{C}_{12}^+$ ($M = \text{V}, \text{Zr}, \text{Hf}, \text{Nb}, \text{Fe}, \text{Cr}, \text{Mo}$)^{16,17} metcars. The $M_8\text{C}_{12}^+$ molecule exhibits unusually strong stability which Castleman suggested was due to a pentagonal dodecahedron structure [Fig. 1.1(a)] in which each metal atom was bonded to three neighboring carbon atoms. Although a highly symmetric cage-like geometry for these clusters seems to have been established,¹⁸ the metcar structures and formation or growth mechanisms remain the subjects of continuing discussion, and recent reports have predicted structures substantially different from Castleman’s [cf. Fig. 1.2(a) and (c)].^{19,20} In mass spectrometric studies on the formation of metcars, Castleman *et al.*²¹ observed an enhanced abundance of neutral $(\text{MC}_2)_n$ ($n < 7$, $M = \text{Ti}, \text{V}$) clusters,

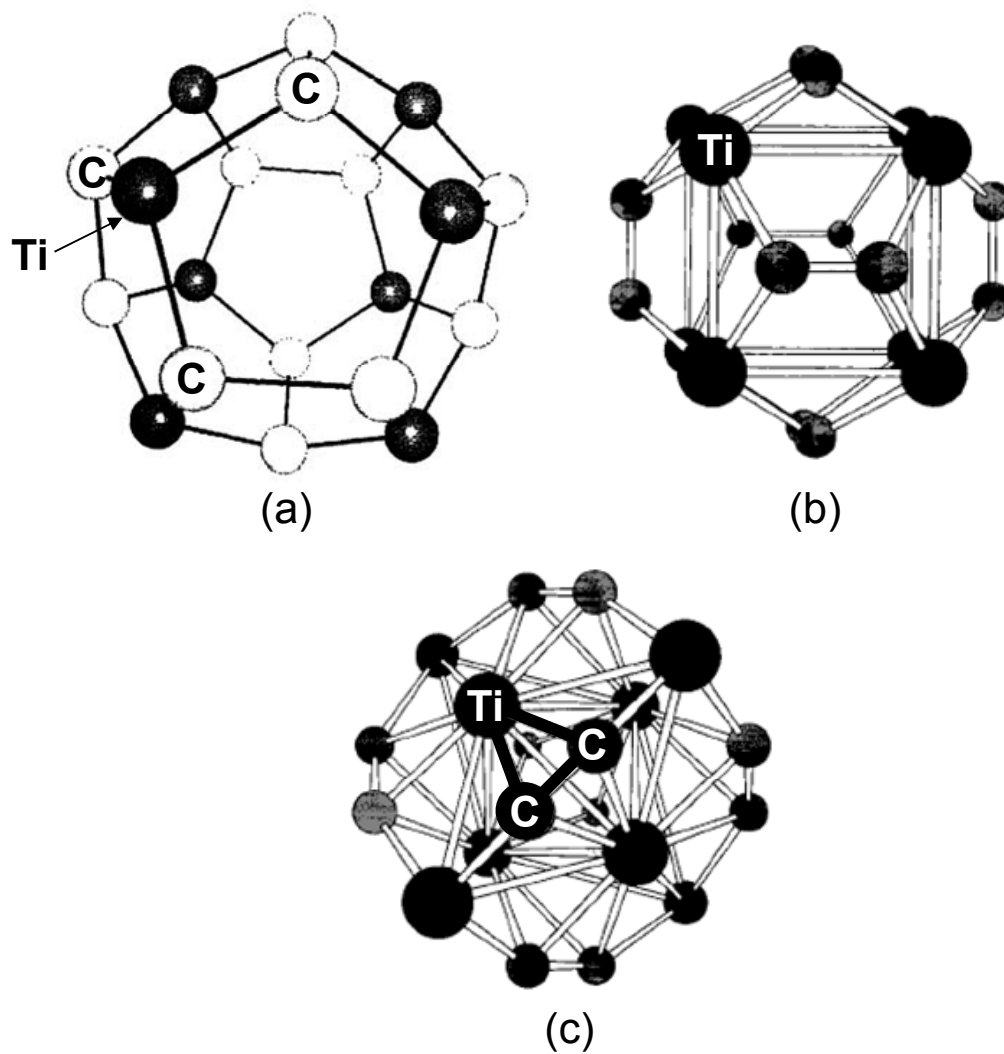


Figure 1.1 The original Ti_8C_{12} metcar structures proposed (a) by Castleman *et al.* (Ref. 15) and (b) modeled by Dance (Ref. 20). Dance's structure in (c) is a better representative of the currently accepted structure and demonstrates the TiC_2 building block which is not observed in (a) or (b).

suggesting that the MC_2 molecule may serve as a type of building block for larger metcar structures.

The structures and growth mechanisms of metcars (neutral and ions) larger than M_8C_{12} have been investigated. The observation of large, multi-cage structures, such as $Zr_{13}C_{22}^+$, $Zr_{14}C_{21}^+$, $Zr_{18}C_{29}^+$, and $Zr_{22}C_{35}^+$, led Wei *et al.*²² to propose that the larger clusters are created by face-sharing M_8C_{12} cages (commonly referred to as “magic numbers” growth). An alternative growth mechanism^{23,24} is that some structures, such as $M_{14}C_{13}^+$ ($M= Ti, V$) and other combinations larger than the $M_8C_{12}^+$ structure where the M/C ratio is approximately 1:1, grow by adding layers to cubic lattice structures or nanocrystals. Theoretical and experimental research investigating the structures of small (MC , MC_2 , M_nC_3 , *etc.*) transition-metal carbide clusters aims to elucidate the nature of the structures and growth mechanisms of these large metcar structures.²⁵

1.3 PREVIOUS RESEARCH

Small transition-metal carbide clusters have been the subject of several experimental and theoretical studies with the interest of determining the structures, spectra, bonding, and other properties of such clusters.

1.3.1 Previous Experimental Results

Previous experimental observations and measurements of small transition-metal carbide clusters are limited exclusively to mass spectrometry or photoelectron spectroscopy experiments. In addition to the original identifications of large metcars, mass spectrometry has been used to observe smaller metcars such as Ni_2C_3 ,²⁶ $Ti_4C_9^+$,²⁷ and various other metcar structures such as

$(MC_2)_n$ ($n < 7$, $M = \text{Ti, V}$) clusters,²¹ among others. Although mass spectrometry provides information on the atomic composition of molecules and possible fragmentation and formation pathways, it does not determine molecular structures or provide information about their infrared spectra.

The few photoelectron (PE) spectroscopy studies of small transition-metal carbides are mostly limited to the first row of transition metals including MC_2 ($M = \text{Sc, V, Cr, Mn, Fe, Co}$) clusters,²⁸ MC_3 ($M = \text{Sc, V, Cr, Mn, Fe, Co, Ni}$) clusters,²⁹ several TiC_n ($n = 2-5$) clusters,³⁰ Co_2C_n ($n = 2, 3$) and V_2C_n ($n = 2-4$) clusters,²⁵ and CrC_n^- and CrC_n ($n = 2-8$) clusters.³¹ Investigations for second-row transition metals include YC_2 ,³² Y_3C_2 (and cation),³³ NbC_n ($n = 2-7$),³⁴ and Nb_2C_3 .³⁵ The results of PE surveys provide more useful information than mass spectrometry studies, for example, vibrational fundamentals and the energy separation between the different electronic states of the molecule. Combined with theoretical studies, they give insight into the nature of the structure and chemical bonding of the molecule.

Unfortunately, results from PE spectroscopy investigations of transition-metal carbides have several problems. First, the measured frequencies typically have uncertainties of $\pm 20 \text{ cm}^{-1}$ or greater (even $\pm 60 \text{ cm}^{-1}$), an accuracy which makes the results from this technique unsuitable for astrophysical use. Second, PE spectroscopy investigations do not necessarily confirm the geometry of the molecule. Nonetheless, PE investigation results provide a useful starting point for further experimental investigations that aim to determine molecular structure and vibrational fundamentals, as is the case with the present research, and are also useful in subsequent theoretical investigations of those molecules.

1.3.2 Previous Theoretical Results

There have been numerous theoretical investigations of small transition-metal carbide clusters. For example, density functional theory (DFT) investigations accompanied the PE results of MC_3 ($M=$ Sc, V, Cr, Mn, Fe, Co, Ni) and TiC_n ($n=2-5$) clusters,^{29,30} although it is common for theoretical investigations to be unaccompanied by experimental results. Most investigations have focused on first-row transition-metal carbide clusters (MC_n , $M=$ metal), for example, ScC_n ($n=1-8$) and VC_n ($n=1-8$).^{36,37} There have been fewer second- and third-row theoretical transition-metal carbide investigations, including yttrium carbides and lanthanum carbides.³⁸

The purpose of the theoretical studies is generally to determine the ground state structures of molecules and the nature of molecular orbitals, chemical bonding, and various other properties (electronic, thermal, *etc.*). Vibrational fundamentals are computed and can aid in interpreting experimental data (*e.g.*, determining frequencies ranges to watch for potential molecular absorptions). Though useful, theoretical investigations alone are not sufficient for determining the properties of a molecule. When multiple structures or isomers for a molecule are very close in energy, experimental investigation is needed to determine the ground state structure, as will be discussed for ScC_3 in Chapter V. Furthermore, theoretical predictions for vibrational fundamentals may differ significantly from their experimentally measured quantities, thus making the predicted fundamentals alone unsuitable for identification of a molecule. The technique of isotopic substitution (§2.3) is a solution to this problem. Isotopic substitutions of the atoms in a molecule (*e.g.*, a ^{13}C for a ^{12}C atom) will produce unique spectral patterns for different molecular structures. Experimentally measured shift patterns then can be compared to isotopic spectra predicted by theoretical models, enabling molecular identification.

1.4 OVERVIEW OF THE DISSERTATION RESEARCH

The previous discussions have outlined the need for research on the structures and vibrational fundamentals of small transition-metal carbide molecules. These reasons include the potential for such clusters to be observed in astrophysical environments and their role as building blocks for larger metal carbide structures, such as the metallocarbohedrenes. Despite their potential applications, there have been few investigations of these clusters. Although they have been the subject of some experimental studies, primarily by PE spectroscopy, the measured vibrational frequencies in these studies have very large uncertainties ($\geq 20 \text{ cm}^{-1}$) that make them unsuitable for astrophysical identifications of the molecules. The structures of the molecules, based on PE spectroscopy results, are not clear. Furthermore, the results of theoretical investigations, though useful to subsequent experimental investigations, do not always provide conclusive results for the ground state structures.

The TCU Molecular Physics Laboratory utilizes the complementary relationship between experimental data and theoretical predictions to unambiguously identify the structures and infrared spectra of molecular clusters. As will be discussed in Chapter II, experimental spectra are obtained using Fourier transform infrared (FTIR) spectroscopy, matrix isolation trapping, and isotopic substitution, and theoretically simulated isotopic spectra are computed for a variety of molecular structures. Molecular and vibrational fundamental identifications are made by comparing the experimental isotopically enriched spectra to theoretically simulated isotopic spectra. This approach has been used previously to identify a variety of molecular clusters in the Molecular Physics Laboratory including carbon clusters (C_n), silicon-carbon clusters (Si_mC_n), germanium-carbon clusters (Ge_mC_n), and silicon-germanium-carbon (SiC_nGe) clusters.

New investigations on transition-metal carbides reported in this work have been motivated by the astrophysical and metcar applications described previously. This research, and the

contemporaneous research by Bates,³⁹ is the first to identify unambiguously the structures and vibrational fundamentals of transition-metal carbides using comparisons of the ^{13}C isotopic shift patterns obtained by FTIR spectroscopy to those predicted by DFT simulations. The first observation of linear NiC_3Ni and the identification of its $\nu_3(\sigma_u)$ asymmetric carbon stretching fundamental is discussed in Chapter III. This investigation of NiC_3Ni is the first experimental and theoretical investigation of the structure and spectrum of the molecule. The investigation of TiC_3 (Chapter IV) confirmed the fanlike structure previously predicted for TiC_3 and measured two new vibrational fundamentals and a tentative third fundamental. The investigation of ScC_3 (Chapter V) confirmed the fanlike structure previously predicted for the molecule and identified its electronic ground state. Three new vibrational fundamentals of ScC_3 were measured. The measured $\nu_3(a_1)$ vibrational fundamentals of TiC_3 and ScC_3 resulting from the present work are significantly more accurate than measurements provided by PE spectroscopy.^{29,30} New experimental techniques used to produce and identify these molecules will be described in Chapter II.

CHAPTER II

TECHNIQUES AND PROCEDURES

This chapter outlines the various experimental procedures, including the technique for trapping molecules in solid Ar during an experiment (§§2.1-2.2); the strategy for identifying molecular species and vibrational fundamentals using ^{13}C isotopic shifts (§2.3); and the method for fabricating sample rods with appropriate ^{13}C enrichment (§2.4) for laser ablation. A modification to the laser evaporation technique⁴⁰ which has proved to be an important innovation in the formation and detection of the transition-metal carbide clusters (*e.g.*, MC_3) that are the focus of this research will be discussed (§2.5). The use of theoretical modeling simulations to aid in the interpretation of isotopic spectra will also be briefly discussed (§2.6).

2.1 MATRIX TRAPPING

As the effects peculiar to trapping molecules in matrix samples will play an important role in later chapters, it is worthwhile to review this experimental technique. Although observation of a molecule in its gas phase ideally yields the most useful spectral information, the trapping of molecules within a solid matrix of rare gas (*e.g.*, Ne, Ar) is a very useful technique for observing molecular spectra and can yield important information concerning molecular structure and bonding. The cryogenic temperatures (~ 10 K) necessary for freezing these gases makes them ideal for studying molecules in their ground electronic and vibrational states. With few exceptions (*e.g.*, OH), rotation of the molecule is prevented by the matrix. Furthermore, trapping chemically reactive molecules in an Ar matrix at ~ 10 K in a $\sim 1:1000$ ratio effectively isolates the molecules from one another and restricts diffusion. Matrix trapping also makes it possible to

build up and maintain a sufficient concentration of reactive molecules for measurement of their electronic or infrared spectra. Spectra of molecular species trapped in solid Ar can be taken efficiently over a broad frequency range, in contrast to the narrow frequency ranges (*e.g.*, $\sim 10\text{-}20\text{ cm}^{-1}$) of the tunable dye lasers used in gas phase studies. An additional advantage to the matrix technique is that trapping the molecular products of laser ablation conserves the isotopic material needed for measuring isotopic shifts. In gas phase techniques, the continuous generation of new molecules is required for the duration of measuring the spectrum.

Although trapping the molecule in a solid may perturb the frequencies of vibrational fundamentals, a comprehensive study by Jacox⁴¹ has shown such perturbations are small. The vibrations of diatomics and polyatomics trapped in Ar and Ne matrices are typically within 2% of their gas phase values. Moreover, a careful comparison^{41,42} of gas phase and matrix frequencies to theoretical predictions shows that the Ar or Ne matrix frequencies are much closer to the gas phase values.

Another result of matrix trapping is that the molecule may be trapped in several different trapping sites within the matrix, resulting in multiple absorption bands separated by a few cm^{-1} corresponding to the same vibrational mode. Annealing the matrix by heating and then quenching to $\sim 10\text{ K}$ will diminish or remove secondary trapping sites so that the absorption corresponding to the lowest energy trapping site is dominant.

2.2 EXPERIMENTAL PROCEDURES

2.2.1 *General Experimental Procedures*

The experimental apparatus in this discussion, including the Ar delivery system (Fig. 2.1) and the sample chamber system (Fig. 2.2), was assembled by Bates.³⁹ Metal-carbon matrix

samples were prepared using a dual laser ablation technique⁴⁰ using two 1064 nm pulsed Nd:YAG lasers (Spectra Physics, Quanta Ray models DHS-2, GCR-11, and INDI) to ablate a pair of transition metal and carbon rods in the sample chamber held at a vacuum of 10^{-7} Torr or better. The low vacuum pressure serves to minimize contaminants (*e.g.*, H₂O, CO₂) in the sample chamber. Argon gas from the delivery system sweeps the vapor produced by laser ablation of the rods toward a gold-plated mirror maintained at ~ 10 K by a closed-cycle helium refrigeration system (ARS, Displex). The Ar condenses when it comes in contact with the mirror's surface, thus trapping the vapor in a matrix.

Following sample deposition, spectra are taken using a Bomem DA3.16 Fourier transform spectrometer. Mid-infrared spectra are taken over a range of approximately 450-4000 cm^{-1} . The spectrometer is equipped with a liquid nitrogen cooled HgCdTe detector (also referred to as MCT) and a KBr beamsplitter. Spectra are recorded with a resolution of 0.2 cm^{-1} . Figure 2.1 is a schematic of the overall experimental apparatus and process, including the laser ablation in the sample deposition chamber (enlarged in Fig. 2.2), the Ar delivery system, and the light path from the Bomem spectrometer for taking infrared spectra.

Following deposition, the matrix is annealed by heating, allowing neighboring clusters to combine to form larger clusters. Annealing the matrix also allows molecules with multiple trapping sites within the matrix to relax to the lowest energy site (§2.1).

2.2.2 *Special Experimental Considerations*

Several parameters in the experimental procedures which affect the production of the matrix sample should be considered. These parameters were optimized to trap predominantly small carbon chains, specifically C₃, and observe $M_n\text{C}_3$ clusters.

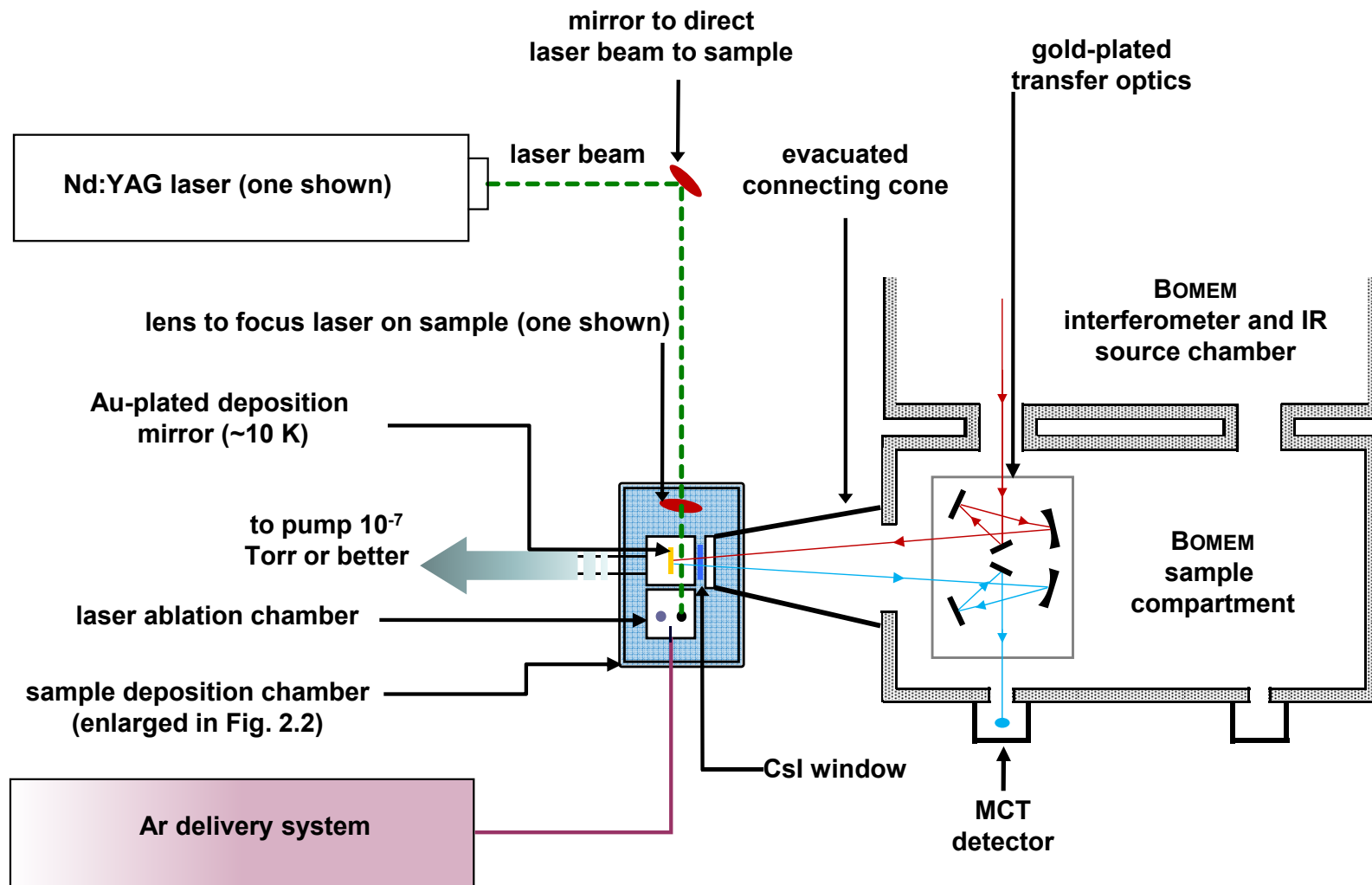


Figure 2.1 General schematic of the experimental apparatus. Only one laser optics system is shown. The sample deposition chamber (shown in the blue, shaded box) is enlarged in Fig. 2.2. The Au mirror here is positioned for scanning by the Bomem (deposition and scanning are not done simultaneously). [Modeled after Bates (Ref. 39)].

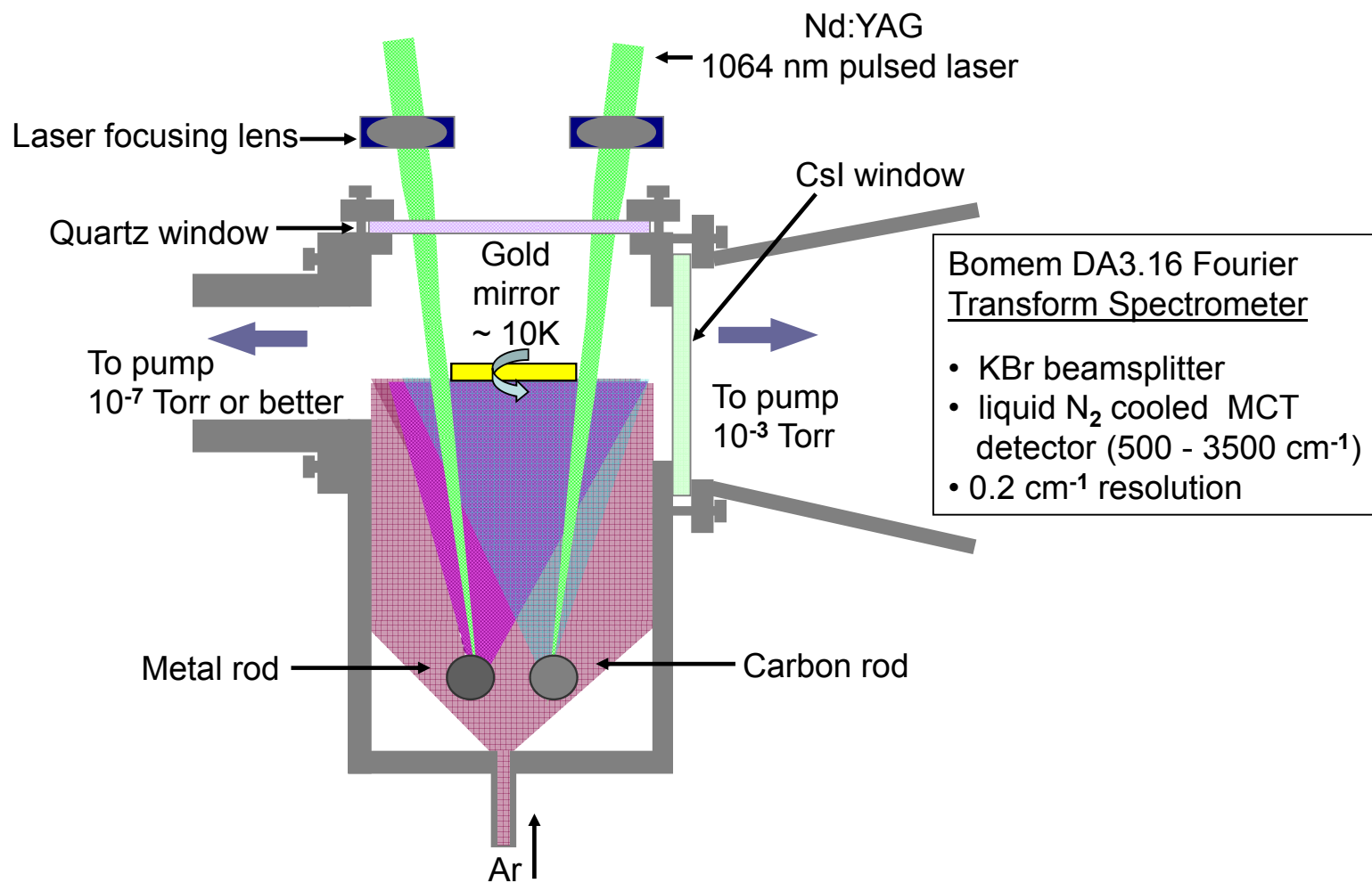


Figure 2.2 Top-view schematic (not to scale) of the sample deposition chamber during deposition. [Modeled after Bates (Ref. 39).]

First, the *Ar flow rate*, a measure of how rapidly Ar flows into the sample chamber during sample deposition, must be optimized for trapping molecules in a matrix. If the flow rate is too great, an excess of Ar will be deposited, resulting in a dilute matrix on the gold mirror. Clusters trapped in such a matrix will have a low concentration. A dilute matrix may make the annealing process less effective as the materials in the matrix are not sufficiently concentrated to allow formation of new molecular species. On the other hand, a flow rate that is too low will not effectively isolate materials in the matrix. Fewer molecular clusters may be observed, and the signal strength in spectra will be weak. Typically, the Ar flow rate that is used causes a ~ 1 Torr/min pressure decrease in the Ar delivery system.

Second, the *laser powers* used on the carbon and metal rods, which determines the evaporation rate of the surfaces, are very important. The laser powers used on various carbon rods depends on their manufacture, the ^{13}C enrichment (see §2.4.1), and also on whether larger or smaller molecular clusters should be produced. Commercially manufactured (ESPI) graphite (^{12}C) rods are the most durable, and can be ablated at higher power ($\sim 2\text{-}3$ W). For lab-manufactured carbon rods enriched with ^{13}C , the laser power that is needed will decrease significantly below the power used for graphite rods to between 0.1 and 1 W. (During deposition the laser power and laser focus are factors that must be considered simultaneously. The “low-power” laser ablation technique discussed in §2.5 takes this into consideration.) The laser powers used to ablate metals rods vary with respect to the properties of the rod and are determined by experiment. The evaporation rate of the metal should be such that atoms, and not metal clusters or microcrystals, result from ablation. Too low an evaporation power on the metal rod will produce too little metal to react with the carbon clusters, thus yielding insufficient metal carbide clusters for observation. However, too high an evaporation rate for the metal will likely

produce large clusters of metal atoms instead of the single atoms required to make M_nC_3 metal-carbon molecules.

Third, the *laser focus* refers to how tight the laser beam is focused on the rod. A “loose” focus (≥ 2 mm diameter) spreads the radiation over a larger surface of the rod, and a “tight” focus (~ 1 mm diameter) focuses the beam on a smaller surface. A tight focus is used on the metal rods. The laser focus and the laser power must be considered simultaneously, thus making the power per unit area a relevant factor, particularly when ablating ^{13}C -enriched carbon rods. Carbon rods that are not baked (so called “soft” rods) require lower powers to avoid rapid degradation of the surface, and so either a low laser power with a tight focus or a higher power with a looser focus is used.

2.3 ISOTOPIC SUBSTITUTION

Carbon-13 isotopic substitution is an essential technique for the unambiguous identification of a new molecular species. The substitution of ^{13}C for ^{12}C atoms in a molecule will result in new absorptions (isotopic shifts) appearing to the low energy side of the vibrational fundamental of the molecule containing only ^{12}C . Carbon-13 enriched rods are prepared (§2.4.1) from thoroughly mixed ^{12}C and ^{13}C powders to ensure random substitutions of ^{13}C at each site in the molecule (*i.e.*, each ^{12}C atom in the molecule has an equal probability of being replaced by a ^{13}C). Isotopic substitution is particularly useful because it can reveal important clues to the symmetry and structure (and, hence, possibly the identity) of a molecule even before theoretical calculations are carried out.

A simple example is the linear C_3 molecule shown in Fig. 2.3(a). By symmetry, the C atoms at the ends of the molecule are equivalent on a 180° rotation about an axis perpendicular to the molecular axis; these C atoms at equivalent sites are labeled C_α . The center C atom is unique

and is labeled C_β . During deposition, any of the three $^{13}\text{C}-^{12}\text{C}-^{12}\text{C}$, $^{12}\text{C}-^{12}\text{C}-^{13}\text{C}$, and $^{12}\text{C}-^{13}\text{C}-^{12}\text{C}$ single ^{13}C -substituted isotopomers has an equal probability of being made. As shown in Fig. 2.3(b), two of the isotopomers, $^{13}\text{C}-^{12}\text{C}-^{12}\text{C}$ and $^{12}\text{C}-^{12}\text{C}-^{13}\text{C}$, are equivalent for ^{13}C (shaded disc) substitution at the C_α sites. In contrast, the $^{12}\text{C}-^{13}\text{C}-^{12}\text{C}$ isotopomer is unique, as shown in Fig. 2.3(c). Using $\sim 10\%$ ^{13}C enrichment, most of the C_3 deposited will be $^{12}\text{C}_3$, but each single ^{13}C -substituted isotopomer will contribute an isotopic shift with $\sim 10\%$ the intensity of the $^{12}\text{C}_3$ absorption. Because of the molecule's symmetry, the two equivalent isotopomers (^{13}C substitution for either C_α) will thus contribute to a single isotopic shift with $\sim 20\%$ of the intensity of the $^{12}\text{C}_3$ absorption, and the unique isotopomer (^{13}C substitution for C_β) will contribute one additional shift with $\sim 10\%$ of the intensity of the $^{12}\text{C}_3$ absorption. Fig. 2.4 shows the $\nu_3(\sigma_u)$ asymmetric carbon stretch of linear $^{12}\text{C}_3$ is at 2038.9 cm^{-1} ($\sim 4.9\text{ }\mu\text{m}$). The 2:1 intensity ratio of the isotopic shifts at 2026.4 and 1987.5 cm^{-1} indicates that these shifts result from ^{13}C substitutions at the equivalent and unique carbon sites, respectively. Additionally, absorptions are observed for the doubly substituted isotopomers at 1974.5 ($^{13}\text{C}-^{13}\text{C}-^{12}\text{C}$) and 2012.9 ($^{13}\text{C}-^{12}\text{C}-^{13}\text{C}$) cm^{-1} . The fully ^{13}C -substituted isotopomer ($^{13}\text{C}_3$) is observed at 1960.3 cm^{-1} .

Figure 2.5 illustrates the carbon sites for some of the more commonly predicted MC_3 structures. The addition of a transition metal M to the end of a C_3 chain [Fig. 2.5(a)] results in three unique carbon sites. The fanlike [Fig. 2.5(b)] and kite-shaped [Fig. 2.5(c)] MC_3 structures have two equivalent carbon sites (C_α) and one unique carbon site (C_β). The principal axis of symmetry for each structure is represented by an arrow.

Finally, naturally occurring enrichment of metal isotopes may enable the observation of isotopic shifts resulting from substitution of different metal isotopes at the molecule's metal site(s). Such metal isotopic shifts will only be observed for vibrational modes in which the metal atom significantly participates in the vibration [e.g., Fig. 4.5(c) and 4.5(f)].

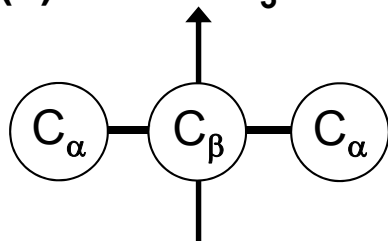
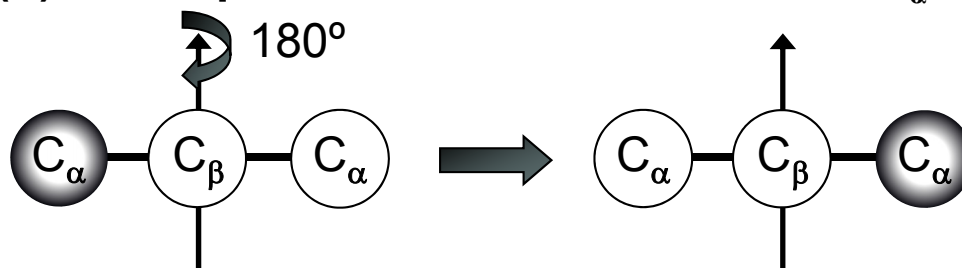
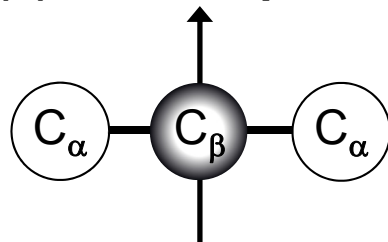
(a) Linear C₃ sites**(b) Two equivalent ¹³C substitutions at C_α:****(c) One unique ¹³C substitution at C_β:**

Figure 2.3 Carbon sites in C₃. C_α denotes equivalent C sites and C_β denotes the unique site. Shaded discs represent single ¹³C substitutions in (b) the two equivalent isotopomers and (c) the unique isotopomer.

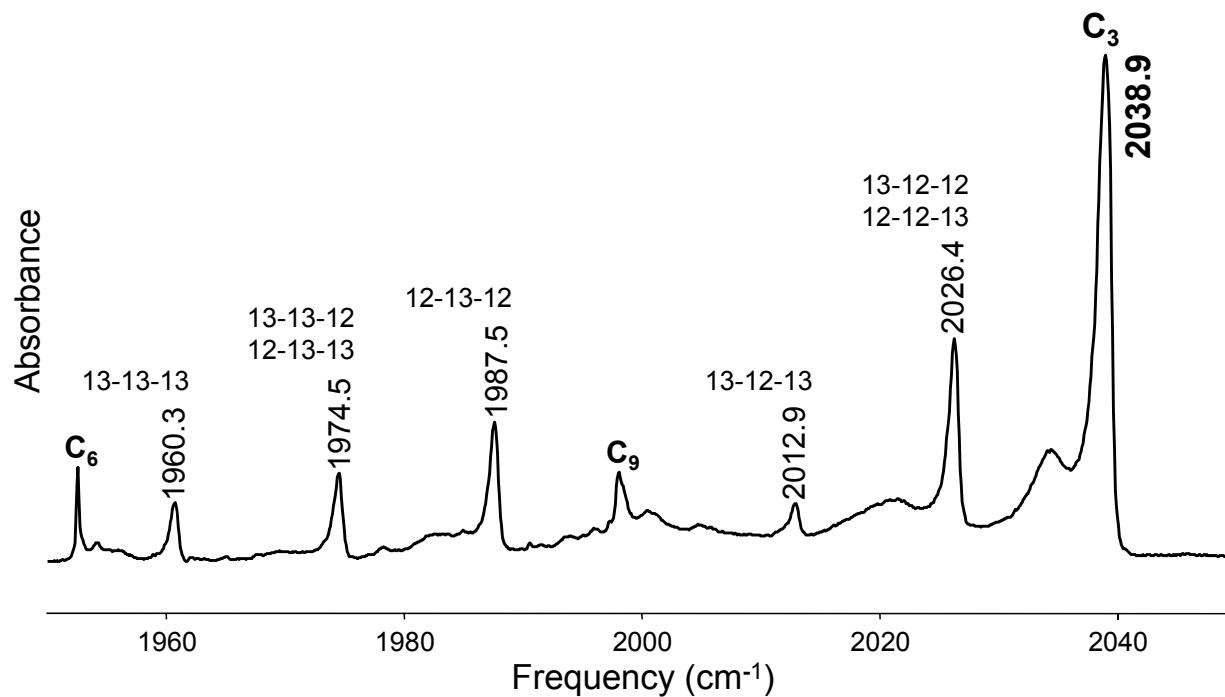


Figure 2.4 The isotopic shift spectrum of the $\nu_3(\sigma_u)$ fundamental of linear C_3 . The isotopomers corresponding to the isotopic shifts are labeled in the C_α - C_β - C_α convention of Fig. 2.3.

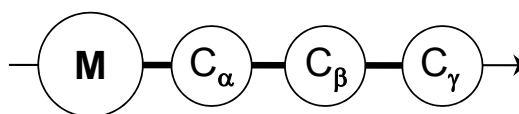
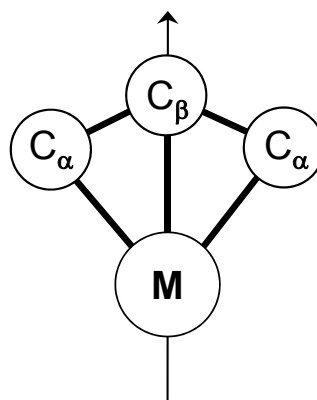
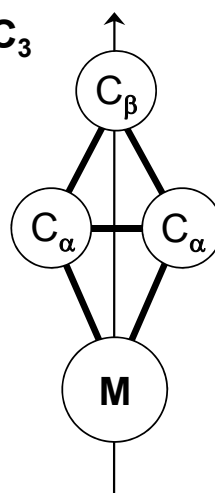
(a) Linear MC_3 **(b) Fanlike MC_3** **(c) Kite-shaped MC_3** 

Figure 2.5 Commonly predicted structures for MC_3 transition-metal carbide clusters. Equivalent and unique carbon sites are labeled in the fashion of Fig. 2.3. The arrows represent the principal axis of symmetry for each geometry.

2.4 SAMPLE ROD PREPARATION

2.4.1 Carbon Sample Rods

Two types of carbon rods are used in various experiments. The first is a commercially manufactured (ESPI, Aeromet) ^{12}C rod used in early experiments to identify potential metal-carbon absorptions. Later, lab-fabricated rods composed of ^{12}C powder (Alfa Aesar, 99.9995% purity) enriched with ^{13}C powder (Isotec, 99.3% purity) are used to produce isotopic shifts. The two powders are thoroughly mixed and pressed into rods at pressures of $\sim 4 \times 10^5$ kPa. The lab-fabricated rods measure ~ 0.9 cm in diameter and ~ 1.4 cm in length. Lab-fabricated carbon rods may be baked overnight at ~ 2100 °C in a vacuum of 10^{-6} Torr or better to evaporate O_2 and CO_2 impurities. Baking for approximately one month allows sintering of the ^{12}C and ^{13}C materials, thus improving the rod's integrity for use over several experiments.⁴³ Since this baking process takes such a long time, unbaked (“soft”) ^{13}C -enriched rods may be used.

Unfortunately, the integrity of the soft rods is rather limited. Low laser power must be used during deposition to ensure that the rod is not destroyed. Typically, soft rods are only good for one experiment; however, if the rod is long enough, it can be inverted so that one rod may be used for two experiments. This is in stark contrast to the 15+ experiments that can be made using just one baked rod (depending on laser power used). Finally, as the soft rods are evaporated at low power to maximize their integrity, they are useful for producing smaller carbon chains (*e.g.*, C_3 , C_4 , C_5). Long carbon chains require higher evaporation rates, and the laser powers needed to obtain the higher evaporation rates would destroy the rod. However, when soft rods are ablated using the “low-power” laser technique described in §2.5, the experiment is found to be optimized for producing molecules bearing three carbon atoms.

2.4.2 *Metal Sample Rods*

Metal sample rods are usually purchased from commercial manufacturers; ESPICorp, Inc. is the usual supplier. However, should the commercially made rods prove unsuitable, as they may be strong sources of contaminants such as CO or CO₂, there are options for manufacturing metal rods in the laboratory.

Metal sample rods may be pressed from commercially available metal powders (Alfa Aesar) using the same press and pressures as are used for carbon rods. A new procedure, first used to prepare a pure nickel rod (§3.2), bakes the metal powder in the furnace just below melting point overnight. This procedure significantly removed CO and CO₂ contaminants found in commercially available nickel rods and powders and facilitated the observation of NiC₃Ni. A final procedure that may be utilized, and will be reviewed in more detail in §6.2.1, is a sintering technique for creating sample rods composed of various ratios of ¹²C, ¹³C, and metal.

2.5 THE “LOW-POWER” EVAPORATION TECHNIQUE

A recent modification of the laser evaporation technique has proven critical for the observation of small metal carbide molecules (*i.e.*, MC₃ and M₂C₃). In contrast to previous experiments which used baked rods ablated at 1.4+ W to produce ¹³C isotopic shifts, the “low-power” laser ablation technique involves ablating an unbaked (soft) carbon rod, prepared using the procedures of §2.4.1, at low laser powers (typically <1 W) to maximize the production of small carbon clusters, specifically C₃ clusters. This low-power technique was developed over several experiments – specifically, experiments leading up to the observation of TiC₃ (Chapter IV) – in which the power of the laser ablating the carbon rod was reduced by small increments.

The laser was fired at ~ 1.2 W for initial experiments. Subsequent experiments reduced the power in intervals of 0.2 W such that, after multiple experiments, a laser power of 0.6-0.8 W provided an optimum evaporation rate of rods with $\sim 20\%$ ^{13}C enrichment.

There were several important observations made during the development of the low-power evaporation technique. As the laser power was reduced, absorptions from smaller carbon chains (*e.g.*, C_3 , C_4 , C_5 , and C_6) began to dominate the spectra as the absorptions from larger chains (*e.g.*, C_8 , C_9 , C_{10}) became less intense. Spectra were dominated by the $\nu_3(\sigma_u)$ vibration of C_3 at 2038.9 cm^{-1} , although C_4 , C_6 , C_7 , and, to a lesser extent, C_9 vibrations were also prominent. The intensity of the latter three chains might be attributed to the combination of two or three C_3 chains to form C_6 and C_9 , respectively, and C_3 and C_4 chains (or two C_3 chains and a C monomer) to form C_7 . Those absorptions identified as potential metal carbide species gained intensity as laser power on the carbon rod was decreased. Since the most noticeable difference between the low-power and higher power evaporation rates was the significant increase of C_3 production, it was likely that the candidate metal carbide responsible for the absorptions contained only three carbon atoms. With lower evaporation rates, deposition times for the preparation of matrix samples increased from less than 30 min to as high as 120 min, thus allowing for longer depositions of metal carbon clusters.

In general, the low-power technique combines the laser focusing lens and the laser power to ablate the carbon rod with a low energy per unit area, typically $<1\text{ W/mm}^2$, thus decreasing the depth the laser penetrates into the rod and preserving the carbon rod's integrity over the course of the experiment. It should be noted that the low-power ablation technique is highly dependent on the position of the lens focusing the laser on the carbon rod. If the lens is positioned such that there is a very tight focus on the rod, the laser power will need to be decreased. Once the lens

position is established, the laser power may be decreased to even lower levels to ablate rods with higher ^{13}C -enrichment.

There are several advantages to using of the low-power technique. First, the high yield of C_3 makes this technique very practical for producing $M_n\text{C}_3$ species and thus serves as an effective method for restricting the types of new clusters that may be observed (*i.e.*, small metal carbides, specifically $M_n\text{C}_3$ clusters). Second, very long deposition times (~ 2 hours) allow for greater production of molecular clusters. This is particularly useful for molecules with low-intensity absorptions such as the cyclic (fanlike) structures. Third, spectra that are recorded when this approach is used can be very clean and uncluttered, particularly in the $1800\text{-}2100\text{ cm}^{-1}$ range in which many high intensity carbon chain absorptions are found. Lower production of longer clusters will result in fewer features in such regions.

To date, the low-power technique has been used in the observation of several transition-metal carbide clusters including NiC_3Ni , TiC_3 , and ScC_3 discussed in following chapters; CrC_3 ,⁴⁴ CoC_3 ,⁴⁵ and metal-carbides AlC_3Al and AlC_3 (Ref. 46) observed by Bates *et al.*; and the $\nu_1(\sigma)$ fundamental of GeC_3 by Gonzalez *et al.*⁴⁷ In future research it will serve as a good first step in trying to identify new molecular species and vibrational fundamentals.

2.6 THEORETICAL SIMULATIONS

Theoretical simulations provide a complementary set of data to experimental observations that help to enable the unambiguous identification of a molecular species and its vibrational fundamentals. Most previous investigations do not report the calculated fundamentals, much less the intensities of the fundamentals, and so new simulations of clusters are necessary to calculate the fundamentals, their intensities, and the isotopic shift patterns. When the molecular species has not been previously investigated by theorists, analysis of the experimentally observed

isotopic shift pattern can suggest a candidate molecule's possible symmetry and species. Theoretical simulations can then be undertaken to model different candidate clusters, including their structures, fundamentals, and isotopic shift patterns. Simulations in this work have used DFT in the GAUSSIAN 03 program suite.⁴⁸ The parameters for the modeling for all the molecular clusters are discussed in their respective chapters.

CHAPTER III

FTIR OBSERVATION OF THE $\nu_3(\sigma_u)$ VIBRATIONAL FUNDAMENTAL OF LINEAR NiC₃Ni IN SOLID Ar

3.1 INTRODUCTION AND PREVIOUS RESEARCH

Molecules bearing first-row transition metals are expected to be observed in astrophysical sources⁴⁹ and may provide insight for understanding the formation mechanisms and abundances of the “iron-peak” transition metals (Cr, Mn, Fe, Co, Ni, Cu, Zn) in asymptotic giant branch stars.⁵⁰ However, the paucity of experimentally observed frequencies for such molecules precludes astrophysical identifications. Some nickel bearing species have been studied using microwave and electronic spectroscopy, *e.g.*, the rotational spectrum of NiCl in its $^2\Pi_{3/2}$ ground electronic state has been experimentally recorded by Yamazaki *et al.*⁴⁹ and the millimeter wave spectrum of NiC, a species potentially observable in circumstellar shells of carbon rich stars such as IRC+10216, has been studied by Brewster and Ziurys.⁵⁰ Lambert and Mallia reported the observation of NiH in sunspot spectra using electronic spectroscopy⁵¹ and ^{58}Ni and ^{60}Ni have both been reported in the solar photosphere.⁵²

Small transition-metal carbide clusters are also of interest because of possible applications to understanding the formation and bonding of metallocarbohedrenes (metcars) and other large metal-carbon structures. The metal dicarbide MC_2 clusters have been studied extensively as potential metcar building blocks.⁵³ Cage-like metallocarbohedrenes, M_8C_{12} ($M = \text{Ti, V, Zr, Hf}$), were first produced by evaporating metal targets with a pulsed laser in a hydrocarbon environment by Castleman *et al.*^{15,16} Tono *et al.*²⁵ have pointed out that early transition metals (*e.g.*, Ti, V) more readily react in the hydrocarbon plasma to form metal carbides than do late

transition metals (*e.g.*, Co, Ni). More drastic methods, such as laser ablation of composite metal-carbon samples, are needed to form late transition-metal carbide clusters, although even such extreme methods do not produce structures as complex as metallocarbohedrenes (see Ref. 25 and references therein). In mass spectrometric studies Reddic and Duncan²⁶ produced various late-transition-metal carbides (*e.g.*, NiC₃, Ni₂C₃, Ni₂C₆, Ni₂C₁₁) using laser evaporation of a composite nickel-carbon target. Their spectra were dominated by the Ni monomer and NiC₃, although Ni₂C₃ was present. Wang and Li reported the observation of NiC₃ in a combined PE spectroscopy and DFT investigation of various MC₂ and MC₃ clusters.^{28,29} A vibrational frequency at 480±60 cm⁻¹ was reported for NiC₃, though a structure for the molecule was not proposed. No data were reported for NiC₂. With the exception of the mass spectroscopy study by Reddic and Duncan,²⁶ no other experimental or theoretical investigations of the NiC₃Ni cluster have been reported.

There have been further theoretical investigations of nickel-carbon clusters. Andriotis *et al.*⁵⁴ have reported DFT and coupled-cluster calculations for the ground state structures of NiC_n (*n*=3,4) and Ni₂C_n (*n*=4-6) clusters. Subsequently, Rey *et al.*⁵⁵ reported DFT calculations for several nickel carbide clusters including NiC_n (*n*=1-6) and Ni₂C_n (*n*=4-6). The two investigations obtained conflicting results for the structures of NiC₃ and NiC₄. The kite-shaped structure initially predicted for NiC₃ by Andriotis *et al.*⁵⁴ and the linear NiC₃ structure reported by Rey *et al.*⁵⁵ are shown in Fig. 3.1(a) and (b), respectively. Later DFT investigations of the NiC₃ cluster by Froudakis *et al.*⁵⁶ and Longo *et al.*⁵⁷ reached a consensus that NiC₃ should have a cyclic (fanlike) structure [Fig. 3.1(c)] with an energetically close-lying linear structure. Longo and Gallego⁵⁸ reported the results of a DFT investigation of the structures of Ni₂C_n (*n*=7-11) clusters. No theoretical investigation has reported results for Ni₂C₃. Furthermore, there was no agreement on the most stable structures for the Ni₂C_n clusters studied. Andriotis *et al.*⁵⁴ reported

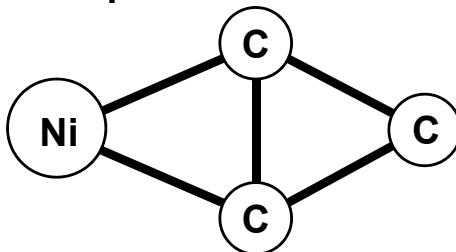
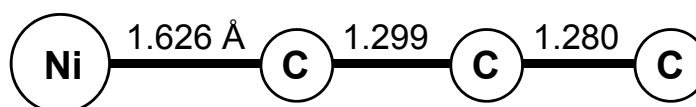
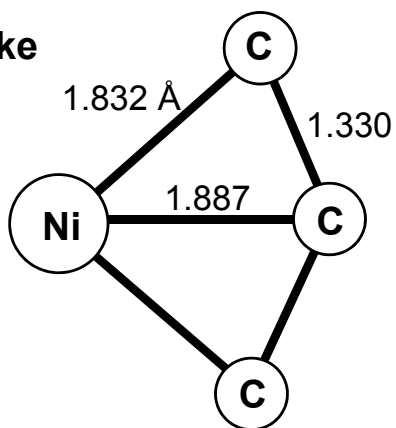
(a) Kite-shaped**(b) Linear****(c) Fanlike**

Figure 3.1 The (a) kite-shaped, (b) linear, and (c) fanlike geometries modeled for NiC_3 . The fanlike is predicted to be the ground state structure. Bond lengths are in angstroms (\AA) (linear and fanlike only). [(a) adapted from Longo *et al.* (Ref. 57); (b)-(c) adapted from Froudakis *et al.* (Ref. 56).]

three-dimension cage-like structures for Ni_2C_n ($n=4-6$) whereas Rey *et al.*⁵⁵ reported linear structures for Ni_2C_4 and Ni_2C_5 and ringlike structures for Ni_2C_6 and Ni_2C_7 .

Here is presented the first experimental and theoretical investigation of the structure and infrared spectrum of linear NiC_3Ni . A comparison of experimentally measured and DFT predicted ^{13}C isotopic shifts has enabled assignment of the $\nu_3(\sigma_u)=1950.8\text{ cm}^{-1}$ asymmetric carbon stretching fundamental.

3.2 EXPERIMENTAL PROCEDURES

NiC_3Ni was produced by the simultaneous evaporation of a nickel rod and a carbon rod using two pulsed ($\sim 10\text{ Hz}$), tightly focused 1064 nm Nd:YAG lasers (Spectra Physics). During evaporation the rods were continuously rotated and translated to ensure uniform evaporation of the rods' surfaces. The resulting vapor was co-deposited with Ar (Matheson, 99.9995% purity) onto the surface of a gold-plated mirror maintained at $\sim 10\text{ K}$ by a closed cycle refrigeration system (ARS, Displex).

To obtain isotopic shifts, carbon rods were prepared from mixtures of ^{12}C (Alfa Aesar, 99.9995% purity) and ^{13}C (Isotec, 99% purity) powders to produce isotopic shift spectra with effective enrichments of $\sim 12\%$ ("low") and $\sim 50\%$ ("medium") ^{13}C . Laser powers of ~ 0.2 and $\sim 0.1\text{ W}$ were used for the low and medium enrichment carbon rods, respectively. Deposition times were typically $\sim 25-30\text{ min}$ for low-enrichment experiments and $\sim 25-40\text{ min}$ for medium-enrichment experiments in a vacuum of 10^{-7} Torr . A nickel rod was fabricated by heating nickel powder (Alfa Aesar, $\sim 99.8\%$ purity) enclosed within a graphite cell in a vacuum of $\sim 10^{-7}\text{ Torr}$ pressure for $\sim 12-18$ hours. Heating at $\sim 1200\text{ }^\circ\text{C}$ removed most contaminants (*e.g.*, CO , CO_2) and sintered the powder into a solid rod $\sim 1\text{ cm}$ in length and $\sim 0.8\text{ cm}$ in diameter.

Absorption spectra in the range of 500-3500 cm^{-1} were recorded with a resolution of $\pm 0.2 \text{ cm}^{-1}$ using a Bomem DA3.16 Fourier transform spectrometer equipped with a KBr beamsplitter and liquid nitrogen cooled HgCdTe detector. Following deposition, the matrix sample was annealed for ~ 5 min at specified temperatures between 15 K and 30 K and immediately quenched to ~ 10 K. Annealing enables diffusion and recombination of neighboring clusters to form larger clusters and helps to sharpen absorption bands. Since there was no synchronization between the firing of the two lasers during deposition, gas phase reaction between Ni and C_3 is probably minimal and reaction on the matrix surface more likely. Subsequent annealing at ~ 20 -25 K sharpened the bands but the signal of the molecule's isotopic spectrum was not increased significantly.

3.3 EXPERIMENTAL RESULTS AND ANALYSIS

Potential nickel carbide absorptions in the 500-3500 cm^{-1} range were found by comparing the spectra produced by the simultaneous ablation of a nickel and a ^{12}C rod to spectra produced by a single ^{12}C rod (see Fig. 3.2). An unidentified absorption potentially belonging to a nickel carbide species was observed at 1950.8 cm^{-1} [Fig. 3.2(a)].

The measurement of isotopic shifts is a decisive test for the identification of molecular species and their vibrational fundamentals. To facilitate the observation of ^{13}C shifts, carbon rods with the low and medium ^{13}C enrichments discussed earlier were evaporated simultaneously with the nickel rod. The relatively low laser powers (~ 0.1 - 0.2 W) used to evaporate the ^{13}C -enriched rods produce predominantly smaller carbon chains such as C_3 and C_3^- , C_4 , C_5 , and C_6 and C_6^- . During deposition spectra were dominated by the $\nu_3(\sigma_u)$ vibrational fundamental of C_3 at 2038.9 cm^{-1} . It was thus expected that using the low laser evaporation rates would produce predominantly smaller nickel carbide clusters. Previous research by this lab indicates that

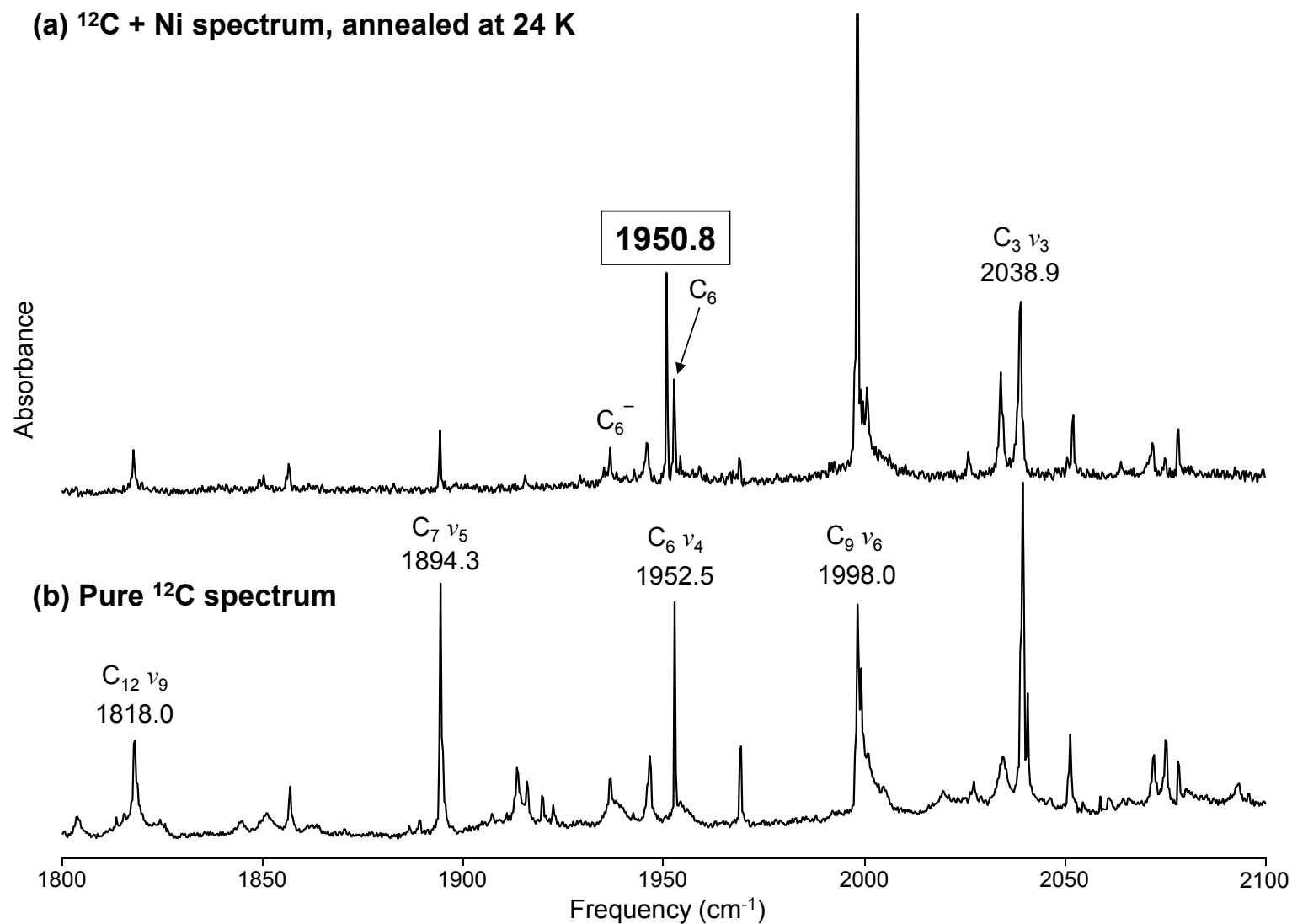


Figure 3.2 A survey spectrum in the $1800\text{-}2100 \text{ cm}^{-1}$ range showing the spectra produced (a) from the ablation of nickel and graphite rods and (b) from graphite ablation only. Vibrational fundamentals of known carbon bands are labeled. The intense absorption at 1950.8 cm^{-1} is unique to (a) which suggests it belongs to a nickel-carbon cluster.

monomers predominantly result from the laser ablation of the metal rods as has been observed for the transition-metal carbides TiC_3 (Chapter IV), CrC_3 ,⁴⁴ CoC_3 ,⁴⁵ the group IV molecules^{59,60} GeC_3Ge , GeC_5Ge , and the linear aluminum carbides⁴⁶ AlC_3 and AlC_3Al .

Figure 3.3(a) shows the spectrum in the 1860-1960 cm^{-1} region for $\sim 12\%$ ^{13}C enrichment. The spectrum was produced after ~ 30 min of deposition followed by annealing at 25 K for 5 min and then quenching to 10 K. Isotopic shifts of the band at 1950.8 cm^{-1} are found at 1938.1 and 1903.2 cm^{-1} . The 1938.1 cm^{-1} isotopic shift band, which is somewhat overlapped on its low frequency side by a band of C_6^- at 1936.4 cm^{-1} , has an intensity approximately twice that of the 1903.2 cm^{-1} band, which is $\sim 12\%$ the intensity of the band at 1950.8 cm^{-1} . This result suggests a molecule that has three carbon atoms, with one unique C site and two equivalent C sites. This vibration could therefore result from the asymmetric carbon-carbon stretching mode of a Ni-bearing centrosymmetric molecule containing a linear C_3 chain. The simplest of these, linear NiC_3Ni , may thus be the carrier. The spectrum in Fig. 3.3(a) also exhibits vibrational fundamentals and isotopic shifts for the $\nu_4(\sigma_u)=1952.5$ cm^{-1} fundamental of C_6 , the $\nu_4(\sigma_u)=1936.4$ cm^{-1} fundamental of C_6^- (see Ref. 45), and the $\nu_5(\sigma_u)=1894.3$ cm^{-1} fundamental of C_7 . There are overlapping isotopic shifts for C_6 at 1929.1 cm^{-1} and C_6^- at 1928.6 and 1929.2 cm^{-1} . Another, unidentified band at 1898.2 cm^{-1} is present, but it behaves independently of the 1950.8 cm^{-1} band and is therefore not a candidate for an isotopic shift [*cf.* Fig. 3.3(b)]. Several other possible isotopic shifts from the 1950.8 cm^{-1} band are observed at ~ 1924.5 , 1889.7, and 1875.5 cm^{-1} . If it is assumed that the nickel atoms do not participate significantly in the vibration, the frequency for the fully ^{13}C -substituted species of linear NiC_3Ni can be estimated using the formula $\sqrt{12/13} \times 1950.8$ $\text{cm}^{-1}=1874.3$ cm^{-1} . This result is very close to an absorption observed at 1875.5 cm^{-1} thus making it a likely candidate for the fully ^{13}C -substituted isotopic shift.

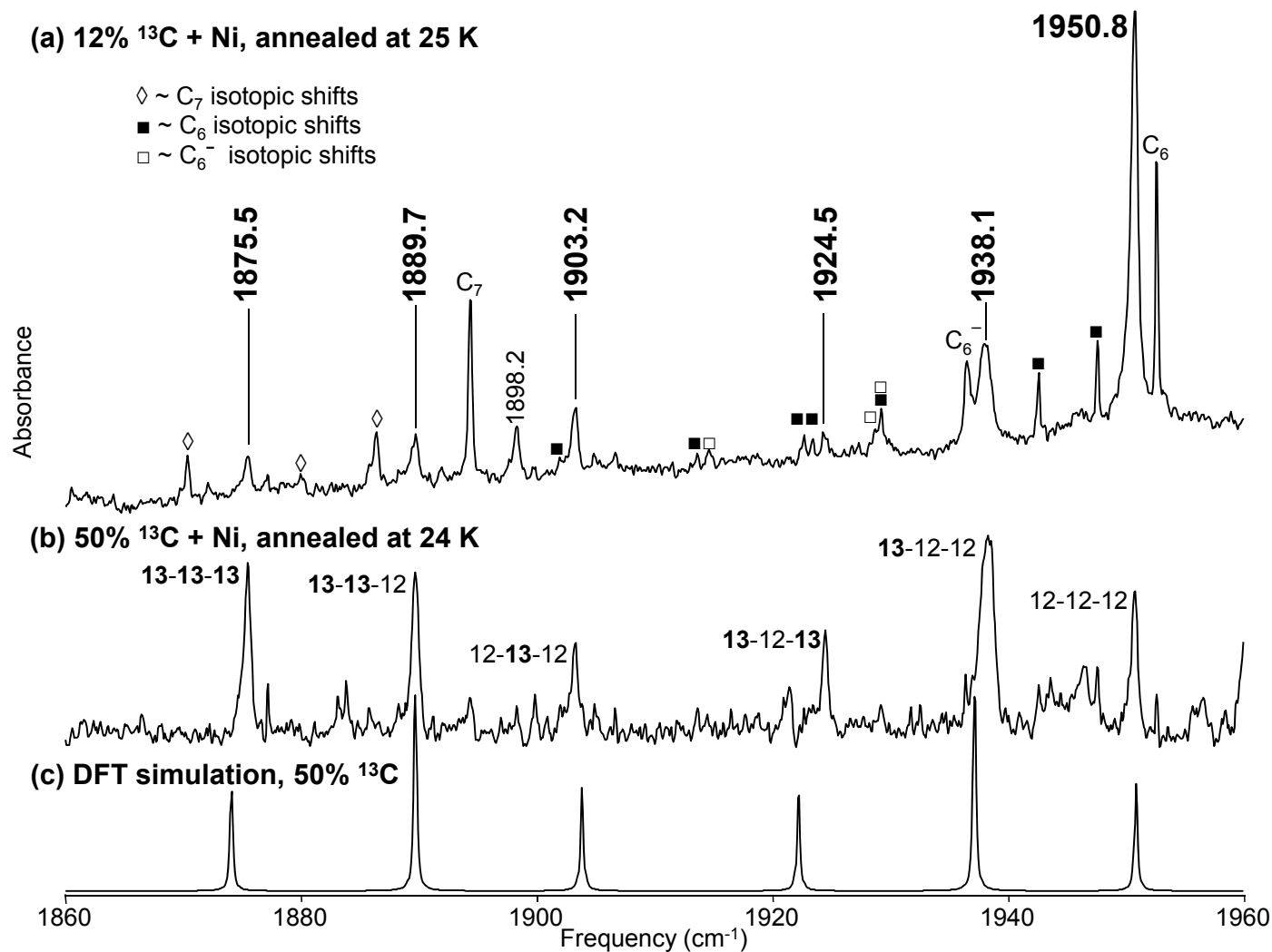


Figure 3.3 The ^{13}C isotopic substituted spectra in the $1860\text{-}1960\text{ cm}^{-1}$ range showing (a) the spectrum with $\sim 12\%$ ^{13}C enrichment and (b) $\sim 50\%$ ^{13}C enrichment. Isotopomers are assigned in (b) following the convention of Table 3.2 and Fig. 3.4. Spectrum (c) shows the 50% ^{13}C -enriched DFT calculated isotopic spectrum for linear $\text{Ni}^{13}\text{C}_3\text{Ni}$ off 1950.8 cm^{-1} . All isotopic shifts, including the full $\text{Ni}^{13}\text{C}_3\text{Ni}$ isotopomer, are scaled off the fundamental.

Figure 3.3(b) shows the isotopic spectrum with ~50% ^{13}C enrichment following annealing at 24 K for ~5 min. All of the absorptions in Fig. 3.3(a) proposed as isotopic shifts are easily visible in the spectrum of Fig. 3.3(b). The isotopic shift bands do not exhibit the relative intensities expected for complete randomization of ^{13}C because the evaporation characteristics of the amorphous ^{13}C and the more crystalline ^{12}C are somewhat different. However, the relative intensities of the isotopomer bands are very similar to those observed for the $\nu_3(\sigma_u)$ vibrational mode of C_3 (not shown), consistent with the idea that the 1950.8 cm^{-1} absorption is a vibrational fundamental of centrosymmetric NiC_3Ni . The observed isotopic shifts are labeled in Fig. 3.3(b) where 12 and 13 represent a ^{12}C and ^{13}C substitution, respectively, at the carbon sites of the linear molecule. For brevity, the terminal Ni atoms have been omitted from the C_3 units. A comparison of the observed isotopic shifts to DFT calculated isotopic shifts is necessary to confirm the identification of the molecular species, the vibrational fundamentals, and the electronic state.

3.4 THEORETICAL MODELING AND ANALYSIS

As discussed previously, earlier theoretical investigations^{54,55} of small nickel carbide clusters did not report on Ni_2C_3 ; however, the experimental results already discussed provide evidence that the 1950.8 cm^{-1} absorption belongs to linear NiC_3Ni . DFT calculations were performed with the GAUSSIAN 03 suite⁴⁸ using the B3LYP functional (Becke 3-parameter exchange functional⁶¹ and Lee Yang Parr correlation function⁶²) and employing the 6-311G* basis set. NiC_3Ni in singlet, triplet, and quintet electronic states was considered.

When the molecule is constrained to be linear ($D_{\infty h}$ symmetry) the singlet ($^1\Sigma_g^+$) electronic state has the lowest energy and is energetically well separated from a triplet state ~23 kcal/mol higher and a quintet state ~56 kcal/mol above the singlet state. However, none of the critical

points obtained for the linear geometry is a minimum. The triplet state has imaginary bending frequencies at $393i$, $160i$, $33i$ cm^{-1} and the quintet, at $1235i$ and $593i$ cm^{-1} . The singlet state has an imaginary frequency for only the $\nu_7(\pi_u)$ bending mode at $55i$ cm^{-1} (see Table 3.1). By relaxing the linear structure to allow a slight bend ($\sim 2^\circ$), local minima are found for the singlet (1A_1) and triplet states. The triplet state lies ~ 22 kcal/mol higher than the singlet. The bent quintet state is a transition state ($243i$ cm^{-1}). A similar situation prevailed in the DFT investigation of Ti_2C_3 clusters⁶³ by Sumathi and Hendrickx where, for the linear TiC_3Ti isomer, they introduced $\sim 1^\circ$ bending along the axis for the triplet and quintet electronic states.

Figure 3.4 shows the relaxed NiC_3Ni structure for what is now the 1A_1 ground state with C_{2v} symmetry. The separation between the total energies of the singlet relaxed (1A_1) and linear (${}^1\Sigma_g^+$) structures is very small with the relaxed structure ~ 0.0005 kcal/mol below the linear structure. The small, $\sim 2^\circ$ bending of the relaxed structure suggests that NiC_3Ni is effectively linear with some floppiness. This idea is reinforced by comparing the calculated vibrational fundamentals for the singlet linear (${}^1\Sigma_g^+$) and relaxed (1A_1) structures in Table 3.1. Although the number of vibrational modes differs for the linear and relaxed structures, the frequencies of the vibrational modes are very similar, taking into account the change in symmetry. In particular, the $\nu_3(\sigma_u)$ and $\nu_7(b_2)$ carbon-carbon stretching fundamentals are both calculated to be ~ 2076 cm^{-1} with nearly equal intensities of ~ 2670 km/mol. This mode is the obvious candidate for assignment to the absorption observed at 1950.8 cm^{-1} .

Table 3.2 shows a comparison between the measured and calculated frequencies for the isotopic shifts from the 1950.8 cm^{-1} absorption for NiC_3Ni in the ${}^1\Sigma_g^+$ electronic state and the assignments of the ^{13}C -substituted isotomers' frequencies. Figure 3.3(b) illustrates the isotopomer assignments on the spectrum where, for brevity, the Ni atoms have been omitted from the ends of the C_3 unit. The first column in Table 3.2 lists the isotomers of NiC_3Ni and

the second, the frequencies of the corresponding observed isotopic shifts (ν_{obs}). The DFT predicted frequencies of the vibrational fundamental and its isotopic shift bands are given in the third column (ν_{DFT}), and the isotopic shift frequencies scaled to the observed spectrum are shown in the fourth column (ν_{sc}). Because the anharmonic effects associated with the fully ^{13}C -substituted species are different from the harmonic effects of the fully ^{12}C species, two scaling factors are needed. A scaling factor of $1950.8/2075.9=0.93974$ was used to scale the single ^{13}C isotopic substitutions and $1875.5/1994.3=0.94043$ for the single ^{12}C isotopic shifts (*i.e.*, double ^{13}C substitutions). The last column of Table 3.2 shows the difference between the observed and scaled frequencies ($\nu_{\text{obs}}-\nu_{\text{sc}}$). Since the calculated isotopic shifts for the linear and relaxed structures were effectively the same ($\pm 0.1 \text{ cm}^{-1}$) when scaled to the observed fundamental at 1950.8 cm^{-1} and the fully ^{13}C substituted isotopic shift at 1875.5 cm^{-1} , only the isotopic shifts for the linear $^1\Sigma_g^+$ structure are presented in Table 3.2. Figure 3.3(c) shows the 50% ^{13}C -enriched DFT simulated spectrum for the ^{13}C isotopic shifts from the 1950.8 cm^{-1} vibrational fundamental, scaled by only the ratio of the observed and calculated ^{12}C fundamentals (*i.e.*, $1950.8/2075.9$). There is good agreement between the theoretical predictions and the experimental measurements. All differences between the observed and predicted isotopic shifts are within $\pm 1.5 \text{ cm}^{-1}$. The absorption at 1950.8 cm^{-1} may therefore be assigned to the $\nu_3(\sigma_u)$ vibrational fundamental of linear, NiC_3Ni in its $^1\Sigma_g^+$ state. The only other vibrational fundamental accessible in the $500\text{-}3500 \text{ cm}^{-1}$ range is the $\nu_4(\sigma_u)$ metal-carbon stretch predicted at $\sim 786 \text{ cm}^{-1}$. Although its low intensity ($\sim 28 \text{ km/mol}$) does not necessarily preclude its observation, it was not observed in this study.

Table 3.1 DFT-B3LYP/6-311G* calculated vibrational frequencies for ${}^1\Sigma_g^+$ linear and 1A_1 “relaxed” NiC₃Ni (see Fig. 3.4).

Structure	Vibrational mode	Frequency (cm ⁻¹)	Infrared intensity (km/mol)
<i>D_{∞h}</i> (linear)	$\nu_1(\sigma_g)$	1518	0
	$\nu_2(\sigma_g)$	325	0
	$\nu_3(\sigma_u)$	2076	2676
	$\nu_4(\sigma_u)$	786	28
	$\nu_5(\pi_g)$	275	0
	$\nu_6(\pi_u)$	140	77
	$\nu_7(\pi_u)$	55 <i>i</i>	1.6
<i>C_{2v}</i> (relaxed)	$\nu_1(a_1)$	1518	0
	$\nu_2(a_1)$	326	0
	$\nu_3(a_1)$	194	71
	$\nu_4(a_1)$	56	5
	$\nu_5(a_2)$	275	0
	$\nu_6(b_1)$	157	77
	$\nu_7(b_2)$	2076	2673
	$\nu_8(b_2)$	785	28
	$\nu_9(b_2)$	276	0

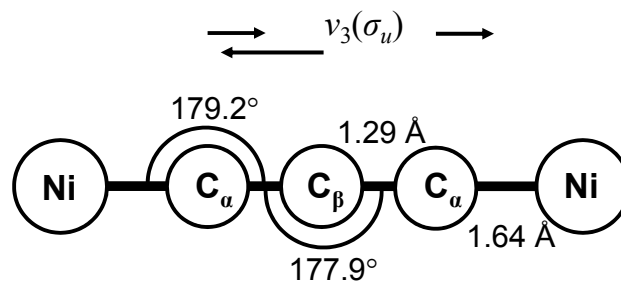


Figure 3.4 The structure of linear NiC₃Ni in the $^1\Sigma_g^+$ and relaxed 1A_1 electronic states. Bond lengths are in angstroms (Å) and are the same for both linear and relaxed structures. The angles denote the bending calculated for the relaxed structure. The vectors above the molecule indicate the displacement of the carbon atoms in the $\nu_3(\sigma_u)$ vibrational mode of the linear structure which corresponds to the $\nu_7(b_2)$ vibrational mode of the relaxed structure.

Table 3.2 Comparison of observed and DFT-B3LYP/6-311G* calculated isotopic shifts for linear ${}^1\Sigma_g^+$ NiC₃Ni (see Fig. 3.3).

Isotopomer	Observed ν_{obs} (cm ⁻¹)	DFT Calculated ν_{DFT} (cm ⁻¹)	Scaled ν_{sc} (cm ⁻¹)	Difference $\nu_{\text{obs}} - \nu_{\text{sc}}$ (cm ⁻¹)
Ni-12-12-12-Ni	1950.8	2075.9	1950.8 ^a	---
Ni- 13 -12-12-Ni	1938.1	2061.3	1937.1	1.0
Ni-12- 13 -12-Ni	1903.2	2025.9	1903.8	-0.6
Ni- 13-13-13 -Ni	1875.5	1994.3	1875.5 ^b	---
Ni- 13-13 -12-Ni	1889.7	2010.9	1891.1	-1.4
Ni- 13 -12- 13 -Ni	1924.5	2045.5	1923.7	0.8

^a The predicted shifts in Column 3 are scaled by a factor of 1950.8/2075.9=0.93974.

^b The predicted shifts in Column 3 are scaled by a factor of 1875.5/1994.3=0.94043.

3.5 CONCLUSIONS

The measurement of ^{13}C isotopic shifts using FTIR spectroscopy combined with DFT calculations has enabled the identification of the $\nu_3(\sigma_u)=1950.8\text{ cm}^{-1}$ vibrational fundamental of linear NiC_3Ni in its $^1\Sigma_g^+$ state in solid Ar. The results of DFT calculations suggest that the molecule may be slightly floppy based on theoretical modeling with linear and relaxed structures. The agreement between measured ^{13}C isotopic shifts and those calculated by theory is very good. Although there have been several studies investigating various nickel carbide structures, none have been reported on the structure of Ni_2C_3 for which only mass spectrometric results have previously been reported.²⁶ This is thus the first report to present results on the structure and vibrational spectrum of NiC_3Ni .

CHAPTER IV

FTIR OBSERVATION OF VIBRATIONAL FUNDAMENTALS OF TiC₃ IN SOLID Ar

4.1 INTRODUCTION AND PREVIOUS RESEARCH

The first report of the metallocarbohedrene, specifically Ti₈C₁₂⁺, by Castleman *et al.*¹⁵ prompted further theoretical and experimental investigations of smaller titanium carbide clusters with the objective of understanding the structures of the smaller clusters and how they combine to form the larger metcar clusters. In an early theoretical study on small Ti_mC_n molecules using a linear combination of atomic orbitals molecular orbital approach, Reddy and Khanna⁶⁴ reported the structures for TiC, TiC₂, Ti₂C₂, and Ti₂C₃, and the analogous titanium nitrides. Cyclic structures were found for all of the polyatomics. An experimental study by Wang *et al.*³⁰ used PE spectroscopy to obtain vibrationally resolved spectra of the TiC_n⁻ (*n*=2-5) anions. They reported metal-carbon stretching frequencies for TiC₂ (560±50 cm⁻¹), TiC₃ (650±30 cm⁻¹), TiC₄ (440±40 cm⁻¹), and TiC₅ (240±60 cm⁻¹). Based on comparisons with earlier theoretical work on LaC_n and YC_n (*n*=2-6) clusters,³⁸ they concluded that the Ti analogs would have C_{2v} ring structures.

Subsequently, Sumathi and Hendrickx undertook extensive DFT calculations on TiC_n (*n*=2-4),^{65,66} Ti₂C₂,⁶⁷ and Ti₂C₃.⁶³ Calculations with the BP86 (Becke and Perdew)^{61,68} and B3LYP^{61,62} functionals confirmed that TiC₂ should have a triangular C_{2v} structure with ionic bonds, in agreement with the earlier work of Reddy and Khanna,⁶⁴ and a ³B₁ ground state. This situation is analogous to the Group IV silicon-carbon clusters in which the SiC₂ structure is C_{2v} with an ionic bond between Si and the C₂ unit.⁶⁹ DFT calculations of harmonic vibrational frequencies predicted a C-C stretch and symmetric and antisymmetric Ti-C stretches at 1676,

587, and 257 cm^{-1} , respectively. The predicted 587 cm^{-1} symmetric Ti-C stretch and the cyclic structure for TiC_2 are in agreement with the $560 \pm 50 \text{ cm}^{-1}$ frequency measured by Wang *et al.*³⁰ and the structure they suggested.

In their DFT-B3LYP investigation of TiC_3 and TiC_4 Sumathi and Hendrickx⁶⁵ determined planar, fanlike C_{2v} structures with transannular Ti-C bonding for both molecules, consistent with the geometries Wang *et al.*³⁰ had deduced from their PE spectroscopy measurements. Figure 4.1 shows the TiC_3 structures that Sumathi and Hendrickx modeled, and Figure 4.2 shows an energy level diagram which plots the relative energies of the structures. The global minimum for TiC_3 has a 1A_1 electronic state with a triplet transition state predicted 7.1 kcal/mol higher in energy. The fanlike isomer should thus be well separated from a triplet kite-shaped isomer lying 21.5 kcal/mol higher in energy and a linear quintet isomer lying at 28.9 kcal/mol. The Ti-C vibrational frequencies of 686.5 and 472.2 cm^{-1} predicted for fanlike TiC_3 and TiC_4 , respectively, are in good agreement with the 650 ± 30 and $440 \pm 40 \text{ cm}^{-1}$ frequencies observed by PE spectroscopy.³⁰

Analogous to rhombic Si_2C_2 ,⁷⁰ a rhomboidal isomer with a transannular Ti-C bond has been predicted as the quintet ground state structure for Ti_2C_2 lying ~ 59 kcal/mol lower than the nearest quintet linear isomer with terminal Ti atoms.⁶⁷ For Ti_2C_3 , a cyclic, pentagonal geometry with a C_2 unit at the base lying ~ 30 kcal/mol below linear TiC_3Ti is predicted for the quintet ground state.⁶³ The predictions for TiC_2 and Ti_2C_2 parallel the experimental and theoretical results for SiC_2 and Si_2C_2 ; however, the analogous Si_2C_3 molecule has been found to be linear.⁷¹ Figure 4.3 shows the Ti_mC_n ground state structures predicted by Sumathi and Hendrickx's investigation.^{63,65-67}

As discussed in Chapter I, transition-metal carbides are also of interest for their potential as astrophysical molecules. Since carbon chains are present in interstellar space and in the

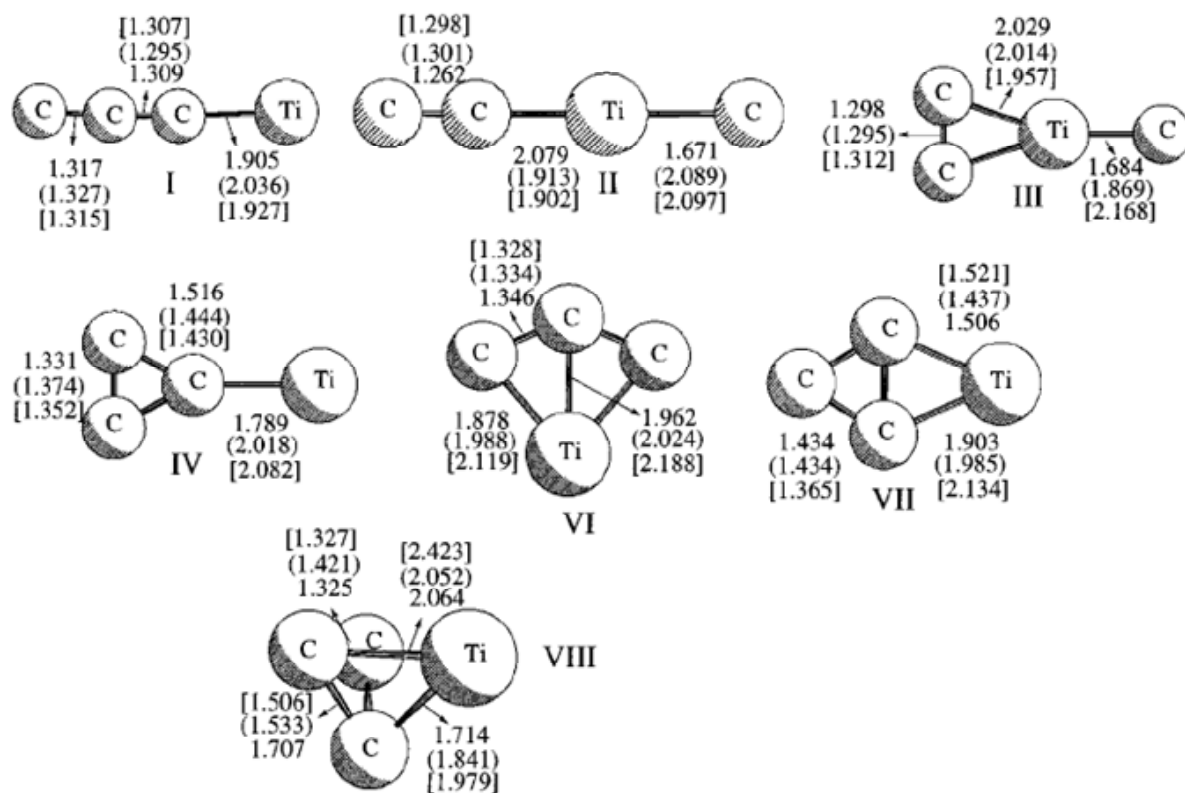


Figure 4.1 Geometries of TiC_3 investigated in the DFT study by Sumathi and Hendrickx (Ref. 65). Bond lengths are given in angstroms (\AA) for singlet, triplet (), and quintet [] electronic states.

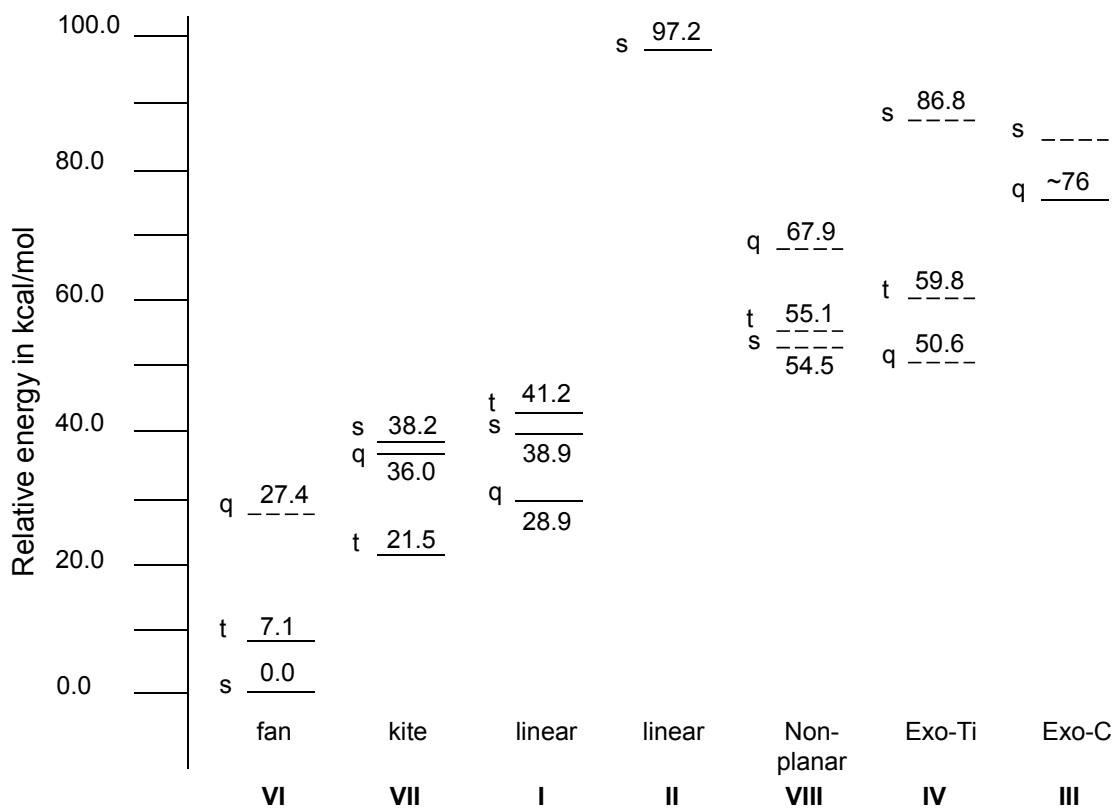


Figure 4.2 Energy level diagram plotting the relative energies of the TiC₃ isomers in Fig. 4.1 by Sumathi and Hendrickx (Ref. 65). The electronic states are singlet (s), triplet (t), and quintet (q). Solid lines represent stable minima and dashed lines represent higher order saddle points or stationary points.

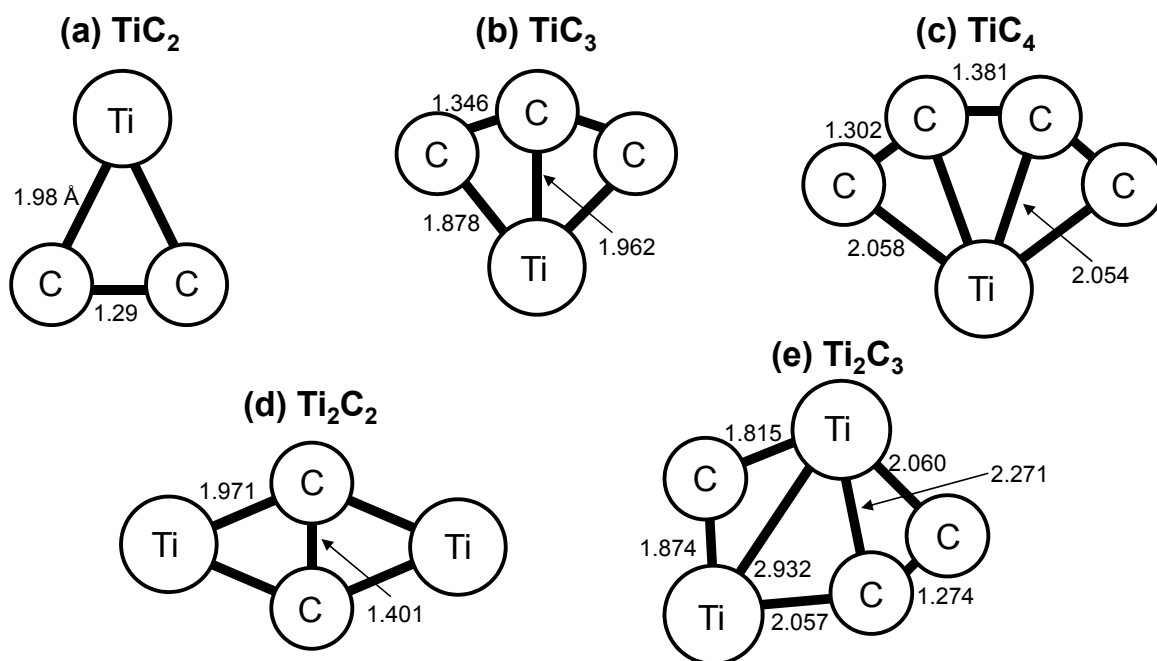


Figure 4.3 Ground state structures for (a)-(c) TiC_n ($n=2-4$) and (d)-(e) Ti_2C_n ($n=2,3$) clusters calculated in the DFT investigations of Sumathi and Hendrickx (Ref. 63,65-67). Bond lengths are in angstroms (Å).

atmospheres of late-type carbon stars like IRC+10216,^{12,72} and small molecules bearing transition metals like Ti have been detected in both stellar and circumstellar spectra, it is anticipated that transition metal–carbon molecules could be present as well. The advent of platforms in space for the observation of infrared spectra has generated a need for the laboratory measurements of the spectra of potentially relevant molecules.

The present discussion on TiC₃ reports the first unambiguous evidence of the molecule's fanlike (C_{2v}) structure in the 1A_1 electronic state and the observation of new vibrational fundamentals. A comparison of experimentally measured and DFT predicted ¹³C isotopic shifts has enabled assignment of the $\nu_5(b_2)$ and $\nu_3(a_1)$ vibrational fundamentals and a tentative assignment of the $\nu_4(b_1)$ fundamental. The observed fanlike structure and fundamentals confirm the conclusions of the previous DFT⁶⁵ and PE³⁰ spectroscopy studies.

4.2 THEORETICAL CALCULATIONS

The DFT-B3LYP investigation of TiC₃ by Sumathi and Hendrickx⁶⁵ has shown that the 1A_1 state with C_{2v} fanlike structure is the global minimum, with a fanlike triplet state lying ~7 kcal/mol higher and a kite-shaped triplet structure lying ~22 kcal/mol above the ground state. As noted, this prediction is consistent with the PE spectroscopy results,³⁰ and so the present investigation has focused on the fanlike structure.

The GAUSSIAN 03 program suite⁴⁸ was used to perform DFT calculations using the B3LYP functional^{61,62} and the 6-311G(3df, 3pd) basis set. Figure 4.4 shows the 1A_1 fanlike structure predicted by this new calculation. The calculated frequencies of the vibrational fundamentals and the infrared intensities are shown in Table 4.1, and Fig. 4.5 illustrates the vibrational modes. As expected, the predicted frequencies are in agreement with the results of Sumathi and Hendrickx (not shown).⁶⁵ The calculated infrared intensities indicate that the $\nu_3(a_1)$ mode at

$\sim 697\text{ cm}^{-1}$ should be most intense, followed by the $\nu_5(b_2)$ at ~ 1549 and $\nu_6(b_2)$ at $\sim 460\text{ cm}^{-1}$. Since isotopic shift patterns are critical for the determination of structure and identification of vibrational modes, ^{13}C isotopic shift frequencies have also been calculated.

4.3 EXPERIMENTAL PROCEDURES

TiC_3 was produced by the simultaneous evaporation of a titanium rod and a carbon rod using two focused 1064 nm Nd:YAG pulsed lasers (Spectra Physics). The rods were continuously rotated and translated during evaporation to ensure uniform evaporation over the rods' surfaces. The resultant molecular vapor was simultaneously deposited with Ar (Matheson, 99.9995% purity) onto a gold-plated mirror maintained at $\sim 10\text{ K}$ by a closed-cycle refrigeration system (ARS, Displex). Laser powers of $\sim 2.9\text{ W}$ tightly focused on the titanium rod and $\sim 0.7\text{ W}$ on the carbon rod produced the best yield of TiC_3 . The low laser power on the carbon rod optimized the yield of C_3 for reaction with Ti (§2.5).

Typically, samples were deposited for $\sim 75\text{ min}$ in a vacuum of 10^{-7} Torr or better. To enable ^{13}C isotopic shift measurements, carbon rods with the required isotopic enrichment were made by pressing a mixture of ^{12}C (Alfa Aesar, 99.9995% pure) and ^{13}C (Isotec, 99.3% purity) powders using $\sim 4 \times 10^5\text{ kPa}$ pressure into rods $\sim 1.4\text{ cm}$ in length and 0.9 cm in diameter.

Absorption spectra were recorded over the range of $500\text{-}3500\text{ cm}^{-1}$ with a resolution of 0.2 cm^{-1} using a Bomem DA3.16 Fourier transform spectrometer equipped with a KBr beamsplitter and HgCdTe detector cooled with liquid nitrogen. Following evaporation, the matrix sample was annealed by heating it to specified temperatures for $\sim 4\text{ min}$ and then quenching to $\sim 10\text{ K}$. This procedure enabled the diffusion and combination of neighboring molecules to form larger clusters and also helped to eliminate multiple trapping site features in the spectra.

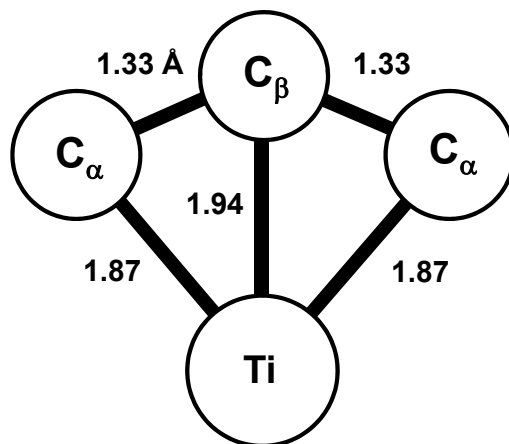


Figure 4.4 The DFT-B3LYP/6-311G(3*df*, 3*pd*) calculated fanlike (C_{2v}) isomer of TiC_3 in the 1A_1 ground state. Bond lengths are in angstroms (Å). Equivalent carbon sites are denoted C_α , and the unique carbon site by C_β .

Table 4.1 DFT-B3LYP/6-311G(3df, 3pd) predicted vibrational frequencies (cm^{-1}) and infrared intensities (km/mol) for the 1A_1 fanlike (C_{2v}) isomer of TiC_3 (see Fig. 4.4 and 4.5).

Structure	Vibrational mode	Frequency (cm^{-1})	Infrared intensity (km/mol)
C_{2v}	$\nu_1(a_1)$	1291	4
	$\nu_2(a_1)$	866	5
	$\nu_3(a_1)$	697	64
	$\nu_4(b_1)$	621	12
	$\nu_5(b_2)$	1549	39
	$\nu_6(b_2)$	460	28

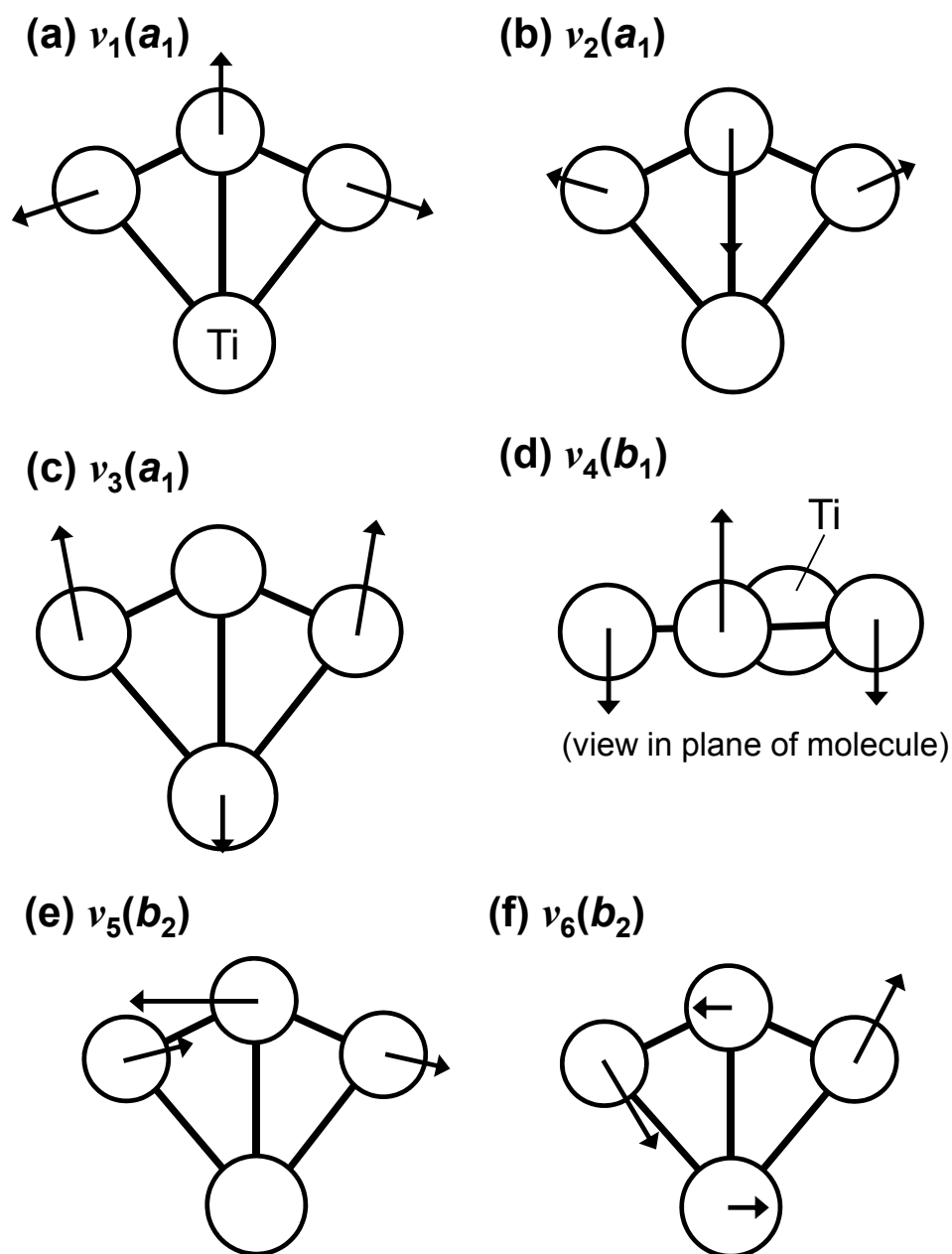


Figure 4.5 The DFT-B3LYP/6-311G(3df, 3pd) calculated vibrational modes of fanlike (1A_1) TiC_3 . Vectors show the displacement of the atoms.

4.4 RESULTS AND ANALYSIS

Potential absorptions belonging to titanium-carbon molecules in the 500-3500 cm^{-1} range were identified by comparing spectra produced by the evaporation of a carbon rod with spectra from the dual evaporation of carbon and titanium rods. Under the experimental conditions used to laser ablate the carbon rod, the spectrum was dominated by a very strong $\nu_3(\sigma_u)$ mode of C_3 at 2038.9 cm^{-1} . Because of the relatively low laser power used and the relatively high vacuum ($\sim 10^{-7}$ Torr), spectra have only very weak absorptions from CO and CO_2 , which are often associated with carbon evaporation, and only trace amounts of H_2O .

With the introduction of the metal by the simultaneous evaporation of carbon and titanium rods, the most prominent new features and thus candidates for titanium-carbon vibrational fundamentals are absorptions at 624.3 and 1484.2 cm^{-1} , with the low frequency band having an integrated intensity about twice that of the high frequency band. The intensities of these absorptions were strongly correlated with the intensity of the $\nu_3(\sigma_u)$ mode of C_3 . As the laser power on the carbon rod was increased from 0.7 W, the intensities of the candidate bands decreased and disappeared at 1.5 W laser power, when the C_3 absorption had lost intensity relative to absorptions of C_6 and C_9 that had grown in strongly. These observations suggest the strong likelihood that the new features are associated with a titanium-carbon species containing a C_3 unit. Table 4.1, which shows the predictions of DFT-B3LYP calculations for the frequencies and intensities of the vibrational fundamentals of fanlike (1A_1) TiC_3 , indicates that the most intense vibrational fundamentals should be the $\nu_3(a_1)$ metal-carbon stretching mode predicted at $\sim 697 \text{ cm}^{-1}$ and the $\nu_5(b_2)$ carbon-carbon stretch at $\sim 1549 \text{ cm}^{-1}$. The $\nu_3(a_1)$ mode is predicted to be ~ 1.6 times the intensity of $\nu_5(b_2)$, which is reasonably close to the observation that the 624.3 cm^{-1} band is approximately two times the intensity of the 1484.2 cm^{-1} band. The frequencies and relative intensities of the two candidate titanium-carbon absorptions are close to the predicted

values, which suggests that the 624.3 and 1484.2 cm^{-1} absorptions are potential candidates for the $\nu_3(a_1)$ and $\nu_5(b_2)$ fundamentals, respectively, of the fanlike TiC_3 isomer.

4.4.1 *The $\nu_5(b_2)$ vibrational fundamental*

Measurement of ^{13}C isotopic shifts is a crucial test for the unambiguous identification of vibrational fundamentals. Figure 4.6(a) shows the isotopic spectrum that results for the 1484.2 cm^{-1} band when a Ti rod and a carbon rod with $\sim 10\%$ ^{13}C enrichment are simultaneously evaporated, and the products deposited at ~ 10 K in solid Ar. Prior to annealing the sample, the 1484.2 cm^{-1} band is accompanied by a satellite band of almost equal intensity 3.4 cm^{-1} lower at 1480.8 cm^{-1} . Additional absorptions appear on the low frequency side of the 1480.8 cm^{-1} band, presumably corresponding to ^{13}C isotopic shifts of the 1484.2 cm^{-1} absorption: two moderately strong bands at 1473.5 and 1450.9 cm^{-1} and a weaker band at 1461.4 cm^{-1} . Similar to the 1484.2 cm^{-1} fundamental, a satellite band 3.4 cm^{-1} lower in frequency accompanies each of the isotopic shift bands. The “doubling” of the spectral features suggests that the molecule is trapped at two different trapping sites in solid Ar, and this distinctive feature in the spectrum of unannealed samples helped initially in the recognition of the ^{13}C isotopic shifts of the 1484.2 cm^{-1} band. Since annealing a matrix sample will often diminish or remove satellite bands as the trapped molecules relax into the lowest energy site, the sample that produced the spectrum in Fig. 4.6(a) was annealed in 2 K intervals from 12 to 24 K for ~ 4 min and then quenched to 10 K after each annealing. During this process the low frequency satellites were steadily reduced in intensity resulting, after the final annealing, in the spectrum shown in Fig. 4.6(b). The spectrum has simplified to two prominent shifts at 1473.5 and 1450.9 cm^{-1} with an intensity ratio of the former to the latter band of 2:1. The weaker 1461.4 cm^{-1} band has sharpened, and another band has been resolved at 1439.9 cm^{-1} .

The presence of two major ^{13}C isotopic shift bands and their 2:1 intensity ratio immediately suggests the possibility that the carrier of the 1484.2 cm^{-1} band is a titanium-carbon molecule containing one unique and two equivalent carbon atoms. It should also be noted that the 1450.9 and 1473.5 cm^{-1} bands are 10 and 20%, respectively, of the 1484.2 cm^{-1} fundamental, which is consistent with the 10% isotopic enrichment of the carbon rod. The observed isotopic shift spectrum, therefore, is exactly what would be expected for fanlike (C_{2v}) TiC_3 and rules out the linear structure with a terminal carbon on one end. The shift pattern does not rule out TiC_3Ti ; however, as noted earlier, DFT calculations⁶³ have shown that the energy of the linear structure is ~ 30 kcal/mol above the ground state for which a planar pentagonal structure with inequivalent carbons is predicted.

Table 4.2 shows a comparison of the measured isotopic shifts for the ^{13}C -substituted isotopomers for the 1484.2 cm^{-1} band to the predictions of DFT-B3LYP/6-311G(3df, 3pd) calculations, and Fig. 4.6(c) shows the DFT simulated isotopic shift spectrum for comparison with the observed spectrum in Fig. 4.6(b). The isotopic shifts in Fig. 4.6(b) are labeled following the $\text{Ti-C}_\alpha\text{-C}_\beta\text{-C}_\alpha$ convention of Table 4.2 and Fig. 4.4; however, the metal atom (*i.e.*, ^{48}Ti) is omitted from the labels in Fig. 4.6(b) for brevity. The first column of Table 4.2 lists the TiC_3 isotopomers and the second column lists the FTIR observed isotopic shifts (ν_{obs}). The third column lists the DFT calculated fundamental and isotopic shifts (ν_{DFT}). The fourth column lists the calculated isotopic shifts scaled for comparison with the measured shifts (ν_{sc}). The DFT predicted isotopic shifts in Table 4.2 and the simulated spectrum in Fig. 4.6(c) have both been scaled by a factor obtained by multiplying the DFT predicted frequencies by the ratio of the observed ^{12}C isotopomer frequency for the $\nu_5(b_2)$ mode to the DFT predicted value ($1484.2/1549.4=0.95792$). The fifth column of Table 4.2 lists the difference between the experimental and theoretical shifts ($\Delta\nu=\nu_{\text{obs}}-\nu_{\text{sc}}$). The strong shifts at 1473.5 and 1450.9 cm^{-1}

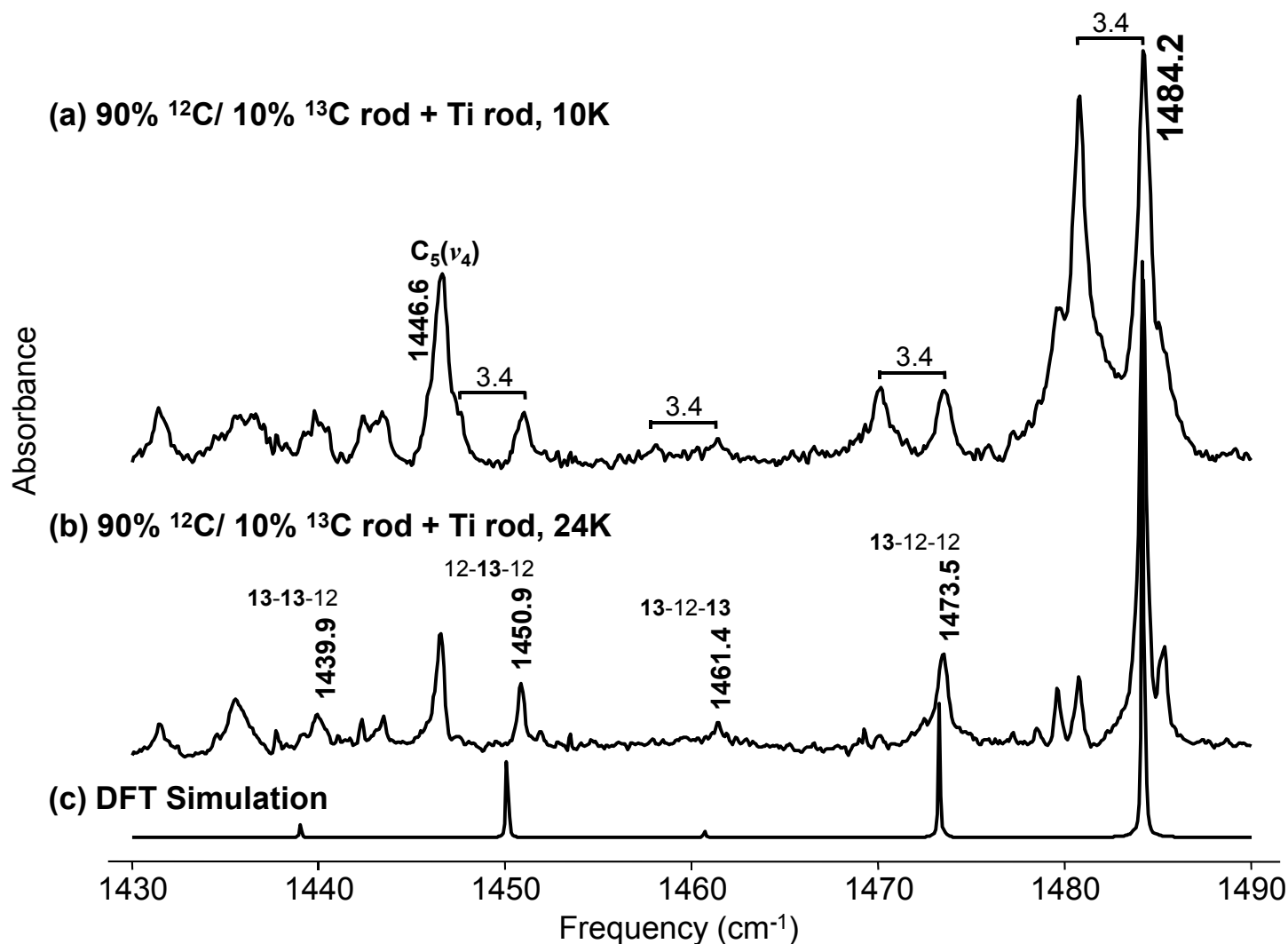


Figure 4.6 The $\nu_5(b_2)=1484.2 \text{ cm}^{-1}$ fundamental of TiC_3 . (a) The spectrum produced in the $1430\text{-}1490 \text{ cm}^{-1}$ region by the simultaneous evaporation of a carbon rod with 10% ^{13}C isotopic enrichment and a titanium rod and (b) the spectrum of the sample after annealing at 24 K. The labeling of isotopic shifts in (b) follows the convention of Table 4.2 and Fig. 4.4 (the metal atom is omitted for brevity). (c) The DFT-B3LYP/6-311G(3df, 3pd) simulated spectrum.

Table 4.2 Comparison between the observed ^{13}C shift frequencies (cm^{-1}) and the DFT-B3LYP/6-311G(3*df*, 3*pd*) predicted isotopomer frequencies for the $\nu_5(b_2)$ mode of the 1A_1 fanlike (C_{2v}) isomer of TiC_3 (see Fig. 4.6).

Isotopomer Ti-C $_{\alpha}$ -C $_{\beta}$ -C $_{\alpha}$	Observed ν_{obs} (cm^{-1})	DFT Calculated ν_{DFT} (cm^{-1})	Scaled ν_{sc} (cm^{-1})	Difference $\Delta\nu$ (cm^{-1})
48-12-12-12	1484.2	1549.4	1484.2 ^a	---
48- 13 -12-12	1473.5	1538.0	1473.3	0.2
48-12- 13 -12	1450.9	1513.8	1450.1	0.8
48- 13-13 -12	1439.9	1502.2	1439.0	0.9
48- 13 -12- 13	1461.4	1524.9	1460.7	0.7
48- 13-13-13	---	1488.6	1426.0	---

^a The predicted shifts in Column 3 are scaled by a factor of $1484.2/1549.4=0.95792$.

correspond to the 13-12-12 and 12-13-12 singly ^{13}C -substituted isotopomers, respectively. The weaker 1439.9 and 1461.4 cm^{-1} absorptions are readily identified as shifts for the two possible double ^{13}C -substituted isotopomers, 13-13-12 and 13-12-13, respectively. Agreement between theory and measurement is very good and confirms the assignment of the 1484.2 cm^{-1} absorption to the $\nu_5(b_2)$ fundamental of fanlike (C_{2v}) TiC_3 .

4.4.2 *The $\nu_3(a_1)$ vibrational fundamental*

Figure 4.7(a) shows the observed isotopic shift spectrum for the 624.3 cm^{-1} absorption, which is the candidate for the $\nu_3(a_1)$ metal-carbon stretching mode. In this case, the observed spectrum is quite simple with only one distinct shift at 616.8 cm^{-1} . However, Table 4.3 shows that the DFT calculations predict coincidences in the shift frequencies. Figure 4.5(c), which illustrates the $\nu_3(a_1)$ mode, shows that the Ti atom and the equivalent (C_α) carbon atoms significantly participate in the vibration, but not the unique carbon atom (C_β). Therefore, any ^{13}C substitution for the C_β site will result in the corresponding isotopic shift being overlapped by other shifts.

Similar to the $\nu_5(b_2)$ fundamental, the isotopic shift frequency predictions in Table 4.3 and the simulated spectrum in Fig. 4.7(b) have both been scaled by the ratio of the observed ^{12}C isotopomer frequency for the $\nu_3(a_1)$ mode to the DFT predicted value (624.3/696.7=0.8961). The scaled frequency for the isotopomer with ^{13}C at the unique center site (12-13-12) will be overlapped by the 624.3 cm^{-1} absorption for the unsubstituted isotopomer (12-12-12). Similarly, the isotopic shift for single substitution at the two equivalent sites (13-12-12) and the shift corresponding to the equivalent double substitution (13-13-12) are predicted to overlap at ~ 616.7 cm^{-1} . At 10% ^{13}C enrichment, the principal contributors to the intensity should be the single shifts corresponding to ^{13}C isotopic substitution at the two equivalent carbon sites and the

observed shift should be ~20% of the fundamental. The DFT predictions are therefore consistent with the single strong shift observed at 616.8 cm^{-1} that has an integrated intensity ~18% of the 624.3 cm^{-1} band. Although the weak feature at 608.4 cm^{-1} is in agreement with the predicted shifts for the overlapping 13-12-13 and 13-13-13 isotopomers, at 10% ^{13}C enrichment, they would not make a significant contribution, and the intensity of the feature at 608.4 cm^{-1} is not reproducible. Other weak bands appearing in the simulation arise from isotopic shifts for the ^{46}Ti , ^{47}Ti , ^{48}Ti , ^{49}Ti , and ^{50}Ti with relative abundances of 8, 7, 74, 6, and 5%, respectively. They undoubtedly contribute to the wings of the 624.3 cm^{-1} fundamental, but could not be resolved. The agreement between measured and predicted spectra is very good and, therefore, confirms the assignment of the $\nu_3(a_1)=624.3\text{ cm}^{-1}$ fundamental of fanlike (C_{2v}) TiC_3 .

4.4.3 *The $\nu_4(b_1)$ vibrational fundamental*

A weak band appearing at 573.8 cm^{-1} and shown in the low-frequency side of the spectrum in Fig 4.7(a) may be the $\nu_4(b_1)$ fundamental. The band at 573.8 cm^{-1} appeared in only titanium-carbon experiments with consistently ~12% the intensity of the observed $\nu_3(a_1)$ fundamental. The DFT simulated spectrum, with the predicted ^{13}C isotopic shifts shown to the low frequency side of Fig. 4.7(b), is again scaled by the ratio of the observed ^{12}C isotopomer frequency for the $\nu_4(b_1)$ mode to the DFT predicted value ($573.8/620.5=0.9247$). Because of the weak intensity of the observed spectrum, however, experimental shifts corresponding to those in the simulated spectrum cannot be observed; therefore, the assignment of the 573.8 cm^{-1} band to $\nu_4(b_1)$ must be considered very tentative.

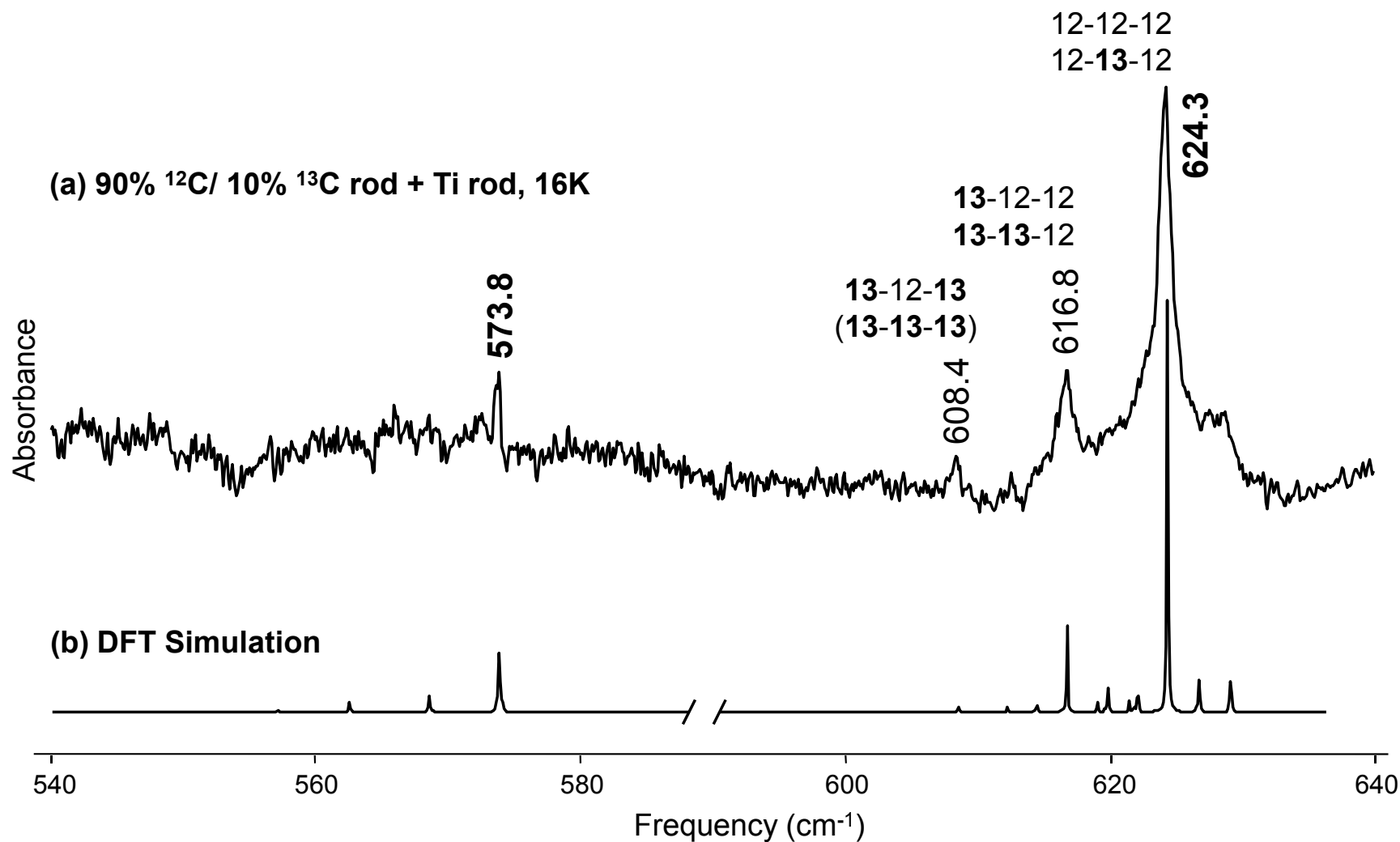


Figure 4.7 The $\nu_3(a_1)=624.3\text{ cm}^{-1}$ and tentatively assigned $\nu_4(b_1)=573.8\text{ cm}^{-1}$ fundamentals of TiC_3 . (a) The spectrum produced in the $540\text{-}640\text{ cm}^{-1}$ region by simultaneous evaporation of a carbon rod with 10% ^{13}C isotopic enrichment and a titanium rod after annealing at 16 K. The labeling of the isotopic shifts follows the convention in Table 4.3 and Fig. 4.4 (the metal atom is omitted for brevity). (b) The DFT-B3LYP/6-311G(3df, 3pd) simulated spectrum.

Table 4.3 Comparison between the observed ^{13}C shift frequencies (cm^{-1}) and the DFT-B3LYP/6-311G(3df, 3pd) predicted isotopomer frequencies for the $\nu_3(a_1)$ mode of the 1A_1 fanlike (C_{2v}) isomer of TiC_3 (see Fig. 4.7).

Isotopomer Ti-C $_{\alpha}$ -C $_{\beta}$ -C $_{\alpha}$	Observed ν_{obs} (cm^{-1})	DFT Calculated ν_{DFT} (cm^{-1})	Scaled ν_{sc} (cm^{-1})	Difference $\Delta\nu$ (cm^{-1})
48-12-12-12	624.3	696.7	624.3 ^a	0.0
48- 13 -12-12	616.8	688.2	616.7	0.1
48-12- 13 -12	Overlapped ^b	696.5	624.1	---
48- 13 - 13 -12	616.8	688.1	616.6	0.2
48- 13 -12- 13	608.4	679.1	608.5	-0.1
48- 13 - 13 - 13	---	679.0	608.4	---

^a The predicted shifts in Column 3 are scaled by a factor of $624.3/696.7=0.8961$

^b Band is overlapped by the main 48-12-12-12 isotopomer absorption.

4.4.4 Other vibrational fundamentals of TiC_3

According to the DFT results shown in Table 4.1, the $\nu_6(b_2)$ fundamental predicted at ~ 460 cm^{-1} should be a strong feature in the spectrum of fanlike TiC_3 . Unfortunately, the 460 cm^{-1} absorption would lie outside the range of the HgCdTe detector and KBr beamsplitter used in this investigation. No candidates were observed for the $\nu_1(a_1)$ and $\nu_2(a_1)$ fundamentals at ~ 1291 and ~ 866 cm^{-1} , respectively, which are predicted to be the weakest fundamentals with less than half the intensity of the $\nu_4(b_1)$ fundamental whose tentative assignment was discussed previously (§4.4.3).

4.5 CONCLUSIONS

On basis of the observed ^{13}C isotopic shift patterns and very good agreement with DFT predictions, the $\nu_5(b_2)$ asymmetric carbon-carbon stretching fundamental has been identified at 1484.2 cm^{-1} , and the $\nu_3(a_1)$ symmetric metal-carbon stretch at 624.3 cm^{-1} , for fanlike (1A_1) TiC_3 trapped in solid Ar. An absorption at 573.8 cm^{-1} has been provisionally assigned to the $\nu_4(b_1)$ fundamental. This is the first observation of the vibrational fundamentals of TiC_3 , and the 650 ± 30 cm^{-1} frequency reported as a symmetric metal-carbon stretch of TiC_3 in a previous PE spectroscopy study^{29,30} is consistent with the $\nu_3(a_1) = 624.3$ cm^{-1} fundamental assigned here. This FTIR and DFT investigation of TiC_3 at ~ 10 K provides the first unambiguous evidence for the fanlike (C_{2v}) isomer in the 1A_1 electronic state previously predicted to be the ground state of the molecule by an earlier DFT investigation.⁶⁵

CHAPTER V

FTIR OBSERVATION OF VIBRATIONAL FUNDAMENTALS OF ScC₃ IN SOLID Ar

5.1 INTRODUCTION AND PREVIOUS RESEARCH

The results for fanlike TiC₃ discussed in Chapter IV significantly aided the interpretation of the spectra and conclusions for fanlike ScC₃ discussed here; the two chapters are thus complementary. Scandium carbides were studied in a PE spectroscopy and DFT investigation of MC₂ ($M = \text{Sc, V, Cr, Mn, Fe, Co}$) and MC₃ ($M = \text{Sc, V, Cr, Mn, Fe, Co, Ni}$) clusters by Li and Wang.^{28,29} For ScC₂ they measured a vibrational frequency of $670 \pm 40 \text{ cm}^{-1}$ corresponding to a metal-carbon stretching mode. Although they did not report on possible MC₂ structures, their results suggest that the bond between the Sc atom and C₂ unit has significant ionic character. This conclusion is supported by later theoretical research by Rayón *et al.*⁵³ predicting C_{2v} T-shaped structures for most first-row transition-metal MC₂ clusters and C_{2v} ring structures for TiC₂, CoC₂, and NiC₂. In their PE spectra for ScC₃ Wang and Li²⁹ assigned a vibrational spacing of $560 \pm 30 \text{ cm}^{-1}$ in the ground state to a metal-carbon stretching mode and reported a $600 \pm 50 \text{ cm}^{-1}$ vibrational spacing for an excited state lying 0.42 eV ($\sim 9.7 \text{ kcal/mol}$) higher in energy. Their DFT investigation of ScC₃ proposed a cyclic C_{2v} ring structure (*i.e.*, fanlike) for the molecule with a doublet electronic ground state (2A_2).

Further theoretical investigations on small scandium carbide clusters are listed in a recent article by Redondo *et al.*³⁶ concerning cyclic and linear ScC_{*n*} ($n=1-8$) clusters. The structures and electronic states of ScC₃ and its anion and cation have been investigated by Roszak *et al.*,⁷³ Hendrickx and Clima,⁷⁴ and Redondo *et al.*^{36,75} All of these studies have predicted a fanlike, C_{2v} geometry for the ground state of ScC₃ (see Fig. 5.1), and Redondo *et al.*³⁶ have calculated that

the linear Sc-C-C-C structures⁷⁵ lie ~ 20 kcal/mol higher in energy. However, there has been disagreement about the symmetry of the electronic ground state of fanlike ScC₃. Roszak *et al.*⁷³ calculated the ground state to be 2A_2 using DFT, and 4B_1 using complete active space self-consistent fields (CASSCF) and multi-reference single double configuration interaction (MRSDCI and MRSDCI+Q) theories. However, they argued that the quartet ground state was more consistent with the PE data of Wang and Li,²⁹ thus reassigning their 560 cm⁻¹ frequency to the 4B_1 state and the 600 cm⁻¹ frequency to the 2A_2 state using DFT predicted vibrational fundamentals. In contrast, Hendrickx and Clima⁷⁴ using CASSCF and complete active space with second-order perturbation (CASPT2) theories and Redondo *et al.*³⁶ using DFT have all predicted that the 4B_1 state lies ~ 6 -10 kcal/mol higher than the 2A_2 state, thus making the doublet electronic ground state more probable. This uncertainty in the electronic ground state has in part motivated this experimental investigation aimed at resolving the issue.

This chapter discusses the results of the FTIR observation of ¹³C-substituted isotopic spectra of fanlike ScC₃ trapped in solid Ar. ¹³-Carbon isotopic shift spectra for both the 2A_2 and 4B_1 electronic states have been simulated using DFT. Assignments of the $\nu_5(b_2)$, $\nu_3(a_1)$, and $\nu_1(a_1)$ vibrational fundamentals of fanlike ScC₃ in its 2A_2 electronic ground state have been made based on the very good agreement between experimentally observed and DFT simulated ¹³C isotopic shift spectra. Although DFT simulated spectra for the 4B_1 electronic state have also been calculated, the isotopic shift spectrum for the $\nu_3(a_1)$ fundamental in this state is shown to be inconsistent with the FTIR measured isotopic shift pattern.

5.2 THEORETICAL MODELING

Previous DFT investigations have consistently predicted that the ground state of ScC₃ has a fanlike (C_{2v}) geometry with a 2A_2 electronic ground state³⁶ and a 4B_1 state ~ 6 -10 kcal/mol higher.

The linear state is ~ 20 kcal/mol above the predicted ground state and is thus not a candidate for the ground state structure.⁷⁵ Both linear and fanlike structures have been observed by the Molecular Physics Laboratory in FTIR matrix studies of metal-tricarbon MC_3 clusters trapped in solid Ar. Comparison of DFT predicted ^{13}C isotopic shifts with measured shifts has shown that CrC_3 has a linear geometry⁴⁴ and TiC_3 , a fanlike structure (Chapter IV) consistent with the “ringlike” geometry suggested by the PE observations of Wang *et al.*³⁰ It is worth noting, however, that the energy separating the linear and fan geometries of CrC_3 is only ~ 7 kcal/mol,³¹ significantly smaller than the ~ 30 kcal/mol separating the fan and linear geometries of TiC_3 .⁶⁵

New DFT calculations for fanlike (C_{2v}) ScC_3 in the 2A_2 and 4B_1 electronic states have been made using the GAUSSIAN 03 suite⁴⁸ with the B3LYP functional^{61,62} and the 6-311G(3*df*, 3*pd*) basis set. Figure 5.1(a) shows the resulting 2A_2 fanlike geometry with bond lengths in angstroms, which differ by only ~ 0.02 Å from those calculated by Redondo *et al.*³⁶ The B3LYP/6-311G(3*df*, 3*pd*) bond lengths for the 4B_1 structure are shown in Fig. 5.1(b) and differ by ≤ 0.06 Å from the 4B_1 bond lengths calculated by Hendrickx and Clima.⁷⁴

Table 5.1 shows the DFT calculated frequencies and infrared intensities of the vibrational fundamentals for the 2A_2 and 4B_1 states. The vibrational frequencies are in good agreement with those calculated by Redondo *et al.*³⁶ Figures 5.2(a)-(f) illustrate the six vibrational modes of the 2A_2 state. The vibrational modes of the 4B_1 state are similar with the exception of the $\nu_3(a_1)$ mode in which the central carbon atom (C_β) participates significantly more in the quartet state [Fig. 5.2(g)] than in the doublet state [Fig. 5.2(c)]. For both the doublet and quartet fanlike ScC_3 structures, the $\nu_3(a_1)$ vibrational fundamental is a good candidate for the 560 ± 30 cm^{-1} symmetric metal-carbon stretch measured in the earlier PE study.²⁹ Since isotopic shift patterns can provide a decisive test for the identification of molecular species and their vibrational fundamentals, the ^{13}C isotopic spectra have been calculated for both the 2A_2 and 4B_1 states of fanlike ScC_3 .

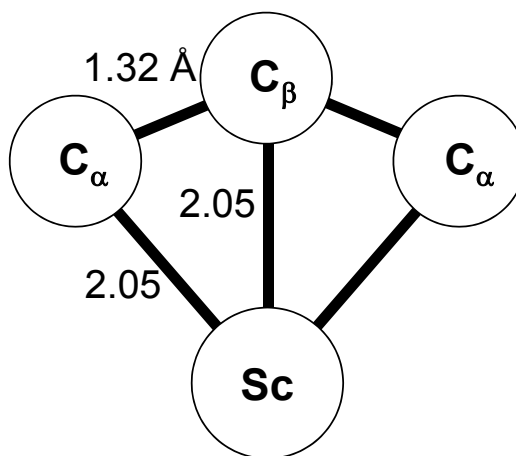
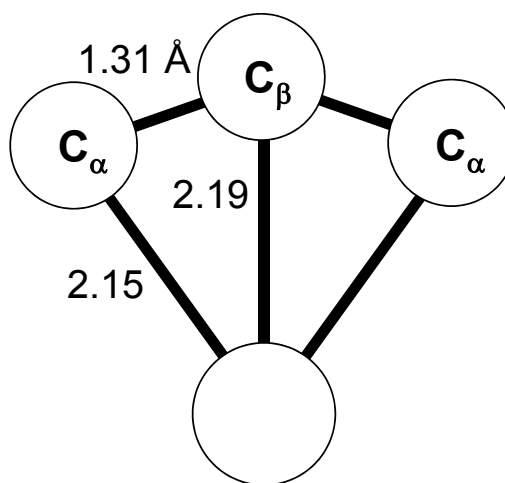
(a) 2A_2 structure**(b) 4B_1 structure**

Figure 5.1 Geometry of fanlike (C_{2v}) ScC_3 in the (a) 2A_2 electronic state and (b) 4B_1 state. Bond lengths in angstroms (Å) are shown for the B3LYP/6-311G(3df, 3pd) simulation. Equivalent and unique carbon sites are labeled C_α and C_β , respectively.

Table 5.1 DFT-B3LYP/6-311G(3*df*, 3*pd*) predicted vibrational modes, frequencies (cm^{-1}), and infrared intensities (km/mol) for cyclic (fanlike, C_{2v}) ScC_3 in 2A_2 and 4B_1 electronic states (see Fig. 5.1 and 5.2).

State	Vibrational mode	Frequency (cm^{-1})	Infrared intensity (km/mol)
2A_2	$\nu_1(a_1)$	1256	4
	$\nu_2(a_1)$	792	2
	$\nu_3(a_1)$	601	80
	$\nu_4(b_1)$	415	70
	$\nu_5(b_2)$	1523	9
	$\nu_6(b_2)$	368	23
4B_1	$\nu_1(a_1)$	1277	10
	$\nu_2(a_1)$	638	26
	$\nu_3(a_1)$	532	89
	$\nu_4(b_1)$	455	8
	$\nu_5(b_2)$	1517	18
	$\nu_6(b_2)$	363	25

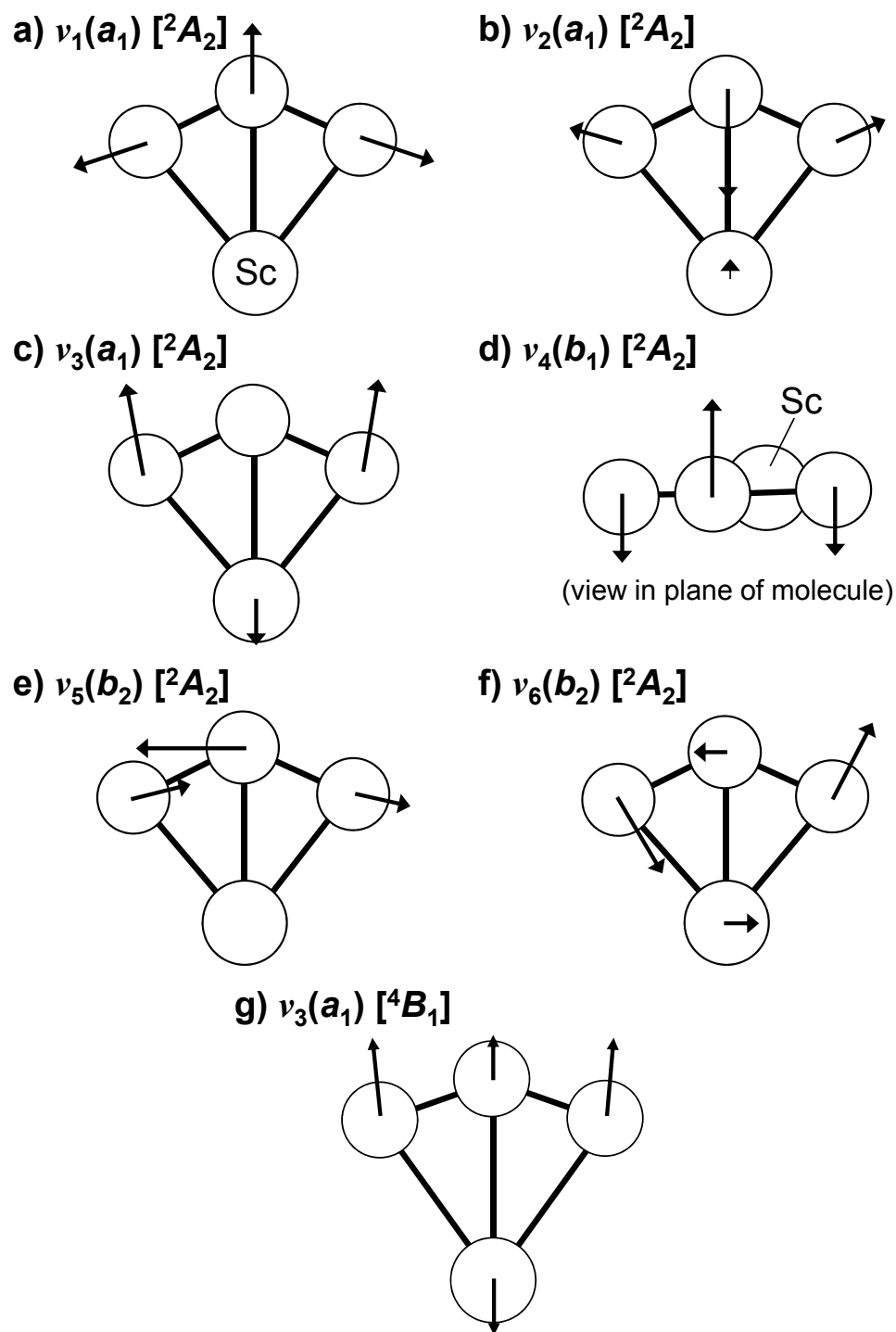


Figure 5.2 [(a)-(f)] The B3LYP/6-311G(3df, 3pd) predicted vibrational modes for ScC_3 in the 2A_2 electronic state. Vectors show the displacement of the atoms. (g) In the $\nu_3(a_1)$ fundamental in the 4B_1 state, the C_β atom significantly participates in the vibration.

5.3 EXPERIMENTAL PROCEDURES

Fanlike ScC₃ was produced by the simultaneous ablation of scandium (ESPI, 99.9% purity) and carbon rods using pulsed 1064 nm Nd:YAG lasers (Spectra Physics) in a vacuum maintained at $\sim 10^{-7}$ Torr or better. The resulting vapor was co-deposited with high purity Ar (99.995% purity, Matheson Tri-Gas) on the surface of a gold-plated mirror maintained at ~ 10 K by a closed-cycle refrigeration system (ARS, Displex). The total deposition time was ~ 100 min. In order to optimize the yield of C₃ for reaction with Sc atoms, laser powers of ~ 1.6 W were used to ablate the scandium rod and ~ 0.18 W for the ¹³C-enriched carbon rod. Both rods were continuously rotated and translated to ensure a uniform evaporation of their surfaces. Carbon rods with $\sim 30\%$ ¹³C enrichment were fabricated in the lab by thoroughly mixing ¹²C (99.9995% purity, Alfa Aesar) and ¹³C (99.3% purity, Isotec) powders and pressing at $\sim 4.5 \times 10^5$ kPa. Typical dimensions for the carbon rods were ~ 0.9 cm diameter and ~ 1.4 cm length.

Infrared absorption spectra were recorded over a range of 500-3500 cm⁻¹ at a resolution 0.2 cm⁻¹ using a Bomem DA3.16 Fourier transform spectrometer with a KBr beamsplitter and a liquid nitrogen cooled HgCdTe detector. After evaporation, the matrix sample was annealed for ~ 6 min at specified temperatures between 20 and 40 K and then quenched to 10 K. This procedure enabled formation of larger molecules from neighboring smaller molecules or atoms by diffusion.

5.4 RESULTS AND ANALYSIS

Potential scandium carbide absorptions in the 500-3500 cm⁻¹ range were identified by comparing spectra produced by the ablation of scandium and pure ¹²C graphite rods to spectra produced by pure graphite ablation. Three candidates for scandium carbide absorption bands

were found at 557.0, 1190.7, and 1478.0 cm^{-1} . The absorption at 557.0 cm^{-1} had the strongest intensity. The intensity ratio of the 1478.0 cm^{-1} absorption to the 557.0 cm^{-1} band was consistently $\sim 27\%$, and of the 1190.7 cm^{-1} absorption to the 557.0 cm^{-1} band was consistently $\sim 5\%$. The intensity ratios of the three bands remained constant with annealing, which suggested that the three absorption bands were vibrations of the same molecule. None of the bands was visible in spectra recorded immediately following deposition, but the all three bands grew in on annealing, particularly at temperatures $\sim 25\text{-}30$ K, which suggests that the molecule did not form during deposition but by diffusion within the matrix. The ablation of a pure scandium rod with a carbon rod pressed from mixed ^{12}C and ^{13}C powders, in order to observe isotopic shifts, produced additional absorption features to the low-frequency side of each of the 557.0, 1190.7, and 1478.0 cm^{-1} candidate scandium carbide bands (§§5.4.1-5.4.3). It should be noted that the intensities of the isotopic shifts in the resulting spectra indicate that the carbon isotopes are not completely randomized because of the different evaporation characteristics of the graphite and ^{13}C materials used to make the carbon rod.

Already, several considerations suggest fanlike ScC_3 as a possible identification for the molecule. As discussed in Chapter II (§2.5), the low laser power used to ablate the carbon rod during deposition produces predominantly C_3 clusters. The dominance of the $\nu_3(\sigma_u)=2038.9$ cm^{-1} fundamental of linear C_3 in the observed spectra suggests that the three candidates for scandium carbide absorptions are vibrations of a C_3 bearing molecule. Additionally, the absorption at 557.0 cm^{-1} is consistent with the 560 ± 30 cm^{-1} frequency measured for ScC_3 in the PE study of Wang and Li and for which their DFT investigation predicted a fanlike geometry.²⁹ Furthermore, the vibrational fundamentals of fanlike TiC_3 (§4.4) observed at 624.3 and 1484.2 cm^{-1} are in the same regions of the spectrum as two of the candidate scandium carbide absorptions, 557.0 and 1478.0 cm^{-1} , respectively.

The observation of ^{13}C isotopic shifts for the observed candidate bands and comparisons with DFT simulated isotopic spectra provide the critical data for identifying the molecular species, its structure, and electronic state. As was discussed, previous theoretical investigations predicted the 2A_2 and 4B_1 electronic states of fanlike ScC_3 to be separated by $\sim 6\text{-}10$ kcal/mol. The doublet state was predicted by several investigations^{29,36,74} to be the ground state, although theoretical simulations in one study⁷³ suggested a quartet ground state; therefore, it is worth comparing the DFT simulated isotopic shift patterns for both electronic states to the observed isotopic shift patterns.

5.4.1 *The $\nu_5(b_2)$ vibrational fundamental*

Figure 5.3(a) shows the isotopic spectrum for the 1478.0 cm^{-1} band in which five distinct isotopic shifts are observed. The isotopic shift pattern for the $\nu_4(\sigma_u)=1446.6\text{ cm}^{-1}$ fundamental of C_5 occurring in the vicinity is also labeled. As can be seen in Table 5.1, the 1478.0 cm^{-1} band is a possible candidate for the $\nu_5(b_2)$ fundamental of either the doublet or quartet state. Figure 5.2(e) for the 2A_2 state shows that $\nu_5(b_2)$ is an asymmetric carbon stretching mode in which the metal does not participate significantly (the vibrational motion is similar for the quartet state). The intensities of the ^{13}C isotopic shifts are consistent with those measured for the $\nu_3(\sigma_u)$ fundamental of C_3 (not shown), thus allowing easy assignment of the isotopic shifts to their respective isotopomers. In Fig. 5.3(a) the strongest shift at 1468.2 cm^{-1} has approximately twice the intensity of the shift at 1442.4 cm^{-1} , which is $\sim 25\%$ of the intensity of the main band at 1478.0 cm^{-1} . These are the singly ^{13}C -substituted isotopic shifts for the equivalent 13-12-12 and unique 12-13-12 isotopomers, respectively. The carbon atoms of the fanlike geometry are labeled following the convention of Fig. 5.1(a) as $\text{C}_\alpha\text{-C}_\beta\text{-C}_\alpha$; for brevity, the metal atom is not included in this notation. Doubly ^{13}C -substituted isotopic shifts, with intensities $\sim 23\%$ and $\sim 11\%$ of the

main band, are observed at 1432.4 and 1457.3 cm^{-1} , respectively, for the equivalent 13-13-12 and unique 13-12-13 isotopomers. Assuming that the Sc atom does not participate significantly in the vibration, the frequency of the fully ^{13}C substituted (13-13-13) isotopic shift can be estimated in the harmonic approximation as $\sqrt{12/13} \times 1478.0 \text{ cm}^{-1} = 1420.0 \text{ cm}^{-1}$, which is very close to the observed 1421.3 cm^{-1} absorption. This confirms that the absorption belongs to the fully ^{13}C -substituted isotopomer.

Figures 5.3(b)-(c) show the DFT simulated ^{13}C shift spectra for the $\nu_5(b_2)$ fundamental measured at 1478.0 cm^{-1} for fanlike ScC_3 in its 2A_2 and 4B_1 states. Visually, the simulated spectra for both states match the experimental data well. Table 5.2 quantifies the agreement between the observed and predicted isotopic shifts for the two states. The first column lists the electronic state and the second, the isotopomers of ScC_3 , following the convention of the spectrum in Fig. 5.3(a). Column 3 (ν_{obs}) lists the experimentally measured frequencies of the fundamental and isotopic shifts. Column 4 (ν_{DFT}) shows the DFT predicted frequencies of the fundamental and shifts and column 5 (ν_{sc}) lists the isotopic shift frequencies scaled for comparison to the experimental frequencies. Scaling for each state is accomplished by multiplying the predicted isotopic shift frequencies (ν_{DFT}) by the ratio of the observed fundamental to the DFT predicted fundamental (see Table 5.2 notes). The last column shows the difference between the measured and predicted isotopic shifts, $\Delta\nu = \nu_{\text{obs}} - \nu_{\text{sc}}$. The agreement of the experimentally measured isotopic shift frequencies with those predicted by theory is very good, with $\Delta\nu \leq 1.5 \text{ cm}^{-1}$ for both electronic states. The singly ^{13}C -substituted equivalent 13-12-12 and unique 12-13-12 shifts are at 1468.2 and 1442.4 cm^{-1} , respectively. The double ^{13}C -substituted shifts are at 1432.4 and 1457.3 cm^{-1} for the equivalent 13-13-12 and unique 13-12-13 isotopomers, respectively. The 13-13-13 isotopic shift is at 1421.3 cm^{-1} . The slightly larger discrepancy for the 13-13-13 isotopomer is likely due to different anharmonicity effects between

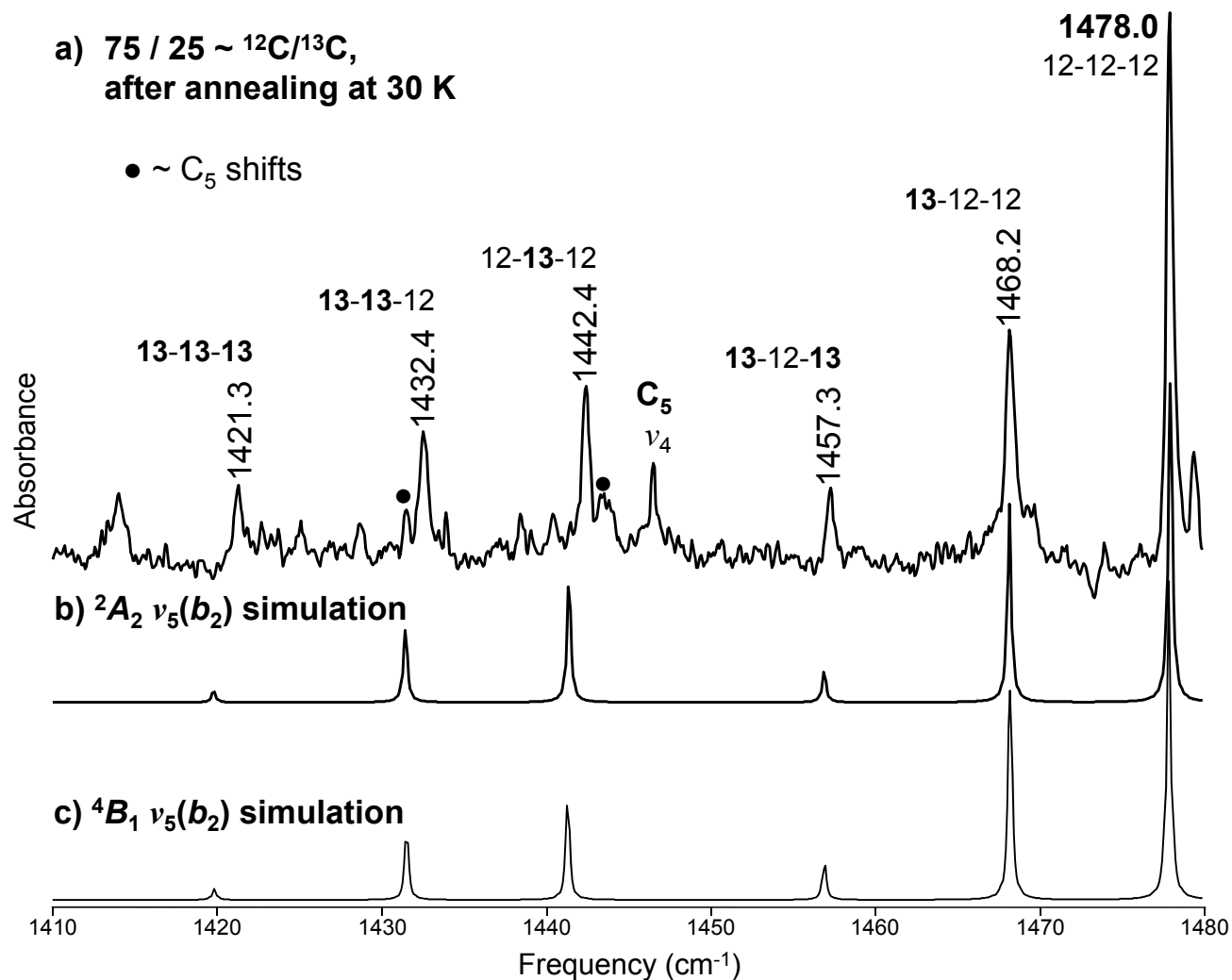


Figure 5.3 The $\nu_5(b_2)=1478.0 \text{ cm}^{-1}$ fundamental of fanlike ScC_3 . (a) ^{13}C -enriched isotopic spectrum after annealing at 30 K; the DFT-B3LYP/6-311G(3df, 3pd) simulated isotopic spectra using 25% ^{13}C enrichment for the (b) 2A_2 and (c) 4B_1 electronic states over the 1410-1480 cm^{-1} region. The isotopic spectrum for C_5 is labeled. Isotopic shift frequencies and isotopomers in the spectrum in (a) are labeled according to the convention of Table 5.2 and Fig. 5.1.

Table 5.2 Comparison of observed ^{13}C isotopic shift frequencies (cm^{-1}) to DFT-B3LYP/6-311G(3df, 3pd) predicted isotopic frequencies for the $\nu_5(b_2)$ mode of fanlike (C_{2v}) ScC_3 in the 2A_2 and 4B_1 electronic states (see Fig. 5.3).

State	Isotopomer Sc-C $_{\alpha}$ -C $_{\beta}$ -C $_{\alpha}$	Observed ν_{obs} (cm^{-1})	DFT Calculated ν_{DFT} (cm^{-1})	Scaled ν_{sc} (cm^{-1})	Difference $\Delta\nu$ (cm^{-1})
2A_2	Sc-12-12-12	1478.0	1522.7	1478.0 ^a	---
	Sc- 13 -12-12	1468.2	1512.6	1468.2	0.0
	Sc-12- 13 -12	1442.4	1485.0	1441.4	1.0
	Sc- 13 - 13 -12	1432.4	1474.8	1431.5	0.9
	Sc- 13 -12- 13	1457.3	1501.0	1456.9	0.4
	Sc- 13 - 13 - 13	1421.3	1462.8	1419.9	1.4
4B_1	Sc-12-12-12	1478.0	1517.1	1478.0 ^b	---
	Sc- 13 -12-12	1468.2	1507.2	1468.4	-0.2
	Sc-12- 13 -12	1442.4	1479.5	1441.4	1.0
	Sc- 13 - 13 -12	1432.4	1469.4	1431.5	0.9
	Sc- 13 -12- 13	1457.3	1495.6	1457.1	0.2
	Sc- 13 - 13 - 13	1421.3	1457.4	1419.8	1.5

^a The predicted 2A_2 shifts in column 5 are scaled by a factor of $1478.0/1522.7=0.97064$.

^b The predicted 4B_1 shifts in column 5 are scaled by a factor of $1478.0/1517.1=0.97423$.

the $^{12}\text{C}_3$ and $^{13}\text{C}_3$ isotopomers. The absorption at 1478.0 cm^{-1} may, therefore, be assigned as the $\nu_5(b_2)$ fundamental of fanlike ScC_3 although, as we have seen, the simulated isotopic shift spectra for this mode do not allow for a definite assignment of the ground electronic state.

5.4.2 *The $\nu_3(a_1)$ vibrational fundamental*

Figure 5.4(a) shows ^{13}C isotopic shifts at 550.0 and 543.0 cm^{-1} that are observed to the low frequency side of the main 557.0 cm^{-1} band. The 557.0 cm^{-1} absorption is the most intense scandium carbide band and is a good candidate for the $\nu_3(a_1)$ fundamental of either the doublet or quartet electronic states predicted at 601 and 532 cm^{-1} , respectively. A similar isotopic shift pattern was observed in the previously discussed study of fanlike TiC_3 (§4.4.2) in which the $\nu_3(a_1)$ fundamental at 624.3 cm^{-1} was accompanied by one very distinct shift at 616.8 cm^{-1} and a second, weaker shift at 608.4 cm^{-1} (see Fig. 4.7). Considerable overlapping of isotopic shifts occurred. The unique 12-13-12 isotopomer shift was overlapped by the fundamental. The equivalent singly ^{13}C -substituted isotopomers (13-12-12) and the equivalent doubly ^{13}C -substituted isotopomers (13-13-12) contributed to the intensity of the stronger shift at 616.8 cm^{-1} . The unique, doubly ^{13}C -substituted isotopomer (13-12-13) and the Ti^{13}C_3 isotopomer contributed to the weaker shift at 608.4 cm^{-1} . Thus, the isotopic shift pattern observed for the $\nu_3(a_1)$ fundamental of fanlike TiC_3 suggests an explanation for the similar pattern observed in the spectrum in Fig. 5.4(a).

An analysis of the spectra of Fig. 5.4(b) and (c) using the illustrations of the $\nu_3(a_1)$ modes in Fig. 5.2(c) and 5.2(g) is instructive. In the doublet state, the major participants are the Sc atom and the outer C atoms (C_α) while the central C atom (C_β) is not significantly displaced [Fig. 5.2(c)], resulting in a significant overlapping of isotopic shifts. In the quartet state, the C_β site is displaced significantly in the vibrational motion [Fig. 5.2(g)], so the isotopic shifts which are

overlapped in the 2A_2 simulated spectrum [Fig. 5.4(b)] are distinguishable in the 4B_1 simulated spectrum [Fig. 5.4(c)].

The shift pattern calculated for the $\nu_3(a_1)$ fundamental in the 2A_2 state, shown in Fig. 5.4(b), matches the isotopic shift pattern measured for the 557.0 cm^{-1} band in Fig. 5.4(a) very well. In contrast, a comparison of the DFT predicted isotopic shift pattern in Fig. 5.4(c) with the experimentally measured pattern for the $\nu_3(a_1)$ fundamental shows that the quartet state cannot be the ground state. An unresolved feature observed on the left shoulder of the main 557.0 cm^{-1} absorption might suggest the possibility that it is the isotopic shift predicted at 555.1 cm^{-1} for the 4B_1 state in Fig. 5.4(c), and if so, that the shifts predicted to the low frequency side of the 551.6 and 545.6 cm^{-1} bands might be unresolved and contained within the envelopes of the observed bands at 550.0 and 543.0 cm^{-1} , respectively. However, the latter two assignments would lead to discrepancies of ~ 1.5 and 2.6 cm^{-1} between predicted and observed shifts which are unacceptably large compared to the 14 cm^{-1} range of the observed spectrum. Moreover, deconvolution of the left shoulder feature observed on the 557.0 cm^{-1} band shows that it is only $\sim 10\%$ the intensity of the main band, which is inconsistent with the $\sim 25\%$ ${}^{13}\text{C}$ enrichment observed in the $\nu_5(b_2)$ isotopic shift spectrum discussed previously (§5.4.1). The better agreement of the observed shifts with the doublet state predictions is clearly demonstrated in Table 5.3. Discrepancies between observed shifts and those predicted for the quartet state are significantly larger than those for the doublet state.

Further evidence that 4B_1 is not the ground state is provided by the absence of a suitable candidate for the $\nu_2(a_1)$ fundamental predicted at 638 cm^{-1} even though, as shown in Table 5.1, its intensity is predicted to be approximately twice that of the observed $\nu_1(a_1)=1190.7\text{ cm}^{-1}$ fundamental (§5.4.3) and more intense than the observed $\nu_5(b_2)=1478.0\text{ cm}^{-1}$ (§5.4.1) if they belonged to the quartet state. The isotopic spectrum in the $620\text{-}680\text{ cm}^{-1}$ region is shown in Fig.

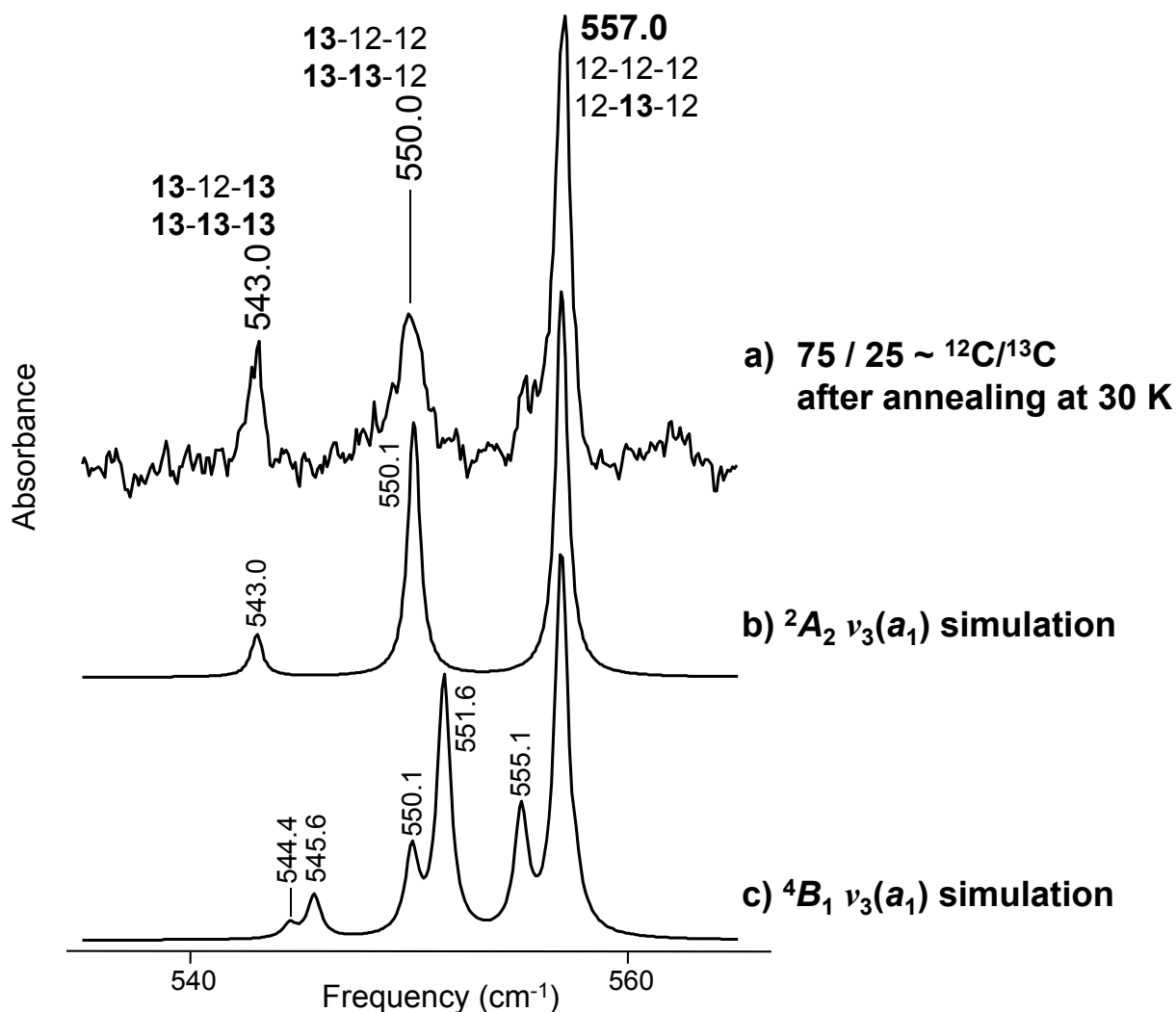


Figure 5.4 The $\nu_3(a_1)=557.0 \text{ cm}^{-1}$ fundamental of fanlike ScC_3 . (a) The ^{13}C -enriched isotopic spectrum after annealing at 30 K; the DFT-B3LYP/6-311G(3df, 3pd) simulated isotopic spectra using 25% ^{13}C enrichment for the (b) 2A_2 and (c) 4B_1 electronic states over the 540–560 cm^{-1} region. Measured and predicted isotopic shift frequencies are labeled. The isotopomers are labeled in (a) following the convention of Table 5.3 and Fig. 5.1.

Table 5.3 Comparison of observed ^{13}C isotopic shift frequencies (cm^{-1}) to DFT-B3LYP/6-311G(3df, 3pd) predicted isotopic frequencies for the $\nu_3(a_1)$ mode of fanlike (C_{2v}) ScC_3 in the 2A_2 and 4B_1 electronic states (see Fig. 5.4).

State	Isotopomer Sc- C_α - C_β - C_α	Observed ν_{obs} (cm^{-1})	DFT Calculated ν_{DFT} (cm^{-1})	Scaled ν_{sc} (cm^{-1})	Difference $\Delta\nu$ (cm^{-1})
2A_2	Sc-12-12-12	557.0	601.2	557.0 ^a	---
	Sc- 13 -12-12	550.0	593.9	550.1	-0.1
	Sc-12- 13 -12	--- ^b	601.0	556.9	---
	Sc- 13 - 13 -12	550.0	593.8	550.1	-0.1
	Sc- 13 -12- 13	543.0	586.1	543.0	0.0
	Sc- 13 - 13 - 13	--- ^c	586.1	543.0	---
4B_1	Sc-12-12-12	557.0	531.7	557.0 ^d	---
	Sc- 13 -12-12	550.0	526.6	551.6	-1.6
	Sc-12- 13 -12	not observed	530.0	555.1	---
	Sc- 13 - 13 -12	550.0	525.2	550.1	-0.1
	Sc- 13 -12- 13	543.0	520.9	545.6	-2.6
	Sc- 13 - 13 - 13	not observed	519.8	544.4	---

^a The predicted 2A_2 shifts in column 5 are scaled by a factor of $557.0/601.2=0.92648$.

^b Shift is overlapped by the fundamental at 557.0 cm^{-1} (Sc-12-12-12).

^c Shift is overlapped by the isotopic shift at 543.0 cm^{-1} (Sc-13-12-13).

^d The predicted 4B_1 shifts in column 5 are scaled by a factor of $557.0/531.7=1.018$.

5.5(a). Three prominent bands are observed in the ^{13}C -enriched spectrum of Fig. 5.5(a) at 639.3, 658.9, and 673.2 cm^{-1} , but none is a suitable candidate for the $\nu_2(a_1)$ fundamental of the quartet state. The band at 639.3 cm^{-1} exhibits no isotopic shifts and is thus immediately excluded from consideration. Comparison of the simulated shift spectrum for $\nu_2(a_1)$ scaled for comparison with the 658.9 and 673.2 cm^{-1} bands similarly eliminates them as candidates. The 658.9 cm^{-1} absorption has a band to the low frequency side at 655.6 cm^{-1} , but with a relative intensity of $\sim 12\%$, it is far too weak to be the single ^{13}C substitution at the two equivalent C_α sites, and there is no evidence of the other expected shifts [Fig. 5.5(b)]. For the 673.2 cm^{-1} absorption, the 670.1 and 655.6 cm^{-1} bands fail as shifts since they do not match the simulated spectrum either in their frequencies or in their intensities relative to the main band [Fig. 5.5(c)]. Thus, none of the three bands in the 620-680 cm^{-1} region can be the $\nu_2(a_1)$ fundamental of the quartet state of ScC_3 , and the assignment of the 557.0 cm^{-1} band to the $\nu_3(a_1)$ fundamental of the 2A_2 state is reinforced. Additionally, the cryogenic temperature of the Ar matrix (10 K) makes it likely that the molecule is in its ground electronic state.⁴¹

Therefore, since the isotopic spectrum measured for the $\nu_3(a_1)$ fundamental at 557.0 cm^{-1} indicates that the molecule is fanlike ScC_3 in the doublet electronic state, which was predicted to be the most likely ground state in previous theoretical investigations,³⁶ it is concluded that the 2A_2 state, and not the quartet state, is the electronic ground state of fanlike ScC_3 . Additionally, the 560 ± 30 cm^{-1} frequency assigned as a symmetric metal-carbon stretch of ScC_3 in its doublet state by a previous PE spectroscopy study²⁹ is consistent with the $\nu_3(a_1)$ fundamental assigned here. It is worth noting that in that study two states of ScC_3 were reported, separated by ~ 9.7 kcal/mol, with the doublet state predicted to be the ground state. Additional theoretical investigations support those conclusions with the quartet state being the higher energy state.^{36,74}

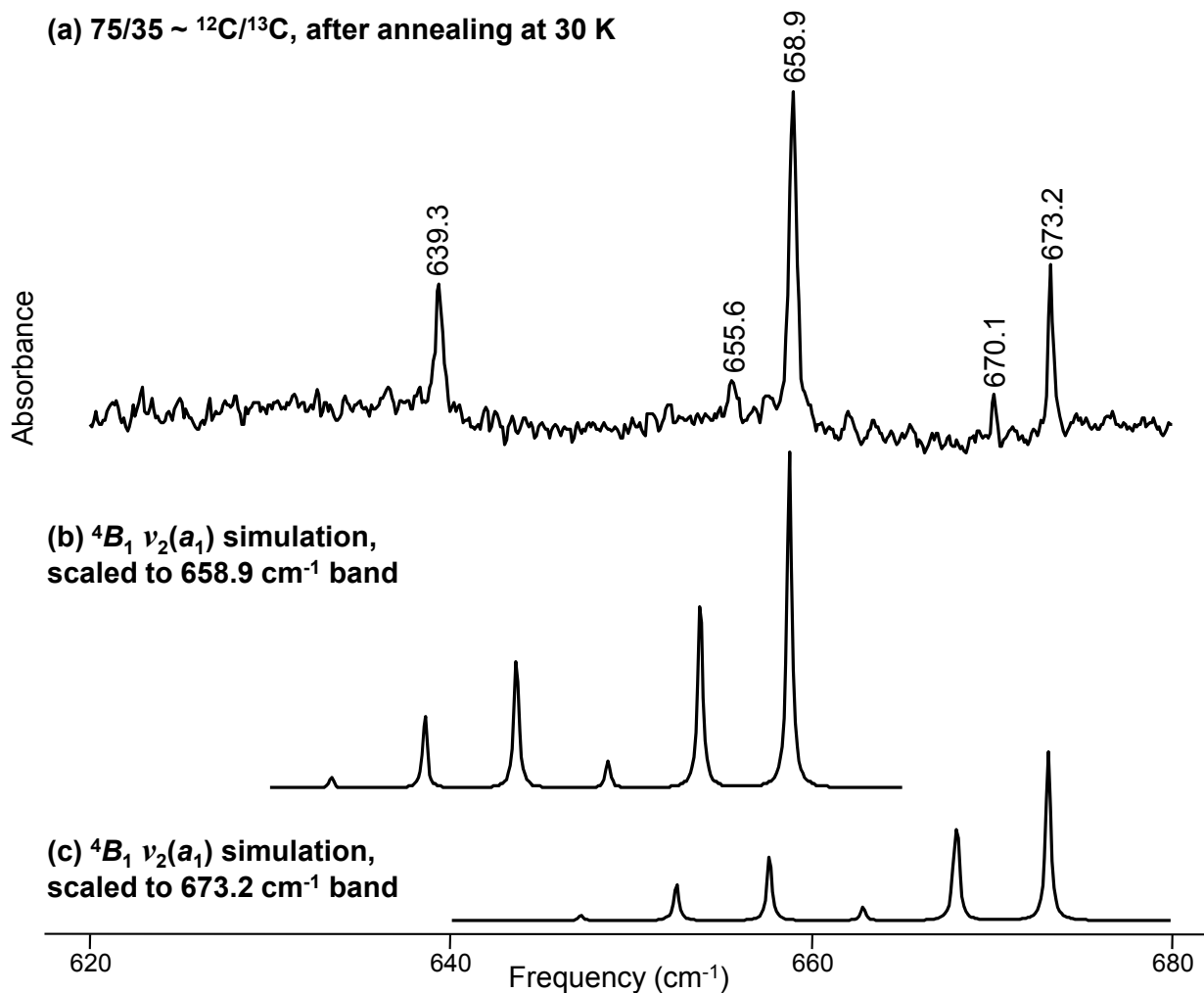


Figure 5.5 (a) The ^{13}C -enriched isotopic spectra after annealing at 30 K in the 620-680 cm^{-1} range. The 4B_1 simulation of the $\nu_2(a_1)$ isotopic spectrum is scaled for comparison with the bands observed at (b) 658.9 and (c) 673.2 cm^{-1} . None of the bands is a suitable candidate for the $\nu_2(a_1)$ fundamental of the quartet state.

5.4.3 The $\nu_1(a_1)$ vibrational fundamental

Figure 5.6(a) shows the isotopic shift spectrum associated with the 1190.7 cm^{-1} band. The analysis of this pattern is complicated by the weakness of the absorption, the low signal-to-noise ratio in this region of the spectrum which complicates measuring the intensities of the shifts, and the isotopic shifts for the $\nu_5(\sigma_u)=1197.3\text{ cm}^{-1}$ fundamental of C_6 , which are labeled. However, the 1190.7 cm^{-1} grew in consistent with the intensities of the other ScC_3 bands at 1478.0 and 557.0 cm^{-1} , suggesting that all three are vibrations of the same molecule. Three isotopic shifts bands in the spectrum can be distinguished at 1182.8 , 1171.6 and 1163.0 cm^{-1} .

Figures 5.6(b)-(c) show the DFT simulated isotopic spectrum shifted from the $\nu_1(a_1)$ fundamental at 1190.7 cm^{-1} for the doublet and quartet states, respectively. Table 5.4 shows that the simulated isotopic shift patterns for both electronic states are, similar to the case for the $\nu_5(b_2)$ fundamental, in good agreement with the measured isotopic shifts; however, the analysis of the $\nu_3(a_1)$ fundamental (§5.4.2) has already shown that the doublet is the ground state. The equivalent singly ^{13}C -substituted isotopomers (13-12-12) contribute to the shift at 1171.6 cm^{-1} . The unique singly ^{13}C -substituted shift (12-13-12) is at 1182.8 cm^{-1} . One of the doubly ^{13}C -substituted shifts, from the equivalent 13-13-12 isotopomers, is observed at 1163.0 cm^{-1} . The noise in this region of the spectrum precludes the observation of the unique double ^{13}C -substituted isotopic shift (13-12-13) and the fully ^{13}C -substituted isotopic shift; however, the measured shifts in combination with the consistent ratio of the intensity of the 1190.7 cm^{-1} band to the other confirmed ScC_3 fundamentals allows for the assignment of the $\nu_1(a_1)=1190.7\text{ cm}^{-1}$ fundamental. Figure 5.2(a) shows that $\nu_1(a_1)$ is a symmetric carbon stretching mode in which the Sc atom does not participate significantly.

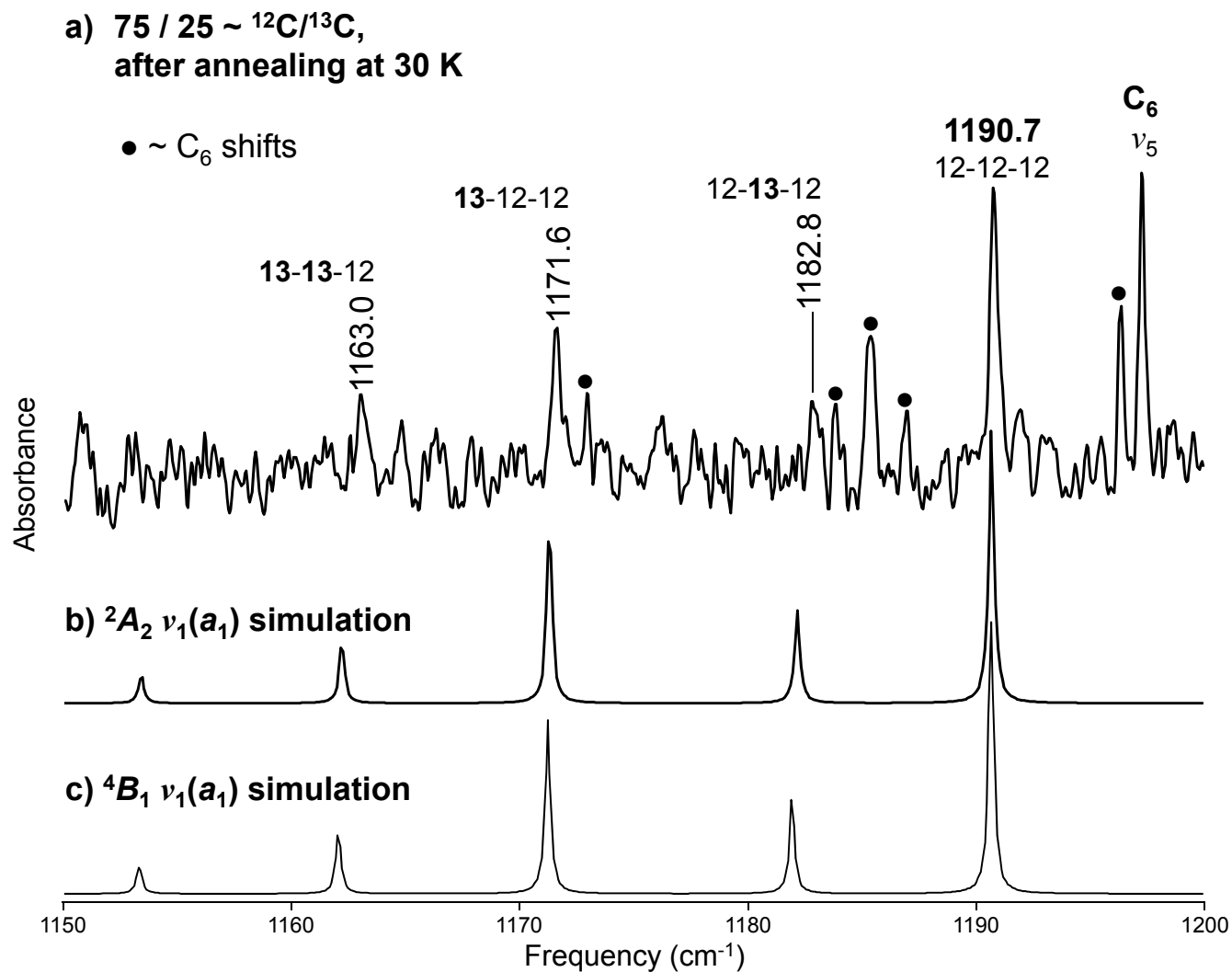


Figure 5.6 The $\nu_1(a_1)=1190.7 \text{ cm}^{-1}$ fundamental of fanlike ScC_3 . (a) The ^{13}C -enriched isotopic spectrum after annealing at 30 K; the DFT-B3LYP/6-311G(3df, 3pd) simulated isotopic spectra using 25% ^{13}C enrichment for the (b) $^2\text{A}_2$ and (c) $^4\text{B}_1$ electronic states over the 1150-1200 cm^{-1} region. The isotopic spectrum for C_6 is labeled. Spectrum (a) shows the isotopic shift frequencies, and isotopomers are labeled following the convention of Table 5.4 and Fig. 5.1.

Table 5.4 Comparison of observed ^{13}C isotopic shift frequencies (cm^{-1}) to DFT-B3LYP/6-311G(3*df*, 3*pd*) predicted isotopic frequencies for the $\nu_1(a_1)$ mode of fanlike (C_{2v}) ScC_3 in the 2A_2 and 4B_1 electronic states (see Fig.5.6).

State	Isotopomer Sc- C_α - C_β - C_α	Observed ν_{obs} (cm^{-1})	DFT Calculated ν_{DFT} (cm^{-1})	Scaled ν_{sc} (cm^{-1})	Difference $\Delta\nu$ (cm^{-1})
2A_2	Sc-12-12-12	1190.7	1256.4	1190.7 ^a	---
	Sc- 13 -12-12	1171.6	1235.9	1171.3	0.3
	Sc-12- 13 -12	1182.8	1247.4	1182.2	0.6
	Sc- 13 - 13 -12	1163.0	1226.3	1162.2	0.8
	Sc- 13 -12- 13	---	1217.1	1153.5	---
	Sc- 13 - 13 - 13	---	1207.1	1144.0	---
4B_1	Sc-12-12-12	1190.7	1277.3	1190.7 ^b	---
	Sc- 13 -12-12	1171.6	1256.4	1171.2	0.4
	Sc-12- 13 -12	1182.8	1267.9	1181.9	0.9
	Sc- 13 - 13 -12	1163.0	1246.5	1162.0	1.0
	Sc- 13 -12- 13	---	1237.1	1153.2	---
	Sc- 13 - 13 - 13	---	1227.1	1143.9	---

^a The predicted 2A_2 shifts in column 5 are scaled by a factor of $1190.7/1256.4=0.94771$.

^b The predicted 4B_1 shifts in column 5 are scaled by a factor of $1190.7/1277.3=0.93220$.

5.4.4 Other vibrational fundamentals of ScC₃

Additional vibrational fundamentals of fanlike ScC₃ in the ²A₂ state are predicted at ~792, 415, and 368 cm⁻¹. The latter two bands are not accessible to the KBr beamsplitter and HgCdTe detector combination used in this study, which has a lower limit of ~500 cm⁻¹. No suitable candidate was observed for the $\nu_2(a_1)$ fundamental predicted at 792 cm⁻¹, the weakest fundamental.

5.5 CONCLUSIONS

This study of ScC₃ using FTIR measurements and DFT calculations has found the ground state structure of ScC₃ to be a fanlike (C_{2v}) geometry with a ²A₂ electronic state, previously predicted to be the ground state,³⁶ and not a nearby ⁴B₁ state. Comparisons of the observed FTIR ¹³C isotopic shift spectra to DFT simulated isotopic spectra have enabled the first identification of three vibrational fundamentals. While the simulated isotopic shift spectra for the $\nu_1(a_1)$ and $\nu_5(b_2)$ fundamentals of both electronic states match measured shifts well, the isotopic spectra for the $\nu_3(a_1)$ fundamental measured at 557.0 cm⁻¹ decisively indicate that the ground electronic state of the molecule is ²A₂. The two remaining vibrational fundamentals that have been assigned are the $\nu_1(a_1)$ =1190.7 cm⁻¹ symmetric carbon stretch and the $\nu_5(b_2)$ =1478.0 cm⁻¹ asymmetric carbon stretch. The absence of a candidate for the strong $\nu_2(a_1)$ fundamental predicted for the quartet state adds further support for the conclusion that only doublet ScC₃ has been produced. Finally, the results of a previous PE spectroscopy investigation²⁹ of ScC₃ are consistent with the assignment of the $\nu_3(a_1)$ metal-carbon stretching fundamental made here.

CHAPTER VI

CONCLUSIONS AND FUTURE RESEARCH

6.1 CONCLUSIONS

This dissertation reports results from FTIR measurements and DFT calculations in the first systematic investigation of the structures and vibrational fundamentals of small transition-metal carbide clusters. Bates³⁹ has reported the results from contemporaneous investigations of CrC₃, CoC₃, and Al_nC₃ ($n=1,2$), and the present work reports the structures and vibrational fundamentals of linear NiC₃Ni, cyclic TiC₃, and cyclic ScC₃. The clusters were produced by trapping the vapor that results from laser ablation of transition metal and carbon rods in solid Ar at ~10 K. Comparisons of observed vibrational fundamentals and ¹³C isotopic shifts to those predicted by DFT have enabled the first unambiguous identification of the molecular structures and vibrational fundamentals for these species.

6.1.1 Linear NiC₃Ni

The investigation of NiC₃Ni reported in Chapter III is the first experimental and theoretical study of the molecule's structure and infrared spectrum. Although Ni₂C₃ was observed in a previous mass spectroscopy study,²⁶ structures for the molecule were not investigated. Furthermore, the possible structures for Ni₂C₃ were not discussed in previous theoretical reports investigating the structures of several Ni_mC_n clusters.⁵⁴⁻⁵⁸ The DFT investigation of linear NiC₃Ni found that the linear ($D_{\infty h}$) structure of the molecule is a transition state lying $\sim 5 \times 10^{-4}$ kcal/mol above a "relaxed", nearly linear (C_{2v}) ground state. The low energy separation of the

two structures suggests that the molecule may be slightly floppy, but is effectively linear. The calculated vibrational modes for both structures were similar, and the simulated isotopic shift spectra for the $\nu_3(\sigma_u)=1950.8\text{ cm}^{-1}$ fundamental of both structures matched the experimentally observed isotopic shift spectra equally well.

The results of this FTIR and DFT investigation of linear NiC_3Ni were published: R. E. Kinzer, Jr., C. M. L. Rittby, and W. R. M. Graham, *Fourier transform infrared observation of the $\nu_3(\sigma_u)$ vibration of NiC_3Ni in Solid Ar*, *J. Chem. Phys.* **128**, 064312 (2008).⁷⁶

6.1.2 Cyclic TiC_3

The investigation of cyclic (fanlike, C_{2v}) TiC_3 provided the first unambiguous evidence for the molecule's 1A_1 fanlike structure, which had been predicted by a previous DFT investigation⁶⁵ to be the ground state of the molecule. Two confirmed vibrational fundamentals and one tentative fundamental were measured. Comparison of FTIR observed and DFT simulated ^{13}C isotopic shift spectra enabled the assignment of the $\nu_3(a_1)=624.3\text{ cm}^{-1}$ symmetric metal-carbon stretch and $\nu_5(b_2)=1484.2\text{ cm}^{-1}$ asymmetric carbon-carbon stretch. An absorption at 573.8 cm^{-1} was provisionally assigned to the $\nu_4(b_1)$ fundamental. This is the first observation of the vibrational fundamentals of TiC_3 , and the $650\pm 30\text{ cm}^{-1}$ frequency reported as a symmetric metal-carbon stretch of TiC_3 in a previous PE spectroscopy study^{29,30} is consistent with the assignment for the $\nu_3(a_1)$ fundamental made in Chapter IV. The low-power evaporation technique, which evaporates the carbon rods with low power per unit area and produces predominantly C_3 chains (§2.5), was also developed during this investigation.

The results of this FTIR and DFT investigation of fanlike TiC_3 were published: R. E. Kinzer, Jr., C. M. L. Rittby, and W. R. M. Graham, *Vibrational spectrum of cyclic TiC_3 in solid Ar*, *J. Chem. Phys.* **125**, 074513 (2006).⁷⁷

6.1.3 Cyclic ScC₃

The investigation of ScC₃ using FTIR measurements and DFT calculations has found the ground state structure of ScC₃ to be a fanlike (C_{2v}) geometry with a ²A₂ electronic state, previously predicted to be the ground state,³⁶ and not a nearby ⁴B₁ state. Comparisons of FTIR observed ¹³C isotopic shift spectra to DFT simulations have enabled the first identification of three vibrational fundamentals. Although the simulated spectra for both electronic states match the measured spectra of the $\nu_1(a_1)=1190.7\text{ cm}^{-1}$ symmetric carbon-carbon stretch and $\nu_5(b_2)=1478.0\text{ cm}^{-1}$ asymmetric carbon-carbon stretch fundamentals equally well, isotopic shift spectra for the $\nu_3(a_1)=557.0\text{ cm}^{-1}$ fundamental decisively indicate that the doublet state, and not the quartet state, is the ground electronic state of the molecule. The absence of a suitable candidate for the $\nu_2(a_1)$ fundamental of the quartet state, which would be stronger than the observed $\nu_1(a_1)$ and $\nu_5(b_2)$ fundamentals, further reinforces the conclusion that only doublet ScC₃ was produced. Finally, the $560\pm 30\text{ cm}^{-1}$ frequency reported as a ScC₃ metal-carbon stretch in a previous PE spectroscopy investigation²⁹ is consistent with the assignment of the $\nu_3(a_1)$ fundamental made in Chapter V.

The results of this FTIR and DFT investigation of fanlike ScC₃ were published: R. E. Kinzer, Jr., C. M. L. Rittby, and W. R. M. Graham, *The vibrational spectrum of fanlike ScC₃ in solid Ar*, J. Chem. Phys. **129**, 184309 (2008).⁷⁸

6.2 FUTURE RESEARCH

6.2.1 Transition-Metal Carbides

The primary goal of future work should be the characterization of the structures and infrared spectra of additional transition metal-carbon clusters. Thus far, FTIR matrix and DFT

investigations have studied NiC_3Ni , TiC_3 , ScC_3 (reported in the present work), CrC_3 ,⁴⁴ CoC_3 ,⁴⁵ (Bates *et al.*), CuC_3 (Wang *et al.*),⁷⁹ and AgC_3 (Szczepanski *et al.*).⁸⁰ These studies are predominantly confined to the first-row transitional metals, and a logical step for further research by the TCU Molecular Physics Laboratory is to continue investigation of second- and third-row transition metals which have already been the subject of some theoretical investigation (*e.g.*, YC_n and LaC_n clusters).³⁸

Smaller and larger transition-metal carbides should be investigated. As was discussed previously (§1.2), MC_2 clusters are particularly relevant as they may serve as building blocks for the larger metcar cage structures [see Fig. 1.1(c)] and have been the subject of extensive theoretical investigation.⁵³ New FTIR investigations of the structures of MC_2 clusters could provide better results than PE spectroscopy and would be important for understanding their roles as metcar building blocks. Additionally, clusters with more than three carbon atoms or with several metal atoms, such as MC_n ($n>3$) and M_mC_n ($m\geq 2$), should be investigated. Experimental results for a large variety of metcar clusters would provide a useful resource for understanding the structures and formations of metallocarbohedrenes.

The low-power laser evaporation technique (§2.5) used in the present work and in work by Bates *et al.*⁴⁴⁻⁴⁶ has produced predominantly M_nC_3 species. The experimental procedures may need to be altered to produce a greater variety of structures. For example, the low-power technique for ablating the carbon rod may be modified so that, instead of using a low laser power (<1 W) over a tight diameter (~1 mm), the laser power may be increased and spread out over a larger diameter (~2-3 mm), thus producing larger carbon chains (C_n , $n>3$) for reaction with the metal atoms. An alternative approach is to use different sample rod materials. A new sintering technique developed in the investigation of germanium-carbon clusters by Gonzalez⁶⁰ may be useful for producing a greater variety of transition-metal carbide clusters. In that work, Ge and C

powders were pressed into a rod and sintered in a furnace for ~2-3 days near the melting point of Ge. This sintering approach facilitated the measurements of GeC_5Ge ,⁶⁰ GeC_3 ,⁴⁷ and low-intensity vibrations of GeC_3Ge .⁸¹ An analogous procedure using transition metals and carbon may be useful for producing metcar clusters besides $M_n\text{C}_3$ and observing low-intensity vibrations.

Finally, two specific clusters, FeC_3 and NiC_3 , should be considered. FeC_3 is important since iron is an astrophysically significant metal. A previous PE spectroscopy investigation of FeC_3 by Wang and Li measured a $480\pm 40\text{ cm}^{-1}$ frequency and predicted a triplet fanlike structure for the molecule.²⁹ Further CASPT2 and DFT theoretical investigations of FeC_3 predicted a 3B_1 fanlike ground state.⁸² A DFT investigation by Noya *et al.*⁸³ reinforced the triplet fanlike ground state and calculated a triplet linear structure only ~6 kcal/mol higher. Future experimental investigations by the Molecular Physics Laboratory may, therefore, be able to observe either the fanlike or linear structures. A previous PE investigation of NiC_3 measured a $480\pm 60\text{ cm}^{-1}$ frequency, but reported no possible structure for the molecule.²⁹ As was discussed in §3.1, the ground state nickel carbide structures, particularly NiC_3 , are subject to theoretical controversy. Competing linear and fanlike structures have been predicted for the ground state of NiC_3 ,^{56,57} and both structures are energetically well separated from the kite-shaped structure. A FTIR isotopic investigation of NiC_3 could observe either of the fanlike or linear states, and the results of such an observation would provide much needed experimental evidence useful for improving the modeling of nickel carbide clusters.

6.2.2 Other Metal Carbides

Future research should continue the investigation of metal (non-transition metal) carbide clusters. The infrared spectra of AlC_3 and AlC_3Al were measured in the Molecular Physics

Laboratory by Bates *et al.*,⁴⁶ and this work should be extended to other metals. Metal–carbon clusters with Al, Mg, Ca, and Na are anticipated to be astrophysically significant species because of the high astrophysical abundance of these metals. Similar to metallocarbohedrenes, metal dicarbides may also serve as building blocks for larger clusters. Therefore, the results of experimental investigations of metal-carbon clusters could also provide useful information needed to understand larger clusters and novel solid state materials.⁸⁴

There have been several theoretical investigations of the MgC_3 and CaC_3 clusters. Table 1.2, which lists confirmed molecules observed in the circumstellar shells of carbon star IRC+10216, shows several magnesium-bearing species, and so it may be anticipated that magnesium carbides such as MgC_3 are astrophysically significant. DFT investigations of MgC_n ($n=1-7$) clusters report that MgC_3 is “rhombic” (*i.e.*, kite-shaped) with isoenergetic singlet or triplet electronic ground states with two linear structures lying within 3 kcal/mol and two fanlike structures at $\sim 5-7$ kcal/mol.⁸⁵⁻⁸⁷ Six different structures are thus predicted within ~ 7 kcal/mol of the ground state,⁸⁵ and any of these structures could be observed in an Ar matrix investigation. Linear and cyclic CaC_3 have been investigated as part of a DFT investigation of CaC_n ($n=1-8$, including anions and cations) clusters.⁸⁸⁻⁹⁰ Fanlike (3B_1) CaC_3 was reported to be the ground state with a kite-shaped (3A_1) structure ~ 8 kcal/mol higher. Several fanlike and kite-shaped isomers lie 10-13 kcal/mol above the predicted ground state, and linear structures are even higher in energy, thus making CaC_3 similar to MgC_3 and its many low-lying isomers. There are no experimental reports of the vibrational frequencies of magnesium or calcium carbide clusters.

6.2.3 Transition Metal–Silicon–Carbon Clusters

Molecules composed of transition metal and silicon atoms are of interest because of the role they may play in a large variety of applications such as semiconductors, high-temperature

coatings, integrated circuits, ceramics, and nanodevices in which small clusters constitute the fundamental building blocks.^{91,92} Transition metal–silicon clusters are the subject of both theoretical and experimental investigation. DFT studies have investigated the structures of various sizes of MSi_n ($n=1-20$) clusters.⁹¹⁻⁹³ The structures reported by the theoretical investigation tend to be non-planar or cage-like, even for small clusters such as MSi_3 for which a pyramidal geometry was predicted to be the ground state structure.⁹¹ Experimental investigations have been principally mass spectroscopy and photodissociation studies which have observed large clusters such as MSi_n ($M= Cr, Ag, Au, Ag$ and $n=7,10,14,16$).^{94,95} The results of these studies suggest that the transition metal–silicon clusters take on very different geometries and “magic” numbers than those found for the metal carbides (§1.2). There have been no investigations of the vibrational spectra of these types of clusters.

Infrared observation of transition metal–silicon clusters will likely be experimentally challenging. Pure silicon clusters have been observed by the Molecular Physics Laboratory,⁴⁰ but because silicon is significantly more massive than carbon (28 vs. 12 amu) the vibrations of pure Si species are found towards the far-IR ($\sim 550\text{ cm}^{-1}$ and below) and a mylar beamsplitter and liquid helium-cooled far-infrared detectors will be necessary to observe the transition metal–silicon species. A possible “intermediate” step towards the characterization of the transition metal–silicon clusters may be the investigation and characterization of molecules composed of transition metal and silicon atoms with a carbon chain backbone. A carbon chain backbone would likely result in vibrational frequencies of fundamentals that are mainly C-C stretching modes that would be observable by the HgCdTe detector and KBr beamsplitter combination normally used in mid-infrared experiments and allow for the investigation of sample fabrication techniques.

REFERENCES

- ¹ B. C. Guo and A. W. Castleman, Jr. Advances in Metal and Semiconductor Research. Ed. Michael A. Duncan. Jai Press, London 1994. Vol. 2, 137.
- ² *Molecules in Space*. Retrieved 10 May 2009 from the Cologne Database for Molecular Spectroscopy (CDMS) at http://www.ph1.uni-koeln.de/vorhersagen/molecules/main_molecules.html. The main page is at <http://www.ph1.uni-koeln.de/vorhersagen/>.
- ³ *The 129 interstellar and circumstellar molecules*. Retrieved 23 March 2009 from NRAO astronomer Al Wooten's web page at <http://www.cv.nrao.edu/~awootten/allmols.html>. Wooten's main page is <http://www.cv.nrao.edu/~awootten/>.
- ⁴ A. Burrows, M. Dulick, C. W. Bauschlicher, Jr., and P. F. Bernath, *Astrophys. J.* **624**, 988 (2005).
- ⁵ G. von Helden, A. G. G. M. Tielens, D. van Heijnsbergen, M. A. Duncan, S. Hony, L. B. F. M. Waters, and G. Meijer, *Science* **288**, 313 (2000).
- ⁶ Y. Kimura, J. A. Nuth III, and F. T. Ferguson, *Astrophys. J.* **632**, L159 (2005).
- ⁷ S. Kwok, K. Volk, and B. J. Hrivnak, *Astrophys. J.* **573**, 720 (2002).
- ⁸ A. Li, *Astrophys. J. Lett.* **599**, L45 (2003).
- ⁹ T. Posch, H. Mutschke, and A. Andersen, *Astrophys. J.* **616**, 1167 (2004).
- ¹⁰ L. M. Ziurys, *Proc. Nat. Acad. Sci.* **103**, 12274 (2006).
- ¹¹ Harris, D. C. and Betrouluci M. D. Symmetry and Spectroscopy: An Introduction to Vibrational and Electronic Spectroscopy. Dover, New York 1989. p. 98.
- ¹² P. F. Bernath, K. H. Hinkle, and J. J. Keady, *Science* **244**, 562 (1989).

- ¹³ *The Next Generation Airborne Observatory*. Retrieved July 2006 from the Stratospheric Observatory For Infrared Astronomy at <http://www.sofia.usra.edu/Sofia/sofia.html>. The main page is located at <http://www.sofia.usra.edu/index.html>.
- ¹⁴ *Seeing Stars with SOFIA*. Retrieved July 2006 from <http://www.sofia.usra.edu/Sofia/sofia.html>. The home page is <http://www.sofia.usra.edu/index.html>.
- ¹⁵ B. C. Guo, K. P. Kerns, and A. W. Castleman, Jr., *Science* **255**, 1411 (1992).
- ¹⁶ B. C. Guo, K. P. Kerns, and A. W. Castleman, Jr., *Science* **256**, 515 (1992).
- ¹⁷ J. S. Pilgrim and M. A. Duncan, *J. Am. Chem. Soc.* **115**, 6958 (1993).
- ¹⁸ J. Muñoz, M.-M. Rohmer, M. Bénard, C. Bo, and J.-M. Poblet, *J. Phys. Chem. A* **103**, 4762 (1999).
- ¹⁹ B. D. Leskiw and A. W. Castleman, Jr., *C. R. Physique* **3**, 251 (2002).
- ²⁰ I. Dance, *J. Am. Chem. Soc.* **118**, 6309 (1996).
- ²¹ S. Wei, B. C. Guo, J. Purnell, S. Buzza, and A. W. Castleman, Jr., *J. Phys. Chem.* **96**, 4166 (1992).
- ²² S. Wei, B. C. Guo, J. Purnell, S. Buzza, and A. W. Castleman, Jr., *Science* **256**, 818 (1992).
- ²³ L. S. Wang and H. Cheng, *Phys. Rev. Lett.* **78**, 2983 (1997).
- ²⁴ J. S. Pilgrim and M. A. Duncan, *J. Am. Chem. Soc.* **115**, 9724 (1993).
- ²⁵ K. Tono, A. Terasaki, T. Ohta, and T. Kondow, *J. Chem. Phys.* **117**, 7010 (2002).
- ²⁶ J. E. Reddic and M. A. Duncan, *Chem. Phys. Lett.* **264**, 157 (1996).
- ²⁷ R. Selvan, L. Gowrishankar, and T. Pradeep, *Proc. Indian Acad. Sci.* **113**, 681 (2001).
- ²⁸ X. Li and L. S. Wang, *J. Chem. Phys.* **111**, 8389 (1999).
- ²⁹ L. S. Wang and X. Li, *J. Chem. Phys.* **112**, 3602 (2000).
- ³⁰ X. B. Wang, C. D. Ding, and L. S. Wang, *J. Phys. Chem. A* **101**, 7699 (1997).

- ³¹ H. J. Zhai, L. S. Wang, P. Jena, G. L. Gutsev, and C. W. Bauschlicher, Jr., *J. Chem. Phys.* **120**, 8996 (2004).
- ³² T. C. Steimle, A. J. Marr, J. Xin, A. J. Merer, K. Athanassenas, and D. Gillett, *J. Chem. Phys.* **106**, 2060 (1997).
- ³³ D. S. Yang, M. Z. Zgierski, and P. A. Hackett, *J. Chem. Phys.* **108**, 3591 (1998).
- ³⁴ H. J. Zhai, S. R. Liu, X. Li, and L. S. Wang, *J. Chem. Phys.* **115**, 5170 (2001).
- ³⁵ D. S. Yang, M. Z. Zgierski, A. Bérces, P. A. Hackett, P. N. Roy, A. Martinez, T. Carrington, Jr., D. R. Salahub, R. Fournier, T. Pang, and C. Chen, *J. Chem. Phys.* **24**, 10663 (1996).
- ³⁶ P. Redondo, C. Barrientos, and A. Largo, *J. Phys. Chem. A* **110**, 4057 (2006).
- ³⁷ P. Redondo, C. Barrientos, and A. Largo, *J. Chem. Theory Comput.* **2**, 885 (2006).
- ³⁸ D. L. Strout and M. B. Hall, *J. Phys. Chem.* **100**, 18007 (1996).
- ³⁹ S. Bates, Dissertation, 2008.
- ⁴⁰ S. Wang, Dissertation, 1997.
- ⁴¹ M. E. Jacox, *Chem. Soc. Rev.* **31**, 108 (2002).
- ⁴² E. F. C. Byrd, C. D. Sherrill, and M. Head-Gordon, *J. Phys. Chem. A* **105**, 9736 (2001).
- ⁴³ R. Cárdenas, Dissertation, 2007.
- ⁴⁴ S. A. Bates, C. M. L. Rittby, and W. R. M. Graham, *J. Chem. Phys.* **125**, 074506 (2006).
- ⁴⁵ S. A. Bates, C. M. L. Rittby, and W. R. M. Graham, *J. Chem. Phys.* **127**, 064506 (2007).
- ⁴⁶ S. A. Bates, C. M. L. Rittby, and W. R. M. Graham, *J. Chem. Phys.* **128**, 234301 (2008).
- ⁴⁷ E. Gonzalez, C. M. L. Rittby, and W. R. M. Graham, *J. Chem. Phys.* **130**, 194511 (2009).
- ⁴⁸ M. J. Frisch, G. W. Trucks, H. B. Schlegel *et al.*, computer code GAUSSIAN 03, Revision B.01, Gaussian, Inc., Pittsburgh PA, 2003.
- ⁴⁹ E. Yamazaki, T. Okabayashi, and M. Tanimoto, *Astrophys. J.* **551**, L199 (2001).

- ⁵⁰ M. A. Brewster and L. M. Ziurys, *Astrophys. J.* **559**, L163 (2001).
- ⁵¹ D. L. Lambert and E. A. Mallia, *Mon. Not. R. Astr. Soc.* **151**, 437 (1971).
- ⁵² J. W. Brault and H. Holweger, *Astrophys. J.* **249**, L43 (1981).
- ⁵³ V. M. Rayón, P. Redondo, C. Barrientos, and A. Largo, *Chem.-Eur. J.* **12**, 6963 (2006).
- ⁵⁴ A. N. Andriotis, M. Menon, G. E. Froudakis, and J. E. Lowther, *Chem. Phys. Lett.* **301**, 503 (1999).
- ⁵⁵ C. Rey, M. M. G. Alemany, O. Diéguez, and L. J. Gallego, *Phys. Rev. B* **62**, 12640 (2000).
- ⁵⁶ G. E. Froudakis, M. Mühlhäuser, A. N. Andriotis, and M. Menon, *Phys. Rev. B* **64**, 241401 (2001).
- ⁵⁷ R. C. Longo, M. M. G. Alemany, B. Fernández, and L. J. Gallego, *Phys. Rev. B* **68**, 167401 (2003).
- ⁵⁸ R. C. Longo and L. J. Gallego, *J. Chem. Phys.* **118**, 10349 (2003).
- ⁵⁹ D. L. Robbins, C. M. L. Rittby, W. R. M. Graham, *J. Chem. Phys.* **114**, 3570 (2001).
- ⁶⁰ E. Gonzalez, C. M. L. Rittby, and W. R. M. Graham, *J. Chem. Phys.* **125**, 44504 (2006).
- ⁶¹ A. D. Becke, *Phys. Rev. A* **38**, 3098 (1988).
- ⁶² C. Lee, W. Yang, and R. G. Parr, *Phys. Rev. B* **37**, 785 (1988).
- ⁶³ R. Sumathi and M. Hendrickx, *J. Phys. Chem. A* **102**, 7308 (1998).
- ⁶⁴ B. V. Reddy and S. N. Khanna, *J. Phys. Chem.* **98**, 9446 (1994).
- ⁶⁵ R. Sumathi and M. Hendrickx, *J. Phys. Chem. A* **102**, 4883 (1998).
- ⁶⁶ R. Sumathi and M. Hendrickx, *Chem. Phys. Lett.* **287**, 496 (1998).
- ⁶⁷ R. Sumathi and M. Hendrickx, *J. Phys. Chem. A* **103**, 585 (1999).
- ⁶⁸ J. P. Perdew, *Phys. Rev. B* **33**, 8822 (1986).
- ⁶⁹ R. A. Shepherd and W. R. M. Graham, *J. Chem. Phys.* **88**, 3399 (1988).

- ⁷⁰ J. D. Presilla-Márquez, S. C. Gay, C. M. L. Rittby, and W. R. M. Graham, *J. Chem. Phys.* **102**, 6354 (1995).
- ⁷¹ (a) C. M. L. Rittby, *J. Chem. Phys.* **100**, 175 (1994); (b) J. D. Presilla-Márquez and W. R. M. Graham, *ibid.* **100**, 181 (1994).
- ⁷² K. W. Hinkle, J. J. Keady, and P. F. Bernath, *Science* **241**, 1319 (1988).
- ⁷³ S. Roszak, D. Majumdar, and K. Balasubramanian, *J. Chem. Phys.* **116**, 10238 (2002).
- ⁷⁴ M. F. A. Hendrickx and S. Clima, *Chem. Phys. Lett.* **388**, 284 (2004).
- ⁷⁵ P. Redondo, C. Barrientos, and A. Largo, *J. Phys. Chem. A* **109**, 8594 (2005).
- ⁷⁶ R. E. Kinzer, Jr., C. M. L. Rittby, and W. R. M. Graham, *J. Chem. Phys.* **128**, 064312 (2008).
- ⁷⁷ R. E. Kinzer, Jr., C. M. L. Rittby, and W. R. M. Graham, *J. Chem. Phys.* **125**, 074513 (2006).
- ⁷⁸ R. E. Kinzer, Jr., C. M. L. Rittby, and W. R. M. Graham, *J. Chem. Phys.* **129**, 184309 (2008).
- ⁷⁹ J. Szczepanski, Y. Wang, and M. Vala, *J. Phys. Chem. A* **112**, 4778 (2008).
- ⁸⁰ Y. Wang, J. Szczepanski, and M. Vala, *J. Phys. Chem. A* **112**, 11088 (2008).
- ⁸¹ E. Gonzalez, C. M. L. Rittby, and W. R. M. Graham, *J. Phys. Chem. A* **112**, 10831 (2008).
- ⁸² M. F. A. Hendrickx and S. Clima, *Chem. Phys. Lett.* **388**, 290 (2004).
- ⁸³ E. G. Noya, R. C. Longo, and L. J. Gallego, *J. Chem. Phys.* **119**, 11130 (2003).
- ⁸⁴ C. Barrientos, P. Redondo, and A. Largo, *Chem. Phys. Lett.* **343**, 563 (2001).
- ⁸⁵ C. Barrientos, P. Redondo, and A. Largo, *Chem. Phys. Lett.* **335**, 64 (2001).
- ⁸⁶ P. Redondo, C. Barrientos, A. Cimas, and A. Largo, *J. Phys. Chem. A* **107**, 6317 (2003).
- ⁸⁷ P. Redondo, C. Barrientos, A. Cimas, and A. Largo, *J. Phys. Chem. A* **107**, 4676 (2003).
- ⁸⁸ A. Largo, P. Redondo, C. Barrientos, and L. M. Ziurys, *Chem. Phys. Lett.* **355**, 509 (2002).
- ⁸⁹ P. Redondo, C. Barrientos, A. Cimas, and A. Largo, *J. Phys. Chem. A* **108**, 11132 (2004).
- ⁹⁰ A. Largo, P. Redondo, and C. Barrientos, *J. Phys. Chem. A* **108**, 6421 (2004).

- ⁹¹ G. K. Gueorguiev, J. M. Pancheco, S. Stafström, and L. Hultman, *Chem. Phys. Lett.* **515**, 1192 (2006).
- ⁹² G. K. Gueorguiev and J. M. Pancheco, *J. Chem. Phys.* **119**, 10313 (2003).
- ⁹³ D. Bandyopadhyay and M. Kumar, *Chem. Phys.* **353**, 170 (2008).
- ⁹⁴ J. B. Jaeger, T. D. Jaeger, and M. A. Duncan, *J. Phys. Chem. A Lett.* **110**, 9310 (2006).
- ⁹⁵ *IR-REMPI Spectroscopy of Metal-Silicon Clusters*. Retrieved 30 April 2009 from the FOM-Institute for Plasma Physics Rijnhuizen web page at www.rijnh.nl/research/guthz/felix_felice/users/user_reports/USERS2003/Duncan_2003.pdf. The main page is <http://www.rijnh.nl/>.

VITA

Personal Background	Raymond Edward Kinzer, Jr. Born 4 August 1982, Houston, TX
Education	Bachelor of Science, Astronomy and Physics, Mathematics minor, Texas Christian University, Ft. Worth, TX, 2004 Doctor of Philosophy, Physics, Texas Christian University, Ft. Worth, TX, 2009
Experience	Physics Tutor, Department of Physics and Astronomy, Texas Christian University, Fort Worth, TX, August 2004-May 2006 Astronomy Laboratory Teaching Assistant, Texas Christian University, August 2002-present Research Assistant, TCU Molecular Physics Laboratory, Texas Christian University, September 2004-present
Awards	Best Graduate Student Poster for Department of Physics and Astronomy, TCU Student Research Symposium, 2006 Robert A. Welch Foundation Graduate Scholarship, 2005-2007 NASA Postdoctoral Program Fellowship, 2009
Professional Memberships	American Association for the Advancement of Science American Physical Society Sigma Xi
Publications	<i>Vibrational Spectrum of Cyclic TiC₃ in Solid Ar</i> , R.E. Kinzer, Jr., C.M.L. Rittby, and W.R.M. Graham, <i>J. Chem. Phys.</i> 125 , 074513 (2006). <i>Fourier Transform Infrared Observation of the $\nu_3(\sigma_u)$ Vibrational Mode of NiC₃Ni in Solid Ar</i> , R.E. Kinzer, Jr., C.M.L. Rittby, and W.R.M. Graham, <i>J. Chem. Phys.</i> 128 , 064312 (2008). <i>The Vibrational Spectrum of Cyclic ScC₃ in Solid Ar</i> , R.E. Kinzer, Jr., C.M.L. Rittby, and W.R.M. Graham, <i>J. Chem. Phys.</i> 129 , 184309 (2008).
Presentations	<i>FTIR Matrix Study of Potential Circumstellar Molecules: TiC₃</i> , R.E. Kinzer, Jr., C.M.L. Rittby, and W.R.M. Graham. 61 st International Symposium on Molecular Spectroscopy, June 2006, The Ohio State University, Columbus, OH. <i>FTIR Matrix and DFT Study of the Vibrational Spectrum of NiC₃Ni</i> , R.E. Kinzer, Jr., C.M.L. Rittby, and W.R.M. Graham. 62 nd International Symposium on Molecular Spectroscopy, June 2007, The Ohio State University, Columbus, OH. <i>FTIR Matrix and DFT Study of the Vibrational Spectrum of Cyclic ScC₃</i> , R.E. Kinzer, Jr., C.M.L. Rittby, and W.R.M. Graham. 63 rd International Symposium on Molecular Spectroscopy, June 2008, The Ohio State University, Columbus, OH.

ABSTRACT

FOURIER TRANSFORM INFRARED SPECTROSCOPY STUDY OF SMALL TRANSITION-METAL CARBIDE CLUSTERS

by Raymond Edward Kinzer, Jr., Ph.D., 2009
Department of Physics and Astronomy
Texas Christian University

Dissertation Advisor:
Dr. W. R. M. Graham, Professor of Physics and Astronomy

Small molecular clusters consisting of transition metals and carbon, which are the focus of the research, are important for their potential as astrophysically significant species and for the information they may provide about the structures and bonding mechanisms of larger transition-metal carbide structures, such as metallocarbohedrenes. Additional applications exist for semiconductors and quantum dots.

The dissertation research is concerned with a new investigation of the structures and infrared signatures of novel transition-metal carbide clusters using Fourier transform infrared (FTIR) spectroscopy and density functional theory (DFT). FTIR absorption spectra were obtained by trapping the vapor produced by the simultaneous evaporation of transition metal and carbon rods with Nd:YAG lasers in an Ar matrix maintained at ~ 10 K in a vacuum at $\sim 10^{-7}$ Torr. Comparison of the vibrational fundamentals and isotopic shifts observed in ^{13}C -enriched vibrational spectra to the isotopic spectra predicted by DFT has enabled the identification of vibrational fundamentals of linear NiC_3Ni , cyclic TiC_3 , and cyclic ScC_3 .

The $\nu_3(\sigma_u)$ asymmetric carbon stretching mode of linear NiC_3Ni has been observed at 1950.8 cm^{-1} . Although other small nickel-carbon clusters have been investigated theoretically, this is the first experimental or theoretical study of the structure and infrared signature of NiC_3Ni . Two vibrational fundamentals of cyclic TiC_3 (a fanlike geometry with a transannular metal-carbon bond) were observed at $\nu_3(a_1)=624.3$ and $\nu_5(b_2)=1484.2\text{ cm}^{-1}$, corresponding to

symmetric metal-carbon and asymmetric carbon-carbon stretching modes, respectively. A third frequency at 573.8 cm^{-1} has provisionally been assigned to the $\nu_4(b_1)$ fundamental. Three vibrational fundamentals of cyclic ScC_3 were observed including the $\nu_5(b_2)=1478.0\text{ cm}^{-1}$ asymmetric carbon stretch, the $\nu_3(a_1)=557.0\text{ cm}^{-1}$ symmetric metal-carbon stretch, and the $\nu_1(a_1)=1190.7\text{ cm}^{-1}$ symmetric carbon stretch. The results for TiC_3 and ScC_3 provide the first unambiguous evidence of the cyclic structures suggested by earlier photoelectron spectroscopy studies, significantly improve the accuracy of the $\nu_3(a_1)$ measurements, and identify three new vibrational fundamentals.

FTIR measured isotopic spectra for all of the fundamentals are in good agreement with the predictions of DFT simulations using the B3LYP hybrid functional. Innovative sample preparation techniques have also been developed in this investigation.